ISTANBUL TECHNICAL UNIVERSITY ★ GRADUATE SCHOOL

AUTOMATIC LANDING WITH MODEL PREDICTIVE CONTROL

M.Sc. THESIS

Talha ULUKIR

Department of Mechatronic Engineering

Mechatronic Engineering Programme

January 2022

ISTANBUL TECHNICAL UNIVERSITY ★ GRADUATE SCHOOL

AUTOMATIC LANDING WITH MODEL PREDICTIVE CONTROL

M.Sc. THESIS

Talha ULUKIR

Department of Mechatronic Engineering

Mechatronic Engineering Programme

Thesis Advisor: Assist. Prof. Dr. İlker ÜSTOĞLU

January 2022

ISTANBUL TEKNİK ÜNİVERSİTESİ ★ LİSANSÜSTÜ EĞİTİM ENSTİTÜSÜ

MODEL ÖNGÖRÜLÜ KONTROL İLE OTOMATİK İNİŞ

YÜKSEK LİSANS TEZİ

Talha ULUKIR
(518191029)

Mekatronik Mühendisliği Anabilim Dalı

Mekatronik Mühendisliği Programı

Tez Danışmanı: Dr. Öğr. Üyesi İlker ÜSTOĞLU

Ocak 2022

Talha ULUKIR, a M.Sc. student of İTU Graduate School student ID 518191029 successfully defended the thesis entitled "AUTOMATIC LANDING WITH MODEL PREDICTIVE CONTROL", which he prepared after fulfilling the requirements specified in the associated legislations, before the jury whose signatures are below.

Thesis Advisor :	**Assist. Prof .Dr. İlker ÜSTOĞLU** İstanbul Technical University	.....
Jury Members :	**Assoc. Prof. Dr. Yaprak YALÇIN** Istanbul Technical University	.....
	Prof. Dr. Şeref Naci ENGİN Yildiz Technical University	.....

Date of Submission : 24 November 2021

Date of Defense : 04 January 2022

To my wife,

FOREWORD

First of all, I would like to thank my thesis advisor, Dr. İlker Üstoğlu, who helped this thesis emerge with his advice and guidance throughout my university and further education life, as well as within the scope of his thesis work. I will always be indebted to him on his way to becoming a controls engineer.

I would like to thank my friends at TUSAŞ - UAV Guidance and Control team, which is the first workplace where I worked as a control engineer, for their understanding and help.

I would like to thank my very dear wife, Melike, for being with me no matter what I experience in life and for her understanding that she never lacks, I would not have been able to complete this thesis without her valuable support.

I would like to thank my parents, Mehmet Ünsal and Güldiye, who have been with me since the first day I opened my eyes to the world and have trusted me since the first day, and my dear brothers Sare, Behram and Berat.

January 2022 Talha ULUKIR

(Control Engineer)

TABLE OF CONTENTS

Page

FOREWORD ..... **ix**
TABLE OF CONTENTS ..... **xi**
ABBREVIATIONS ..... **xiii**
SYMBOLS ..... **xv**
LIST OF TABLES ..... **xvii**
LIST OF FIGURES ..... **xix**
SUMMARY ..... **xxi**
ÖZET ..... **xxiii**
1. INTRODUCTION **1**
1.1 Purpose of Thesis 1
1.2 Literature Review 1
1.3 Motivation 3
2. MODELLING **5**
2.1 Mathematical Modelling 5
2.1.1 Reference frames 5
2.1.1.1 Inertial axis system 5
2.1.1.2 Earth-fixed axis system 5
2.1.1.3 Navigational axis system 6
2.1.1.4 Body axis system 6
2.1.1.5 Stability axis system 6
2.1.1.6 Wind axis system 6
2.1.2 Forces and moments 7
2.1.3 Angles, angular velocity and rates 8
2.1.4 Equation of motions 9
2.1.4.1 Translational equation of motion 9
2.1.4.2 Rotational equation of motion 12
2.1.5 Translational kinematics 13
2.1.6 Rotational kinematics 14
2.2 Actuator Modelling 15
2.3 Disturbance Modelling 16
2.3.1 Gust modelling 16
2.3.2 Wind shear modelling 17
2.4 Sensor Modelling 18
2.5 Linearization 20
2.5.1 Trim 20
2.5.1.1 Trimmed states 21
2.5.1.2 General trim algorithm 21
2.5.2 Linearization 22
2.6 Linear and Nonlinear Model Comparision 25
2.7 Longitudinal and Lateral Modes 27
2.7.1 Longitudinal modes 27
2.7.2 Lateral modes 30

3. AUTOMATIC LANDING 33
3.1 Base Leg 34
3.2 Glide 35
3.3 Flare 35
3.4 Touchdown 36
4. FLIGHT CONTROL ARCHITECTURES 39
4.1 Stability Augmentation System 39
4.1.1 Longitudinal stability augmentation system 40
4.1.2 Lateral stability augmentation system 41
4.2 Control Augmentation System 42
4.2.1 Longitudinal control augmentation system 42
4.2.2 Lateral control augmentation system 43
4.3 Autopilot Systems 44
4.4 Flight Control System General Architecture 45
4.5 Flight Control Robustness, Stability and Flight Quality Criterias 45
5. AUTOMATIC LANDING ARCHITECTURES 51
5.1 Longitudinal Automatic Landing Architectures 51
5.2 Lateral Automatic Landing Architectures 55
6. AUTOMATIC LANDING CONTROLLER DESIGN 59
6.1 Automatic Landing with PID Controller 62
6.1.1 Mathematical background 62
6.1.2 Automatic landing with PID controller 63
6.1.2.1 Longitudinal autopilot 64
6.1.2.2 Lateral autopilot 69
6.2 Automatic Landing with Linear Quadratic Integrator (LQI) 74
6.2.1 Mathematical background 74
6.2.2 Automatic landing with LQI controller 76
6.2.2.1 Longitudinal autopilot 76
6.2.2.2 Lateral autopilot 81
6.3 Automatic Landing with Model Predictive Control (MPC) 85
6.3.1 Mathematical background 85
6.3.2 Automatic landing with MPC controller 90
6.3.2.1 Longitudinal autopilot 91
6.3.2.2 Lateral autopilot 93
6.4 Automatic Landing with Algebraic Model Predictive Control (A-MPC) 96
6.4.1 Mathematical background 96
6.4.1.1 Input constraints handling 97
6.4.1.2 State constraints handling 99
6.4.2 Automatic landing with input constraint AMPC controller 100
6.4.2.1 Longitudinal autopilot 101
6.4.2.2 Lateral autopilot 103
6.4.3 Automatic landing with state constraint AMPC controller 105
6.4.3.1 Longitudinal autopilot 105
6.4.3.2 Lateral autopilot 107
7. RESULTS 111
REFERENCES 115
CURRICULUM VITAE 119

ABBREVIATIONS

ILS **:** Instrument Landing systems
NDI **:** Nonlinear Dynamic Inversion
MPC **:** Model Predictive Control
P **:** Proportional
PI **:** Proportional-Integral
PID **:** Proportional-Integral -Derivative
LQR **:** Linear Quadratic Regulator
LQI **:** Linear Quadratic Integrator
GTM **:** Generic Transport Model
NASA **:** National Aeronautics and Space Administration
TAS **:** True Air Speed
IAS **:** Indicated Air Speed
EAS **:** Estimated Air Speed
GPS **:** Global Positioning System
FAA **:** Federal Aviation Administration
SAS **:** Stability Augmentation System
CAS **:** Control Augmentation System
FCS **:** Flight Control System
SISO **:** Single Input Single Output
MIMO **:** Multi Input Multi Output
AMPC **:** Algebraic Model Predictive Control

SYMBOLS

X, Y, Z	**:** Longitudinal, Lateral and Vertical force
U, V, W	**:** Longitudinal, Lateeral and Vertical speed
L, M, N	**:** Pitching, Rolling, Yawing moment
Ψ, θ, Φ	**:** Azimuth, Pitch and Roll angle
p, q, r	**:** Roll, Pitch and Yaw rate
ρ	**:** Air density
m	**:** Mass
$\mathbf{V_t}$	**:** Speed according to the body axis
$\mathbf{I_b}$	**:** Inertia matrix according to the body axis
$\mathbf{V_{ground}}$	**:** Speed according to the earth
$\mathbf{V_{wing}}$	**:** Wind speed
α	**:** Angle of attack
β	**:** Sideslip angle
γ	**:** Flight path angle
ζ	**:** Damping ratio
$\boldsymbol{\omega_n}$	**:** Natural frequency
$\mathbf{V_n}$, $\mathbf{V_e}$, $\mathbf{V_d}$	**:** North direction, East direction, Vertical speed
$\mathbf{A_x}$, $\mathbf{A_y}$, $\mathbf{A_z}$	**:** Acceleartion on X, Y and Zaxis,
τ	**:** Time constant
$\boldsymbol{\delta_e}$, $\boldsymbol{\delta_a}$, $\boldsymbol{\delta_r}$	**:** Elevator, Aileron and Rudder deflection
$\mathbf{V_{stall}}$	**:** Stall speed
A	**:** Wing area
W	**:** Weight
$\mathbf{CL_{max}}$	**:** Maximum lift coefficient
g	**:** Gravitional force
$\mathbf{I_{xy}}$, $\mathbf{I_{yz}}$, $\mathbf{I_{zx}}$	**:** Inertia moment
x, y, z	**:** Longitudinal, Lateral, Vertical axis

LIST OF TABLES

Page

Table 2.1 : Forces and Moments (According to Body Axis). 7
Table 2.2 : Angles, Rates and Angular Velocities (According to Body Axis). 9
Table 2.3 : Actuators and Actuator Parameters..... 16
Table 2.4 : Air Data System Signals and Parameters..... 19
Table 2.5 : GPS Signals and Parameters. 19
Table 2.6 : Inertial Navigation System Signals and Parameters. 20
Table 2.7 : Longitudinal Modes. 27
Table 2.8 : Lateral Modes. 30
Table 3.1 : Flight Phases. 33
Table 4.1 : Aircraft Classes. 47
Table 4.2 : Flight Quality Levels. 47
Table 4.3 : Short Period Mode Damping Ratio Requirements 48
Table 4.4 : Phugoid Mode Damping Ratio Requirements. 48
Table 4.5 : Dutch Roll Mode Damping Ratio and Frequency Requirements. 48
Table 4.6 : Roll Mode Requirements. 49
Table 6.1 : Longitudinal PID Gains. 65
Table 6.2 : Longitudinal Stability Margins. 68
Table 6.3 : Lateral PID Gains. 70
Table 6.4 : Lateral Stablity Margins. 73
Table 6.5 : Longitudinal Stablity Margins 80
Table 6.6 : Lateral Stablity Margins. 84
Table 7.1 : Controller Compare. 113

LIST OF FIGURES

Page

Figure 2.1 : Body Axis, Stability Axis, Wind Axis 7
Figure 2.2 : Forces and Moments on Aircraft (According to Body Axis) 8
Figure 2.3 : Euler Angles on Aircraft (According to Body Axis)..... 9
Figure 2.4 : Translational Kinematics Transformation..... 11
Figure 2.5 : Actuator Modelling 15
Figure 2.6 : Gust Modelling..... 17
Figure 2.7 : Wind Shear Modelling 18
Figure 2.8 : Sensor Modelling 18
Figure 2.9 : System Matrices 23
Figure 2.10 : Trim Input and States Compare for Different Conditions..... 24
Figure 2.11 : Angular Velocities and Rates According Elevator Doublet..... 25
Figure 2.12 : Angular Velocities and Rates According Aileron Doublet 25
Figure 2.13 : Angular Velocities and Rates According Rudder Doublet..... 26
Figure 2.14 : Linear Velocities According Doublet..... 26
Figure 2.15 : Longitudinal Modes Frequency and Damping Change According Gamma at 80kts Estimated Airspeed 28
Figure 2.16 : Longitudinal Modes Frequency and Damping Change According Estimated Airspeed at 0 Degree Gamma..... 29
Figure 2.17 : Lateral Modes Frequency and Damping Change According Gamma at 80kts Estimated Airspeed..... 31
Figure 2.18 : Lateral Modes Frequency and Damping Change According Estimated Airspeed at 0 Degree Gamma..... 32
Figure 3.1 : Aircraft Accidents and Fatalities Statistics..... 36
Figure 4.1 : General Stability Augmentation System Scheme..... 40
Figure 4.2 : Longitudinal Stability Augmentation System Scheme..... 40
Figure 4.3 : Lateral Stability Augmentation System Scheme..... 41
Figure 4.4 : Control Augmentation System Scheme..... 42
Figure 4.5 : Longitudinal Control Augmentation System Scheme..... 43
Figure 4.6 : Lateral Control Augmentation System Scheme 43
Figure 4.7 : Pitch Hold Scheme 45
Figure 4.8 : Flight Control System Scheme..... 45
Figure 4.9 : Nichols Chart Stability Analysis 46
Figure 5.1 : Desired Altitude Reference at Flare 52
Figure 5.2 : Desired Longitudinal Trajectory Scheme..... 52
Figure 5.3 : Desired Longitudinal Trajectory Scheme..... 53
Figure 5.4 : Pitch Reference Generator Outer Loop 54
Figure 5.5 : Pitch Loop Controller..... 54
Figure 5.6 : Altitude Controller Architecture 55
Figure 5.7 : Landing (Lateral Part) General Scheme..... 56
Figure 5.8 : Landing (Lateral Part) General Scheme..... 56
Figure 5.9 : Landing (Lateral Part) General Scheme..... 57
Figure 6.1 : PID Controller Scheme 63
Figure 6.2 : Longitudinal Controller Scheme 65

Figure 6.3 : Longitudinal Stability Margins (PID Controller) 66
Figure 6.4 : Longitudinal Performance (PID Controller) 66
Figure 6.5 : Longitudinal Performance at Flare (PID Controller) 67
Figure 6.6 : Longitudinal Closed Loop Frequncy Analysis (PID Controller) 67
Figure 6.7 : Sensitivity Bode Diagrams of Longitudinal Actuators (PID Controller) 68
Figure 6.8 : Lateral Controller Scheme 70
Figure 6.9 : Lateral Performance (PID Controller) 71
Figure 6.10 : Lateral Performance at Flare (PID Controller) 71
Figure 6.11 : Lateral Stability Margins (PID Controller) 72
Figure 6.12 : Lateral Closed Loop Frequncy Analysis (PID Controller) 72
Figure 6.13 : Sensitivity Bode Diagrams of Lateral Actuators (PID Controller) 73
Figure 6.14 : LQI Controller Scheme 75
Figure 6.15 : Longitudinal Controller Scheme 77
Figure 6.16 : Longitudinal Performance (LQI Controller) 78
Figure 6.17 : Longitudinal Performance at Flare (LQI Controller) 78
Figure 6.18 : Longitudinal Stability Margins (LQI Controller) 79
Figure 6.19 : Longitudinal Closed Loop Frequncy Analysis (LQI Controller) 79
Figure 6.20 : Sensitivity Bode Diagrams of Longitudinal Actuators (LQI Controller) 80
Figure 6.21 : Lateral Controller Scheme 81
Figure 6.22 : Lateral Performance (LQI Controller) 82
Figure 6.23 : Lateral Performance at Flare (LQI Controller) 83
Figure 6.24 : Lateral Stability Margins (LQI Controller) 83
Figure 6.25 : Lateral Closed Loop Frequncy Analysis (LQI Controller) 84
Figure 6.26 : Sensitivity Bode Diagrams of Lateral Actuators (LQI Controller) 84
Figure 6.27 : Model Predictive Control Approximation Scheme 86
Figure 6.28 : Longitudinal Model Predictive Control Scheme 91
Figure 6.29 : Longitudinal Performance (MPC Controller) 92
Figure 6.30 : Longitudinal Performance at Flare (MPC Controller) 93
Figure 6.31 : Lateral Model Predictive Control Scheme 94
Figure 6.32 : Lateral Performance (MPC Controller) 95
Figure 6.33 : Lateral Performance at Flare (MPC Controller) 95
Figure 6.34 : Longitudinal Algebraic Model Predictive Control Scheme 101
Figure 6.35 : Longitudinal Performance (Input Constraint AMPC Controller) 102
Figure 6.36 : Longitudinal Performance at Flare (Input Constraint AMPC Controller) 102
Figure 6.37 : Lateral Algebraic Model Predictive Control Scheme 103
Figure 6.38 : Lateral Performance (Input Constraint AMPC Controller) 104
Figure 6.39 : Lateral Performance at Flare (Input Constraint AMPC Controller) 104
Figure 6.40 : Longitudinal Algebraic Model Predictive Control Scheme 106
Figure 6.41 : Longitudinal Performance (State Constraint AMPC Controller) 106
Figure 6.42 : Longitudinal Performance at Flare (State Constraint AMPC Controller) 107
Figure 6.43 : Lateral Algebraic Model Predictive Control Scheme 108
Figure 6.44 : Lateral Performance (State Constraint AMPC Controller) 108
Figure 6.45 : Lateral Performance at Flare (State Constraint AMPC Controller) 109

AUTOLAND WITH MODEL PREDICTIVE CONTROL

SUMMARY

In flight control systems, the landing maneuver is one of the most critical time periods for the aircraft, and it is of great importance to both respond to the disruptors and ensure durability in this time period when the disruptor activity is high. Within the scope of this thesis, 4 different controller type automatic landing systems were designed for a twin-engine passenger aircraft, this landing system provides fully automatic landing in both longitudinal and lateral planes. Within the scope of the thesis, different control architectures in the literature for the automatic landing autopilot were examined. Within the scope of the thesis, the change of system inputs and system outputs as a result of linearization under different conditions has been examined. The consistency of the nonlinear model of the aircraft with the linear model was compared, and this comparison was made by examining the behavior of the system variables in response to the binary commands given to the control surfaces. Within the scope of the thesis, what the sub-phases of the automatic landing autopilot are and according to which criteria and conditions these sub-phases are separated from each other are examined. The classical control architectures in the flight control system (stability-enhancing system and control-enhancing system) are discussed, and for what purposes and with what standards these architectures are designed. In fixed-wing aircraft control systems, the longitudinal and lateral states of the system are separable. In the scope of the thesis, the automatic landing architectures in the literature for these separated states are examined. The controllers designed for the descent system in the thesis are: PID, Linear Quadratic Integral, Model Predictive Control and Algebraic Model Predictive Control architectures. One of these four different control architectures (PID) is in a single-input-single-output control structure, while the other three control architectures (LQI, MPC, AMPC) are in a multi-input-multi-output control structure.

Keywords: Automatic landing system, Autoland, PID, LQI, MPC, Autopilot, Model Predictive Control

MODEL ÖNGÖRÜLÜ KONTROL İLE OTOMATİK İNİŞ

ÖZET

Uçuş kontrol sistemlerinde iniş manevrası hava aracı için en kritik zaman dilimlerindendir, bozucu etkinliğinin yüksek olduğu bu zaman diliminde hem bozuculara cevap verebilmek hem de dayanıklılığı sağlamak büyük önem arz etmektedir. Bu tez çalışması kapsamında çift motorlu bir yolcu uçağı için 4 farklı kontrolcü tipinde otomatik iniş sistemi tasarlanmıştır, bu iniş sistemi hem boylamsal hem de yanal düzlemde tam otomatik inişi sağlamaktadır. Tez kapsamında öncelikli olarak otomatik iniş otopilotu için literatürde yer alan farklı kontrol mimarileri incelenmiştir. Hava aracının modellenmesinde; havacılıkta kullanılan eksen takımları ve bunlar arasındaki dönüşüm, kuvvet ve moment denklemleri, eyleyici ve sensör modelleri yer almaktadır. Sisteme etkiyen rüzgar, rüzgar kesme ve ani rüzgar gibi bozucuların modellemesi de anlatılmıştır. Hava aracı kontrol sistemlerinde kontrol mimarisi direkt olarak doğrusal olmayan model üzerine kurulabilecek olsa da literatürde çeşitli koşullarda doğrusal model elde edilip bu model üzerinden kontrol mimarisi inşa edilmektedir, bu nedenle tez içerisinde denge noktasını bulma ve denege noktası etrafında doğrusallaştırma da yer almaktadır. Tez kapsamında farklı koşullarda doğrusallaştırma sonucunda sistem girişlerinin ve sistem çıkışlarının değişimi incelenmiştir. Hava aracının doğrusal olmayan modelinin, doğrusal modeli ile tutarlılığı karşılaştırılmış olup bu karşılaştırma kontrol yüzeylerine verilen ikili komutlara karşılık sistem değişkenlerinin davranışı incelenerek yapılmıştır. Otomatik iniş otopilotu tasarımında uluslararası standartlar ve kabuller mevcuttur, bu standartlar güvenli inişin tanımını yaparken kabuller inişi alt fazlara gölmektedir ve bu alt fazlar tüm sistemlerde aynı şekilde yer almaktadır. Tez kapsamında otomatik iniş otopilotuna ait alt fazların neler olduğu ve bu alt fazların hangi krtilerlere ve koşullara göre birbirinden ayrıldığı incelenmiştir. Uçuş kontrol sisteminde yer alan klasik kontrol mimarileri ele alınıp(kararlılık arttırıcı sistem ve kontrol arttırıcı sistem) bu mimarilerin hangi amaçlarla ve ne standartlarla tasarlandığı ele alınmıştır. Havacılıkta

kullanılan uçuş kontrol sistemlerinin incelenmesinde pilot otoritesinin olduğu kontrol mimarilerinden başlanıp tam otonom mimarilere kadar ve burada yer alan iç içe döngülerin hangi akış ile tasarlandığı ele alınmıştır. Sabit kanatlı hava aracı kontrol sistemlerinde sisteme ait boylamsal ve yanal durumlar ayırılabilir haldedir, tez kapsamında da bu ayırılmış durumlar için literatürde yer alan otomatik iniş mimarileri incelenmiştir. Uçuş kontrolünde boylamsal ve yanal modların kutupları üzerinden sistem karakteristiğine dair incelemeler yapılmaktadır, tez kapsamında ele alınan hava aracı için de boylamsal ve yanal modları kutup, doğal frekans ve sönüm oranı incelenmiştir; farklı koşullarda yapılan doğrusallaştırma sonucunda sistem girişlerinin sistem doğal frekanslarının ve sönüm oranlarının değişimi incelenmiştir. Tez kapsamında iniş sistemi için tasarlanan kontrolörler: PID, Lineer Kuadratik Integral, Model Öngörülü Kontrol ve Cebirsel Model Öngörülü Kontrol mimarileridir. Bu dört farklı kontrol mimarisinden birisi(PID) tek giriş-tek çıkış kontrol yapısındayken diğer üç kontrol mimarisi(LQI, MPC, AMPC) çok giriş-çok çıkış kontrol yapısındadır. PID kontrolörün tsarlanmasının amacı ulaşılabilir ve havacılıkta sık kullanılan bir kontrol yapısı olması ve otomatik iniş problemine uygulanabilirliğini incelemektir. Lineer Kuadratik Integral kontrol mimarisinin uygulanmasının amacı ise yine havacılıkta kullanılan kararlılık arttırıcı sistem(sistem durumlarının stabil hale gelip sönümlenmesini sağlayan mimari) ve kontrol arttırıcı sistem(sistem durumlarından istenilenleri pilot tarafından veya dış döngü kontrolörü tarafından verilecek referans değerlerin takip edilmesini sağlayan mimari) yapıları ile benzerlik kurulabilecek bir yapıda(sistem durumları için durum geribesleme ile kararlı hale getirirken seçilen geribesleme sinyallerini referans takibi yapılacak şekilde hatanın integralden geçirilerek kontrol komutunun oluşturulduğu bir yapıdır) olmasıdır. Uçuş kontrolü kalitesini test etmek için önerilen kontrolör yapıları hem farklı büyüklükte ve yönde sabit rüzgarlar, rüzgar kesme durumları, ani rüzgar durumları kontrol yüzeyi hataları ile bozucu etkisinde bırakılmıştır. Tez kapsamında tasarlanan iniş otopilotu klasik iniş mimarilerinde olduğu gibi süzülme, palye ve teker koyma alt fazlarından oluşmakta olup kontrol sisteminin sınanacağı bozucu durumları hem inişin başında hem alt fazlar arasındaki geçiş anında verilerek kontrolörlerin başarımları incelenmiştir. Uçuş kontrolörleri tasarlanırken kontrol sisteminin davranışı hakkındaki uluslar arası sivil ve askeri standartlar tez kapsamında incelenmiş, tasarlanan kontrolör yapılarından sabit geri beslemeli olan kontrol mimarileri bu kriterlere uygunluk açısından da

değerlendirilmiştir. Tez kapsamında tasarlanan ve çevrimiçi olarak kontrol işaretinin üretildiği Model Öngörülü Kontrol ve Cebirsel Model Öngörülü Kontrol yapılarının kıyaslanmasında hem çevrimiçi çözüm süresi hem de performas kriterleri altındaki başarımı göz önünde bulundurulmuştur. Çevrimiçi kontrol işaretlerinin belirlendiği Model Öngörülü ve Cebirsel Model Öngörülü kontrol yapılarında kararlılık incelemesi klasik geri besleme yöntemlerinde yapıldığı gibi yapılamayacağı için literatürde yer alan varsayımlar ile kararlılıkları incelenmiştir. Kontrolörlerin tasarımı iniş safhasındaki bir durum için doğrusallaştırılmış doğrusal model üzerinden yapılmış olup iniş simülasyonu ve performans analizleri doğrusal olmayan model üzerinden yapılmıştır. Tezin değerlendirme kısmında yanal ve boylamsal durumların tutuşunun belirli kriterler altında, inişin tamamı boyunca, palye fazında ve teker koyma anındaki başarımı değerlendirilerek farklı kontrolör yapılarının iniş otopilotu tasarımındaki başarımı ele alınmıştır.

Anahtar Kelimeler: Otomatik iniş sistemi, Otopilot, PID, LQI, MPC, Model Öngörülü Kontrol

1. INTRODUCTION

1.1 Purpose of Thesis

Within the scope of this thesis;

- With the model predictive control method, it is aimed to develop an algorithm for automatic landing of a fixed-wing aircraft.

- Taking into account that the computation speed of the classical MPC algorithm is high, it is aimed to make automatic landing by using an algorithm that can give results in a lower time with a different MPC approach.

- It is aimed to make performance comparisons of classical feedback control methods (PID, LQI), Model Predictive Control (MPC) and Algebraic Model Predictive Control (AMPC) methods in case of adverse weather conditions.

1.2 Literature Review

The first automatic landing system was implemented in England in 1965, however, many aircraft with automatic landing use the instrument landing system. Automatic landing systems work together with lLS (Instrument Landing systems) at airports. The lLS directs the aircraft with two radio transmitters called glide slope and Joealizer beams to provide the appropriate elevation and approach angle (azimuth) of the aircraft relative to the runway. By starting a flare about 50 feet above the runway surface, the nose of the plane is lifted, the air speed is cut and thus a smooth landing is provided. At altitudes below 200ft, the ILS signs are very noisy, so they stop being used before they fly. Below this altitude a radio altimeter or visual data is used as a reference. The vertical velocity and airspeed of the plane are reduced from the start of the flare to the ground.[1] Several control architectures have been used for automatic descent control. PID and its derivative controllers are used for altitude and descent speed.[2,3]

There are automatic landing algorithms made with the backstepping control method. For automatic landing with this algorithm, roll, yaw angles and altitude, velocity

signals in the longitudinal plane are used. In addition, the gust affecting the aircraft in the study was estimated with an observer structure in 3 axes. [4,5]

Automatic landing algorithms made with the fuzzy control method are available. These studies state that fuzzy logic control is an effective and flexible method for automatic descent when applied to the control law, and that the design method of control law using fuzzy logic control is obtained. [6]

Adaptive Control studies were also carried out for automatic landing systems. [7] In this study, while the glide angle and longitudinal direction are controlled in the first part of the longitudinal axis control, the velocity error and vertical velocity are controlled in the second step. Two reference models and linear observer were used in the related study. The signal predicted by the Observer was used to train the neural network, which is one of the subsystems of the control architecture.

Studies have been carried out in which adaptive control and dynamic inversion methods are used in combination for automatic landing. The Nonlinear Dynamic Inversion (NDI) controller acts as the main controller for this architecture. In the controller, which is designed as two nested loops as inner and outer loop, while the pitch angle, speed, yaw rate commands are controlled in the inner loop, commands to control the descent slope are generated in the outer loop.[8]

Model predictive control method is a method that has been available for a very long time in the control literature. [9–15] The biggest advantages of the model predictive control method are that sub-optimal solutions of the control problem can be easily obtained and control parameters can be adjusted easily.[15,16] In addition to the advantages of the model predictive control method, there are some disadvantages, the most important of which is that the processor power may be insufficient due to online optimization and the processor may take longer than one cycle while obtaining the control signal in the control cycle. Different algorithms have been developed to overcome this situation.[17] In addition, sub-methods have been developed in which some calculations of the model predictive control method are performed offline.[18–20]

Studies have been conducted on model predictive control methods in flight control for a long time.[21,22] Reference model-based approach where used for an MPC controller tries to restore the original functionality of the pilot's controls. For

simulation purposes, methods were studied in which the pilot was simulated with another MPC controller operating at a lower sampling rate. [23] Nonlinear model predictive control methods have also been used in studies on flight control. A nonlinear controller methodology is developed based on nonlinear model predictive control and cluster membership estimation, resulting in a robust controller to model uncertainties and limited noise sources. In the Model Predictive Controller structure, the constraints in the states and control signals can be directly included in the optimization problem and are created within the framework of these constraints while the control signal is generated.[24,25]

In addition to all these studies, no study was encountered in which the model predictive control method was directly used for automatic landing of a fixed-wing aircraft.

1.3 Motivation

The use of model predictive control method in aircraft control is not common, one of the most important reasons for this is that generating the control signal of the MPC solution may impose a heavy computational load on the flight control computer and may send incorrect commands to the aircraft's control surfaces if it cannot reach the optimal solution. It is thought that with the algebraic model predictive control method, which brings an algebraic solution to the model predictive control method, the solution speed of the system will increase and it can be applied on a real aircraft. In terms of performance performance, it will be successful in classical feedback control methods and the solution will not impose more than its capacity on the flight control computer, which will enable the targeted output to be achieved.

2. MODELLING

The aircraft model to be used in the thesis is GTM (GenericTransport Model), which can also be found in the NASA Technology Transfer Program. NASA Aviation Safety Program conducted studies with the T-2 tail numbered aircraft, which was developed within the scope of the General Transport Model, in order to examine the situations caused by loss of control in aircraft. It is aimed to develop flight control technologies that can provide control in case of loss of control due to damage and malfunction in this aircraft. In addition to the aircraft non-linear model, varying behaviors in error scenarios are also included in the model. After the classical aircraft modeling studies, the flights were carried out and the final version of the model was obtained. The aircraft was designed as a geometrically 5.5% subscale version of a passenger plane, but also dynamically scaled. In this context, dynamic scaling techniques [26] were used to scale flight dynamics appropriately.

2.1 Mathematical Modelling

2.1.1 Reference frames

In order for the aircraft to be modeled, the equations must first be expressed in a specific set of axes. Although there are many axis sets in aviation, 6 of them are mentioned in the thesis.

2.1.1.1 Inertial axis system

A non-rotating reference system placed in the center of the earth is assumed. Earth's orbital motion around the sun is ignored. Generally, the z-axis of the inertial axes set is in the direction of the earth rotation axis, and the x and y axes are selected in the equatorial plane.

2.1.1.2 Earth-fixed axis system

The z-axis coincident with the central earth axis is on the earth rotation axis and the x axis rotating with the earth is the set of axes where the lines where the meridian and

the parallel are 0 degrees coincide. An axis system fixed at the center of the earth is useful for obtaining components that can be written from the derivative of the aircraft's position relative to the earth and its position. In this axis system, even in the absence of speed of the aircraft, it is assumed that it moves with the earth and rotates with the earth's rotation.

2.1.1.3 Navigational axis system

It is a set of axes that are on the central navigation system and whose axes are selected in the north, east and down (towards the center of the world) directions. This axis system is useful for obtaining parameters that can be expressed as the position and derivative of the aircraft relative to a point of departure.

2.1.1.4 Body axis system

A set of axes with axes coincident with specific tool directions. For example, the central plane can be chosen at the center of gravity, the x-axis to the nose, the y-axis to the right wing direction, and the z-axis to the right hand rule. The axis system is fixed to the vehicle and moves with the vehicle. In this axis system, the center of mass or center of gravity of the aircraft is selected as the reference point. However, this axis system is useful in determining the forces and moments acting on the aircraft.

2.1.1.5 Stability axis system

In order to obtain linear flight conditions of aircraft, the condition of the aircraft according to the angle of attack is important. The stability axis sysem is used to align the X axis with the incoming flow direction by rotating the aircraft body pivot around the Y axis. As a result, the X-axis of the stability pivot is aligned to the direction of the oncoming air in straight flight. If there is no sideways belt case, the Y-axis will be the same as the Y-axis of the body axis system, and the Z-axis will be the same as the Z-axis of the body axis system.

2.1.1.6 Wind axis system

It is basically based on the body axis system. Unlike the trunk axis system, the X axis is chosen in the direction of wind arrival. The Y axis is chosen to point to the right of the X axis when viewed in the V direction perpendicular to the X axis, and the Z axis

is chosen perpendicular to the X and Y axes in accordance with the right hand rule(Figure 2.1 :).

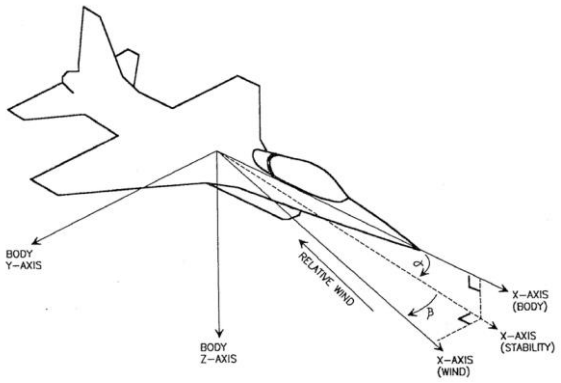

Figure 2.1 : Body Axis, Stability Axis, Wind Axis.

2.1.2 Forces and moments

Newton's second law gives the relationship between the force applied on an object and the mass of the object and the acceleration that this force will add to the object. The force due to the speed difference between the aircraft and the air is called the aerodynamic force. It can be said that the aerodynamic force creates a moment with respect to a reference point on the aircraft. Since the aircraft is not a solid object, there cannot be a single reference point and a single moment. There is a distribution of the force acting at every point of the contacted surface and a moment created by this force at certain reference points (Figure 2.1).

In aerodynamic studies, instead of resultant force and moment, their calculated or measured components in an appropriate axis set are often mentioned. Although these forces and moments can be expressed according to different axis systems, they are generally expressed in the body axis set (Table 2.1).

Table 2.1 : Forces and Moments (According to Body Axis).

Forces	Moments
X	L - Pitching Moment
Y	M - Rolling Moment
Z	N - Yawing Moment

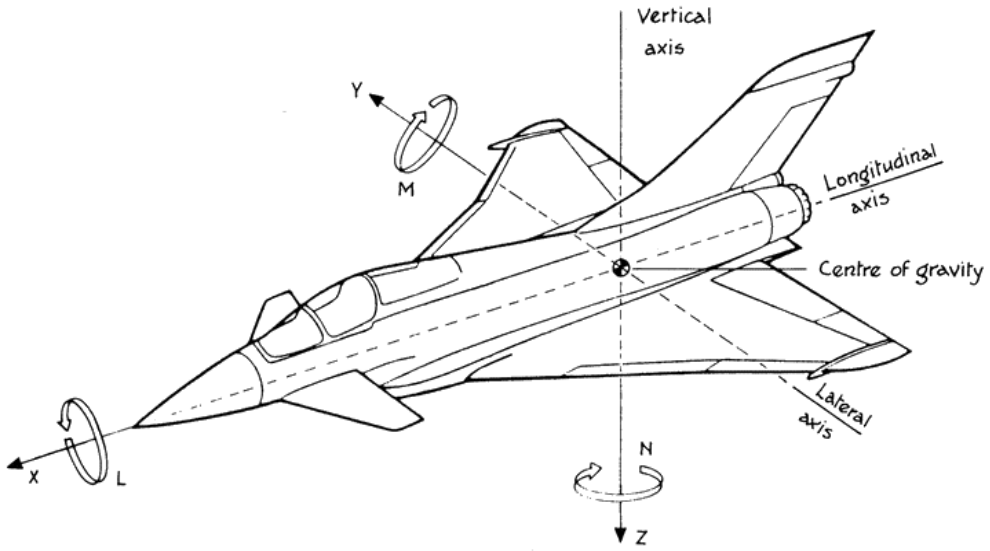

Figure 2.2 : Forces and Moments on Aircraft (According to Body Axis).

2.1.3 Angles, angular velocity and rates

The orientation of a given reference frame with respect to another reference frame is specified by three Euler angles (Ψ, θ, Φ). Ψ, Is called the head or azimuth angle; θ, is called the slope angle; Φ is called bank angle (Figure 2.3).

Euler angle velocities ($\dot{\boldsymbol{\psi}}$,$\dot{\boldsymbol{\theta}}$,$\dot{\boldsymbol{\phi}}$) are not measured directly. The angular velocity components (p, q, r) in the body axes are measured. Conversion is required to obtain the ratios of Euler angle velocities (Table 2.2).

$$\begin{aligned} p &= \dot{\phi} - \dot{\psi} sin\theta \\ q &= \dot{\theta} cos\phi + \dot{\psi} sin\phi cos\theta \\ r &= \dot{\psi} cos\phi cos\theta - \dot{\theta} sin\phi \end{aligned} \tag{2.1}$$

In other words:

$$\begin{aligned} \dot{\phi} &= p + tan\theta(qsin\phi + rcos\phi) \\ \dot{\theta} &= qcos\phi - rsin\phi \\ \dot{\psi} &= sec\theta(qsin\phi + rcos\phi) \end{aligned} \tag{2.2}$$

Table 2.2 : Angles, Rates and Angular Velocities (According to Body Axis).

Angles	Angles Definition	Rates	Rates Definition	Angular Velocities
Ψ - Psi	Heading Angle	p	Yaw Rate	$\dot{\psi}$
θ - Theta	Pitch Angle	q	Pitch Rate	$\dot{\theta}$
Φ - Phi	Roll Angle	r	Roll Rate	$\dot{\phi}$)

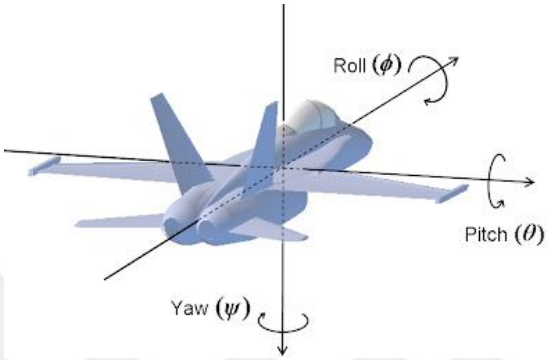

Figure 2.3 : Euler Angles on Aircraft (According to Body Axis).

2.1.4 Equation of motions

We need some pre-assumptions and assumptions before we can write the equations of motion of an airplane.

In order to obtain the Equation of motions, it is assumed that the aircraft is a rigid body, therefore it is assumed that the distance between two points of the aircraft does not change during flight. With respect to Newton's Second Law, some forces and moments applied to the plane and equations of motion expressed through translational and angular accelerations can be established. For this, the rigid body assumption is required. In this way, the movements of the aircraft are expressed in the form of an equation with six degrees of freedom.

2.1.4.1 Translational equation of motion

According to Newton's Second Law:

$$F = ma = m\frac{d}{dt}V_t = \frac{d}{dt}(mV_t) \tag{2.3}$$

And

$$M = \frac{d}{dt}(H) \tag{2.4}$$

F represents the sum of all applied externally.V_t is expressed according to the body axis set, if we arrange this expression according to the world axis system, we express it as follows:

$$(V_t)_E = (V_t)\,|_B + \Theta\, x\, V_t \tag{2.5}$$

Where Θ is define angular position. The rate of change according to the world axis system is given as

$$\frac{d}{d_t}(V_t)_E = \frac{d}{d_t}(V_t)\,|_B + \omega\, x\, V_t \tag{2.6}$$

Where ω is define angular velocity respect to the body axis system. When vectors are expressed in terms of the body axis system, both velocities can be written as the sum of their respective components (Figure 2.4).

$$V_t = i_B U + j_B V + k_B W \tag{2.7}$$

$$\omega = i_B P + j_B Q + k_B R \tag{2.8}$$

$$\frac{d}{d_t}(V_t)\,|_B = i_B \dot{U} + j_B \dot{V} + k_B \dot{W} \tag{2.9}$$

And $\omega\, x\, V_t$ can be describe as:

$$\omega\, x\, V_t = \begin{bmatrix} i & j & k \\ P & Q & R \\ U & V & W \end{bmatrix} = i(QW - VR) + j(UR - PW) + k(PV - UQ) \tag{2.10}$$

If we arrange equation 2.8 and equation 2.9

$$\frac{d}{d_t}(V_t)_E = i_B\dot{U} + j_B\dot{V} + k_B\dot{W} + i(QW - VR) + j(UR - PW) + k(PV - UQ) \quad (2.11)$$

And we can write:

$$a_x = \left(\dot{U} + QW - VR\right) \quad (2.12)$$

$$a_y = \left(\dot{V} + UR - PW\right) \quad (2.13)$$

$$a_z = \left(\dot{W} + PV - UQ\right) \quad (2.14)$$

Therefore:

$$F_x = m\left(\dot{U} + QW - VR\right) \quad (2.15)$$

$$F_y = m\left(\dot{V} + UR - PW\right) \quad (2.16)$$

$$F_z = m\left(\dot{W} + PV - UQ\right) \quad (2.17)$$

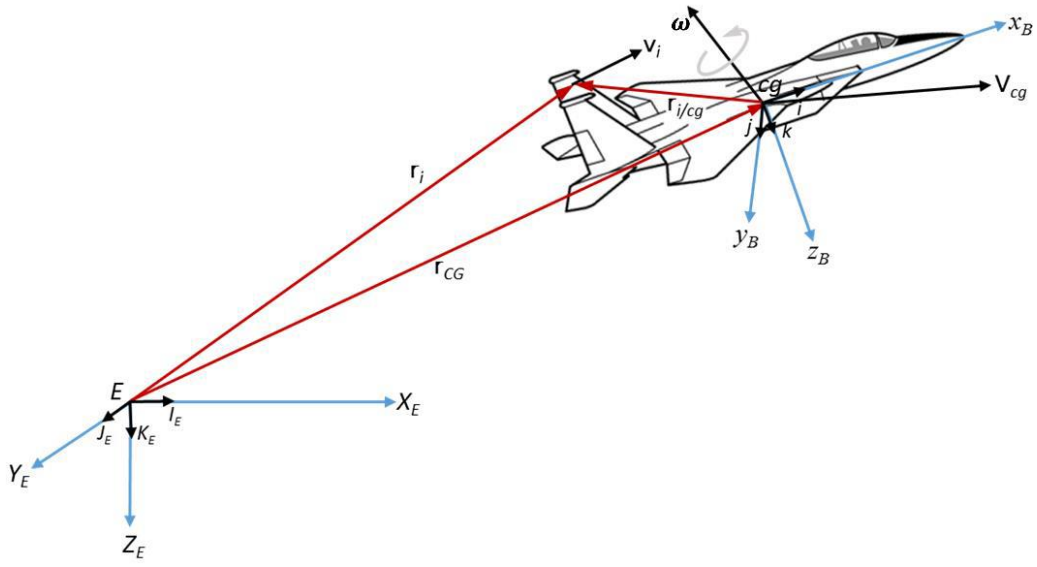

Figure 2.4 : Translational Kinematics Transformation.

2.1.4.2 Rotational equation of motion

Angular momentum for a rigid body can be defined as:

$$H = I\omega \tag{2.18}$$

The inertia matrix, I, is defined as:

$$I = \begin{bmatrix} I_{xx} & -I_{xy} & -I_{xz} \\ -I_{xy} & I_{yy} & -I_{yz} \\ -I_{xz} & -I_{yz} & I_{zz} \end{bmatrix} \tag{2.19}$$

$$M = \frac{d}{d_t}H + \omega * H \tag{2.20}$$

M represents the sum of all applied torques and H is angular momentum. If we write equation 2.18 and 2.20

$$M = \frac{d}{d_t}H + \omega * H = \frac{d}{d_t}I\omega + \omega * H \tag{2.21}$$

And angular momentum for a rigid body can be defined as:

$$H = \begin{bmatrix} I_{xx} & -I_{xy} & -I_{xz} \\ -I_{xy} & I_{yy} & -I_{yz} \\ -I_{xz} & -I_{yz} & I_{zz} \end{bmatrix} \begin{bmatrix} p \\ q \\ r \end{bmatrix} \tag{2.22}$$

Therefore angular acceleration for a rigid body can be defined as:

$$\dot{H} = \begin{bmatrix} I_{xx} & -I_{xy} & -I_{xz} \\ -I_{xy} & I_{yy} & -I_{yz} \\ -I_{xz} & -I_{yz} & I_{zz} \end{bmatrix} \begin{bmatrix} \dot{p} \\ \dot{q} \\ \dot{r} \end{bmatrix} \tag{2.23}$$

$$\dot{H} = \begin{cases} \dot{H}_x = I_{xx}\dot{p} - I_{xy}\dot{q} - I_{xz}\dot{r} \\ \dot{H}_y = -I_{xy}\dot{p} + I_{yy}\dot{q} - I_{yz}\dot{r} \\ \dot{H}_z = -I_{xz}\dot{p} - I_{yz}\dot{q} + I_{zz}\dot{r} \end{cases} \tag{2.24}$$

If we put angular momentum and angular acceleration equations in 2.22

$$\boldsymbol{M} = \left(\dot{H}_x \mathrm{i_B} + \dot{H}_y \mathrm{j_B} + \dot{H}_z \mathrm{k_B}\right) + \begin{vmatrix} \mathrm{i_B} & \mathrm{j_B} & \mathrm{k_B} \\ p & q & r \\ H_x & H_y & H_z \end{vmatrix} \tag{2.25}$$

$$\begin{aligned} M = &\left(\left[I_{xx}\dot{p} - I_{xy}\dot{q} - I_{xz}\dot{r}\right]\mathrm{i_B} + \left[-I_{xy}\dot{p} + I_{yy}\dot{q} - I_{yz}\dot{r}\right]\mathrm{j_B} + \left[-I_{xz}\dot{p} - I_{yz}\dot{q} + I_{zz}\dot{r}\right]\mathrm{k_B}\right) \\ &+\left(\left[qH_z - rH_y\right]\mathrm{i_B} + \left[rH_x - pH_z\right]\mathrm{j_B} + \left[pH_y - qH_x\right]\mathrm{k_B}\right) \end{aligned} \tag{2.26}$$

$$\boldsymbol{M} = L * i_B + M * j_B + N * k_B \tag{2.27}$$

Generally, the aircraft are symmetrical around the XZ aircraft, and the result is usually the following:

$$I_{xy} = I_{yz} = 0 \tag{2.28}$$

And

$$L = I_{xx}\dot{p} - I_{xz}(\dot{r} + pq) + \left(I_{zz} - I_{yy}\right)qr \tag{2.29}$$

$$M = I_{yy}\dot{q} + I_{xz}(p^2 - r^2) + (I_{xx} - I_{zx})pr \tag{2.30}$$

$$N = I_{zz}\dot{r} - I_{xz}p + pq\left(I_{yy} - I_{xx}\right) + I_{xz}qr \tag{2.31}$$

2.1.5 Translational kinematics

The translational velocity components in the body frame

$$V = i_b u + j_b v + k_b w \tag{2.32}$$

The translational velocity components in the earth-fixed frame

$$V_{ground} = i_e \dot{x} + j_e \dot{y} + k_e \dot{z} \tag{2.33}$$

Conversion is required here,

$$V_{ground} = T_B^E V \tag{2.34}$$

Flight path equations or course equations are obtained using the Euler Transform.

$$\begin{bmatrix}\dot{x}\\ \dot{y}\\ \dot{z}\end{bmatrix} = T_B^E \begin{bmatrix}u\\ v\\ w\end{bmatrix} \tag{2.35}$$

Here,

$$T_B^E = \begin{bmatrix}\cos\psi\cos\theta & \cos\psi\sin\theta\sin\phi - \sin\psi\cos\phi & \cos\psi\sin\theta\cos\phi + \sin\psi\sin\phi\\ \sin\psi\cos\theta & \sin\psi\sin\theta\sin\phi + \cos\psi\cos\phi & \sin\psi\sin\theta\cos\phi - \cos\psi\sin\phi\\ -\sin\theta & \cos\theta\sin\phi & \cos\theta\cos\phi\end{bmatrix} \tag{2.36}$$

As a result, the translation kinematic equations are

$$\dot{x} = u(\cos\psi\cos\theta) + v(\cos\psi\sin\theta\sin\phi - \sin\psi\cos\phi) + w(\cos\psi\sin\theta\cos\phi + \sin\psi\sin\phi) \tag{2.37}$$

$$\dot{y} = u(\sin\psi\cos\theta) + v(\sin\psi\sin\theta\sin\phi + \cos\psi\cos\phi) + w(\sin\psi\sin\theta\cos\phi - \cos\psi\sin\phi) \tag{2.38}$$

$$\dot{z} = u(-\sin\theta) + v(\cos\theta\sin\phi) + w(\cos\theta\cos\phi) \tag{2.39}$$

2.1.6 Rotational kinematics

Euler angular velocities are found in terms of aircraft angular accelerations.

$$\begin{bmatrix}p\\ q\\ r\end{bmatrix} = \begin{bmatrix}\cos\theta & 0 & -\sin\theta\\ \sin\phi\sin\theta & \cos\phi & \sin\phi\cos\theta\\ \cos\phi\sin\theta & -\sin\phi & \cos\phi\cos\theta\end{bmatrix}\begin{bmatrix}0\\ 0\\ \dot{\psi}\end{bmatrix} + \begin{bmatrix}1 & 0 & 0\\ 0 & \cos\phi & \sin\phi\\ 0 & -\sin\phi & \cos\phi\end{bmatrix}\begin{bmatrix}0\\ \dot{\theta}\\ 0\end{bmatrix} + \begin{bmatrix}\dot{\phi}\\ 0\\ 0\end{bmatrix} \tag{2.40}$$

Aircraft angular accelerations

$$\begin{bmatrix}p\\ q\\ r\end{bmatrix} = \begin{bmatrix}1 & 0 & -\sin\theta\\ 0 & \cos\phi & \sin\phi\cos\theta\\ 0 & -\sin\phi & \cos\phi\cos\theta\end{bmatrix}\begin{bmatrix}\dot{\phi}\\ \dot{\theta}\\ \dot{\psi}\end{bmatrix} \tag{2.41}$$

Euler angle velocities can be found as:

$$\begin{bmatrix}\dot{\phi}\\ \dot{\theta}\\ \dot{\psi}\end{bmatrix} = \boldsymbol{L}_{\omega}^{-1}\begin{bmatrix}p\\ q\\ r\end{bmatrix} \tag{2.42}$$

Here,

$$\boldsymbol{L_{\omega}^{-1}} = \begin{bmatrix} 1 & \tan\theta\sin\phi & \cos\phi\tan\theta \\ 0 & \cos\phi & -\sin\phi \\ 0 & \sec\theta\sin\phi & \sec\theta\cos\phi \end{bmatrix} \tag{2.43}$$

Euler angle accelerations,

$$\begin{bmatrix} \dot{\phi} \\ \dot{\theta} \\ \dot{\psi} \end{bmatrix} = \begin{bmatrix} 1 & \tan\theta\sin\phi & \cos\phi\tan\theta \\ 0 & \cos\phi & -\sin\phi \\ 0 & \sec\theta\sin\phi & \sec\theta\cos\phi \end{bmatrix} \begin{bmatrix} p \\ q \\ r \end{bmatrix} \tag{2.44}$$

As a result, the rotational kinematic equations are

$$\dot{\phi} = p + \tan\theta(\mathrm{q}\sin\phi + \mathrm{r}\cos\phi) \tag{2.45}$$

$$\dot{\theta} = \mathrm{q}\cos\phi - \mathrm{r}\sin\phi \tag{2.46}$$

$$\psi = \sec\theta(\mathrm{q}\sin\phi + \mathrm{r}\cos\phi) \tag{2.47}$$

It is obtained in the form.

2.2 Actuator Modelling

The actuators in the aircraft model are modeled as a first order system. The deviation value for each actuator is added to the command, and then the position output is obtained by multiplying the delay constant for each actuator with the different frequency(Table 2.3). During modeling, nonlinear actuator speed and position limits are also added to the model. The general scheme of the actuator model is shown in Figure 2.5.

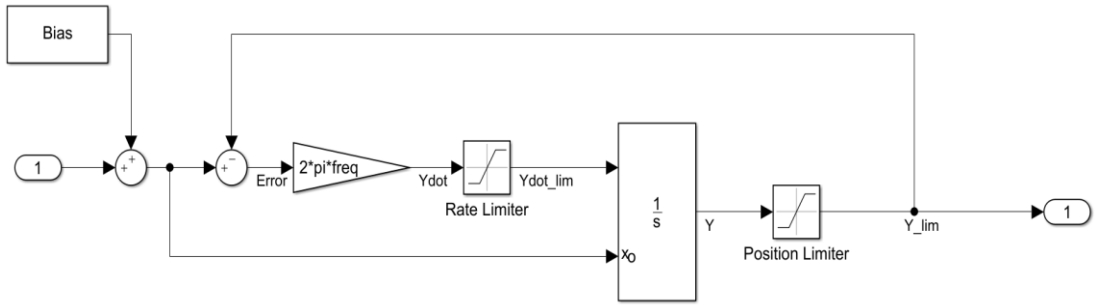

Figure 2.5 : Actuator Modelling.

Table 2.3 : Actuators and Actuator Parameters.

Actuator	Bandwidth	Rate Limits	Position Limits
Elevator	5 Hz	300 deg/s	[-30,+20] degree
Aileron	5 Hz	300 deg/s	[-20,+20] degree
Rudder	5 Hz	300 deg/s	[-30,+30] degree
Throttle			[0,100] percent

2.3 Disturbance Modelling

2.3.1 Gust modelling

Gust; sudden increase in wind speed. In order for the sudden increase in wind speed to be a breakthrough, this increase should be more than 10 Knots, with the increase the wind speed should exceed 16 Knots and its duration should be less than 20 seconds. Short-term wind with a sudden increase, blowing at a speed higher than the average wind speed (at least 10 knots) obtained at the time of the rasat. The farther up from landforms and buildings, the less incident of lunge. Due to convectional currents, edi waves, thermal instability and man-made obstacles on the earth, it is always possible to see a move on the ground.

Gust is defined as in the equation according to MIL-F-8785C[27].

$$V_{wind} = \begin{cases} 0\,, x < 0 \\ \frac{V_m}{2}\left(1 - \cos\left(\pi * \frac{x}{d_m}\right)\right), 0 \le x \le d_m \\ V_m\,, x > d_m \end{cases}$$

Here, V_m gust magnitude is defined as d_m gust length, x traveled distance and V_{wind} as the resulting wind speed in the frame of the body axis.

The Gust model is designed in MATLAB-Simulink environment as shown in the Figure 2.6.

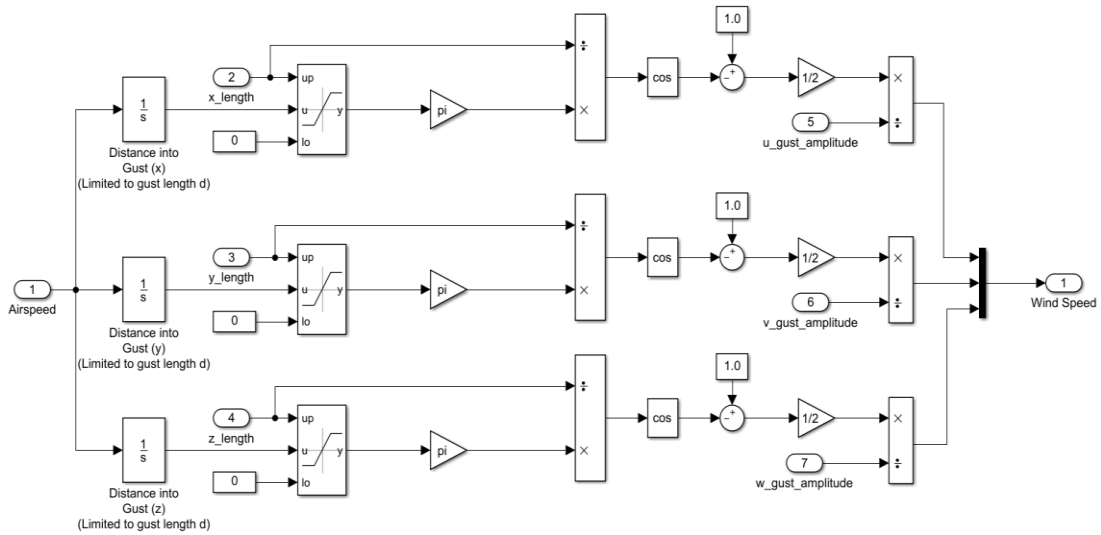

Figure 2.6 : Gust Modelling.

2.3.2 Wind shear modelling

Wind Shear; It can be defined as sudden changes in wind speed or direction, or both, between two specific points in the atmosphere. This change can be horizontal or vertical.

The biggest impact of the wind shear incident is that it poses a great danger to the aircraft in the landing phase. As is known, the speed of the aircraft at the time of landing is much lower than the speed at the time of take-off. This may cause various negative effects to occur at the time of landing on the plane.

Windshear size is defined as in the equation according to MIL-F-8785C[27].

$$u_w = W_{20}\frac{\ln\left(\frac{h}{z_0}\right)}{\ln\left(\frac{20}{z_0}\right)}, \qquad z_0 = \begin{cases} 0.15\ for\ Category\ C\ Flight\ Phase \\ 2.0\ for\ Other\ Flight\ Phases \end{cases}$$

The stages included in Category C Flight Phase are defined in the same standard as follows:

Basic Flight Stages are normally defined by staggered maneuvers using flight path control:

a. Takeoff (TO)

b. Catapult takeoff (CT)

c. Approach (PA)

d, Wave-off / go-around (WO)

e. Landing (L)

The Windshear model is designed in accordance with Category C Flight Phase in MATLAB-Simulink environment as shown in the Figure 2.7.

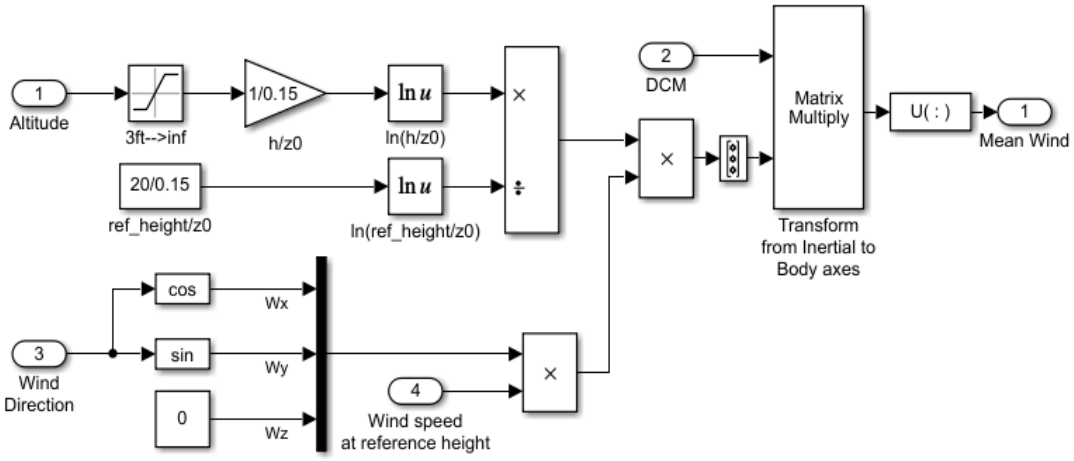

Figure 2.7 : Wind Shear Modelling.

2.4 Sensor Modelling

Another important sub-model in the aircraft model is the Sensor Model. State variables for the relevant aircraft are measured with 3 different systems; air data system, GPS / INS system and inertial navigation system.

Model outputs are passed through the sensor subsystem. In the Figure 2.8, the general scheme for a variable in this subsystem is given.

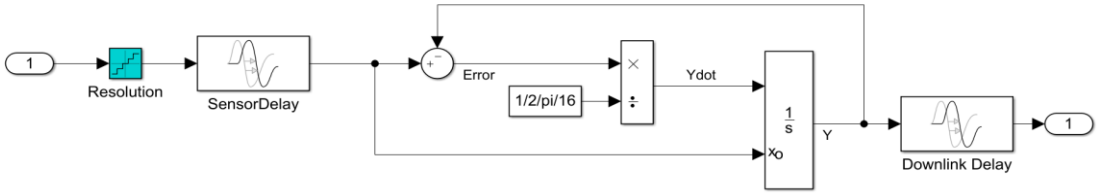

Figure 2.8 : Sensor Modelling.

With the air data system, Alpha (Angle of Attack), Beta (Sideslip Angle), qbar (Dynamic Pressure), TAS (True Air Speed), Ambient Temperature, Altitude variables are measured. Anti-aliasing filter frequency and downlink delay for these variables are as in the Table 2.4.

Table 2.4 : Air Data System Signals and Parameters.

Signal Name	Anti-aliasing Filter Frequency	Downlink Delay
Alpha	100 Hz	0.015s
Beta	100 Hz	0.015s
QBar	100 Hz	0.015s
TAS	100 Hz	0.015s
Ambient Temperature	100 Hz	0.015s
Altitude	100 Hz	0.015s

With the GPS system, Phi (Rotation Angle), Theta (Pitch Angle), Psi (Yaw Angle), Latitude, Longitude, Altitude, Vn (North Direction Speed), And (East Direction Speed), Vd (Vertical Speed) variables are measured. Anti-aliasing filter frequency and downlink delay for these variables are as in the Table 2.5.

Table 2.5 : GPS Signals and Parameters.

Signal Name	Resolution	Sensor Delay	Anti-aliasing Filter Frequency	Downlink Delay
Phi	0.01 degree	0.040 second	100 Hz	0.015s
Theta	0.01 degree	0.040 second	100 Hz	0.015s
Psi	0.01 degree	0.040 second	100 Hz	0.015s
Latitude	10^{-7} degree	0.040 second	100 Hz	0.015s
Longitude	10^{-7} degree	0.040 second	100 Hz	0.015s
Vn	$0.01\ \frac{meter}{second}$	0.040 second	100 Hz	0.015s
Ve	$0.01\ \frac{meter}{second}$	0.040 second	100 Hz	0.015s
Vd	$0.01\ \frac{meter}{second}$	0.040 second	100 Hz	0.015s

Pb (Rotation Angle Speed Relative to Body Axis), qb (Pitch Angle Speed Relative to Trunk Axis), rb (Yaw Angle Speed Relative to Body Axis), Ax (Acceleration on X Axis), Ay (Acceleration on Y Axis), Az (Acceleration in Z Axis) variables are

measured with Inertial Navigation System. Anti-aliasing filter frequency and downlink delay for these variables are as in the Table 2.6.

Table 2.6 : Inertial Navigation System Signals and Parameters.

Signal Name	Anti-aliasing Filter Frequency	Downlink Delay
pb	100 Hz	0.015s
qb	100 Hz	0.015s
rb	100 Hz	0.015s
Ax	100 Hz	0.015s
Ay	100 Hz	0.015s
Az	100 Hz	0.015s

2.5 Linearization

2.5.1 Trim

Trim basically aims to balance the forces and moments acting on the aircraft. This equilibrium position can also be expressed as zero longitudinal and lateral forces, and zero rolling and yaw moments. In cases where the aircraft is stable, the equilibrium situation is expected to continue under the conditions where the trim process is applied - if there is no disruptive effect.[28]

Obtaining aircraft trim conditions is of paramount importance. Trim defines aircraft flight envelope and performance characteristics and is also used in both analysis and design of engineering studies. Trim itself is of great importance, as well as the data to be derived from it. Linear models are derived at trim points (Figure 2.10). In flight control, controllers designed around linear models are used, so both model accuracy and the success of the trim are of great importance in flight control. The change of state of the control surface and variables at various trim points can be seen in Figure 2.9.

2.5.1.1 Trimmed states

Equilibrium point or trim point is defined in a classical concept in nonlinear systems theory. The system equilibrium point invariant with time is specified as x_{eq} and the function $g(\dot{x}, x, u)$ at the equilibrium point is defined as

$$g(0, x, u) = 0 \tag{2.48}$$

When $\dot{x}_{eq} = 0, u_{eq} = 0$ or $u_{eq} = u_0$

What is expressed by steady-state flight is a condition where the derivatives of the aircraft motion variables are zero. This also means that the linear and angular accelerations are zero.

The general steady state flight condition can be defined as:

$$Tranlational\ Rates: (\dot{u} = \dot{v} = \dot{w} = 0)\ or\ \left(\dot{V}_T = \dot{\beta} = \dot{\alpha} = 0\right)$$

$$Rotational\ Rates: (\dot{p} = \dot{q} = \dot{r} = 0)\ or\ (\dot{p}_w = \dot{q}_w = \dot{r}_w = 0)$$

$$Tranlational\ Velocities: (u = v = w = C)\ or\ (V_T = \beta = \alpha = C)$$

$$Rotational\ Velocities: (p = q = r = C)\ or\ (p_w = q_w = r_w = C)$$

$$Control\ Inputs: \delta_e = \delta_a = \delta_r = \delta_T = C$$

C represents predetermined or appropriate values for each state or control input.

Steady-state conditions $(\dot{p} = \dot{q} = \dot{r} = 0)$, require angular velocities to be zero or constant (as in fixed turns) and therefore aerodynamic and thrust moments must be zero or constant. Steady-state conditions $(\dot{u} = \dot{v} = \dot{w} = 0)$, require that the air velocity angle of attack and the side slip angle be constant, and therefore the aerodynamic forces must be zero or constant. A steady state solution can only be found on a digital computer using a numerical method, due to its nonlinearity.

2.5.1.2 General trim algorithm

The most common method of finding aircraft steady-state is based on minimizing a cost function. With this method, the set of unknown parameters is obtained by minimizing the cost function in line with certain requirements. For the aircraft, the situation is as follows: the nonlinear equation of the aircraft is minimized under the

specified conditions to obtain the aircraft's control inputs and unspecified state variables in these conditions.

2.5.2 Linearization

Nonlinear models are used to evaluate the control system performance of the aircraft, while linear models are used for control system design. Mostly, linear models are obtained from nonlinear models by numerical method. The most recent developments in the understanding of aircraft dynamics and the control system have come from working with linear equations using the small disturbance method. The small disturbance method was proposed by G.H.Brayn in 1911. The small disturbance method, under non-accelerated flight conditions, the sum of the forces and moments generated by small disturbance is equal to the force and moment the aircraft is subjected to. This method is still used in control system development. Using the stability derivatives in the small disturbance method, forces and moments acting on the aircraft can be calculated in certain flight conditions. The mathematical model required for the control of the aircraft is obtained by using the stability derivatives obtained according to the aircraft configuration and flight conditions and the inertial parameters of the aircraft in the small disturbance method.

In the small disturbance theory, it is assumed that the motion of the plane makes small deviations during non-accelerated flight, and with this assumption, the product of small changes in the variables is very small compared to the others, so the terms sine and cosine that are negligible or non-linear are cleared from the equations with the small angle approach. Control inputs are constant while equations of motion are linearized. For the case where angular accelerations and linear accelerations are considered to be zero or very small, the equations of motion can be divided into longitudinal and lateral accelerations.

$$\begin{bmatrix} \dot{u} \\ \dot{v} \\ \dot{w} \\ \dot{p} \\ \dot{q} \\ \dot{r} \\ \dot{Lat} \\ \dot{Lon} \\ \dot{Alt} \\ \dot{Phi} \\ \dot{Theta} \\ \dot{Psi} \end{bmatrix} = \begin{bmatrix} -0.0379 & -0.0013 & 0.1259 & 9.56*10^{-14} & -10.699 & 7.21*10^{-13} & 0 & 0 & -0.0001096 & 0 & -32.0632 & 0 \\ -0.000183 & -0.531147 & -0.00331 & 11.389 & 0 & -134.011 & 0 & 0 & -5.76*10^{-7} & 32.0630 & 0.00082911 & 0 \\ -0.259 & 0.0011845 & -2.54 & 9.05431*10^{-14} & 128.55 & 6.7171*10^{-12} & 0 & 0 & 0.00094248 & 0.009955 & -2.6702 & 0 \\ 0.005109 & -0.680063 & -0.05767 & -6.4201 & -0.1537 & 2.0757 & 0 & 0 & 1.435*10^{-7} & 0 & 0 & 0 \\ 0.018521 & 0.006065 & -0.33 & -0.00685 & -3.521 & 0.04402 & 0 & 0 & -4.190*10^{-6} & 0 & 0 & 0 \\ 0.0004056 & 0.22008 & -0.00255 & -0.4872 & -0.0442 & -1.4282 & 0 & 0 & 9.02679*10^{-8} & 0 & 0 & 0 \\ -2.590*10^{-21} & -4.7844*10^{-8} & -1.485*10^{-11} & 0 & 0 & 0 & 0 & 0 & 8.0236*10^{-18} & 5.401*10^{-7} & 9.5867*10^{-22} & -6.50772*10^{-6} \\ 6.0365*10^{-8} & -1.56099*10^{-12} & 5.0272*10^{-9} & 0 & 0 & 0 & 6.39735*10^{-6} & 0 & -3.942*10^{-13} & 1.7621*10^{-11} & -3.755*10^{-17} & -2.1231*10^{-10} \\ 0.0829939 & 0.000309 & -0.99655 & 0 & 0 & 0 & 0 & 0 & 0 & -0.003493 & 136.017 & 0 \\ 0 & 0 & 0 & 1 & -2.5858*10^{-5} & 0.08328 & 0 & 0 & 0 & -6.74899*10^{-17} & 1.2422*10^{-17} & 0 \\ 0 & 0 & 0 & 0 & 1 & 0.0003104 & 0 & 0 & 0 & -1.233*10^{-17} & 0 & 0 \\ 0 & 0 & 0 & 0 & -0.00031 & 1.0034 & 0 & 0 & 0 & -8.1319*10^{-16} & 1.030*10^{-18} & 0 \end{bmatrix} \begin{bmatrix} u \\ v \\ w \\ p \\ q \\ r \\ Lat \\ Lon \\ Alt \\ Phi \\ Theta \\ Psi \end{bmatrix} +$$

$$\begin{bmatrix} 0.0060128 & -0.04284 & 0.001587 & -0.0323494 & -0.03234 & -0.06689 & 0.02372 & 0.07220 & 0.07220 \\ 0 & -0.0214 & 0.42176 & 0.011490 & -0.01149 & 0 & 0 & 0.00280 & -0.0015 \\ -0.5979 & 0.1554 & 0.0899 & 0.22889 & 0.22889 & -0.7097 & -0.9322 & -0.0024 & -0.0024 \\ -0.01437 & -0.9459 & 0.2387 & -0.4986 & 0.50682 & -0.0121 & -0.0221384 & 0.00924 & -0.00924 \\ -0.78448 & 0.08945 & 0.002359 & 0.0130346 & 0.01432 & 0.052491 & -1.16447 & 0.009702 & 0.009702 \\ -0.000727 & -0.053456 & -0.45423 & -0.057812 & 0.05846 & -0.0003406 & -0.0011753 & 0.02800 & -0.02800 \\ 0 & 0 & 0 & 0 & 0 & 0 & 0 & 0 & 0 \\ 0 & 0 & 0 & 0 & 0 & 0 & 0 & 0 & 0 \\ 0 & 0 & 0 & 0 & 0 & 0 & 0 & 0 & 0 \\ 0 & 0 & 0 & 0 & 0 & 0 & 0 & 0 & 0 \\ 0 & 0 & 0 & 0 & 0 & 0 & 0 & 0 & 0 \\ 0 & 0 & 0 & 0 & 0 & 0 & 0 & 0 & 0 \end{bmatrix} \begin{bmatrix} Elevator \\ Aileron \\ Rudder \\ L\ Spoiler \\ R\ Spoiler \\ Flaps \\ Stabilizer \\ L\ Throttle \\ R\ Throttle \end{bmatrix}$$

Figure 2.9 : System Matrices.

Aircraft is linearized at 500ft Altitude, 80 kts Indicated Airspeed and 0° Gamma angle.

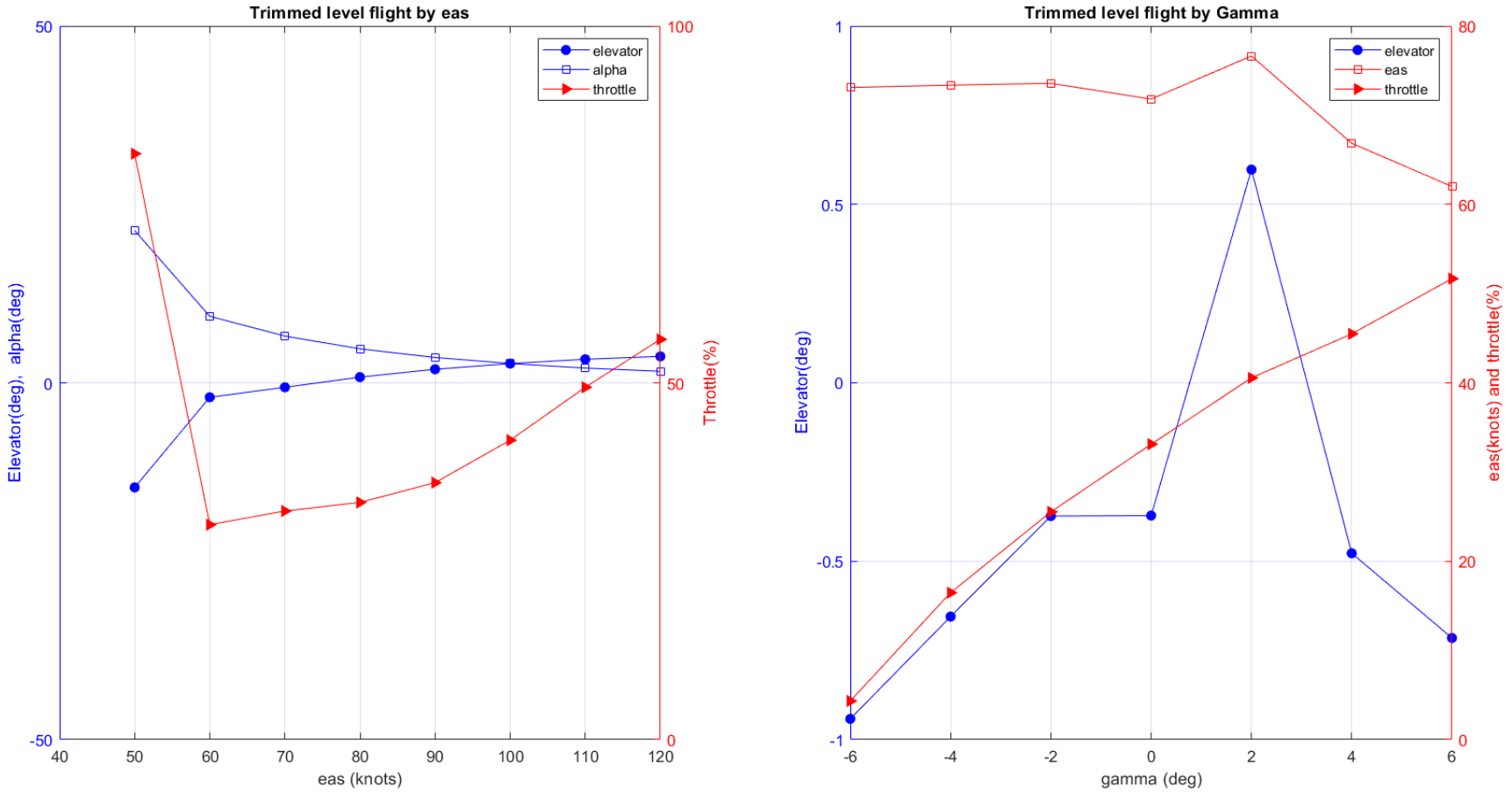

Figure 2.10 : Trim Input and States Compare for Different Conditions.

2.6 Linear and Nonlinear Model Comparision

In order to test the accuracy of aircraft linearization, doublet type signals to aircraft control surfaces and comparison of the states of the linear model and the nonlinear model is a method generally followed. The results are shown in the Figure 2.11, Figure 2.12, Figure 2.13, Figure 2.14, as can be understood from the figures, the consistency of the aircraft model obtained as a result of linearization with the nonlinear model is in question.

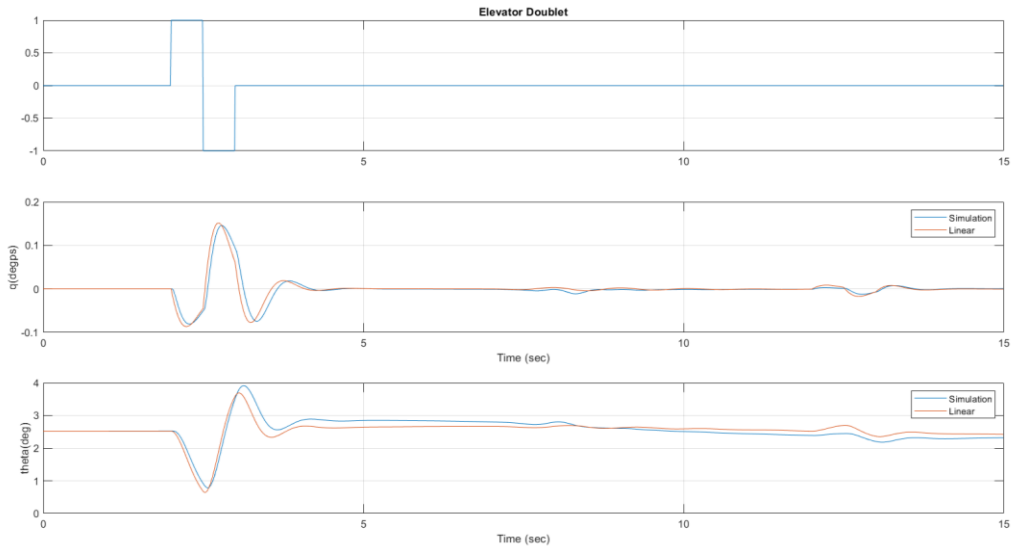

Figure 2.11 : Angular Velocities and Rates According Elevator Doublet.

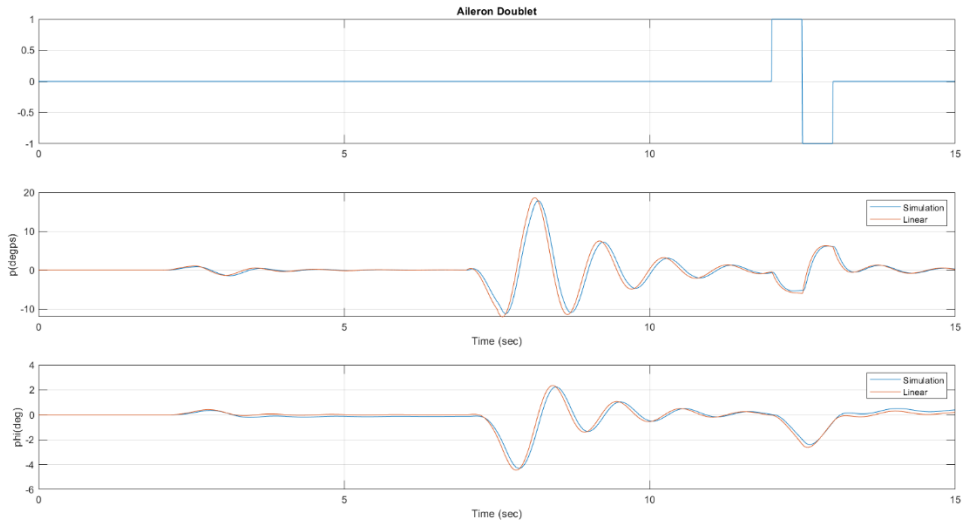

Figure 2.12 : Angular Velocities and Rates According Aileron Doublet.

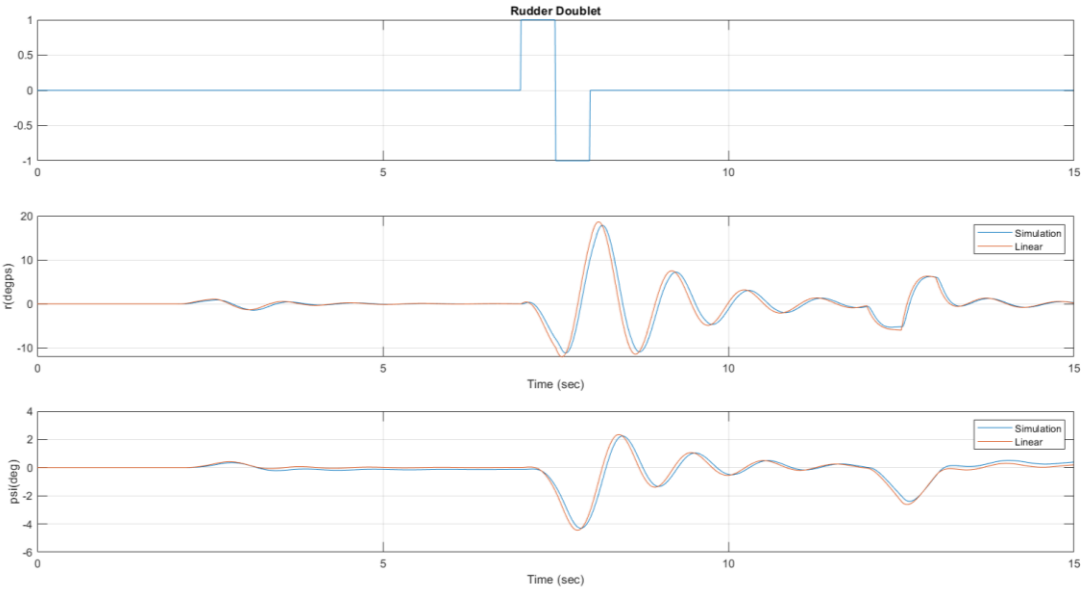

Figure 2.13 : Angular Velocities and Rates According Rudder Doublet.

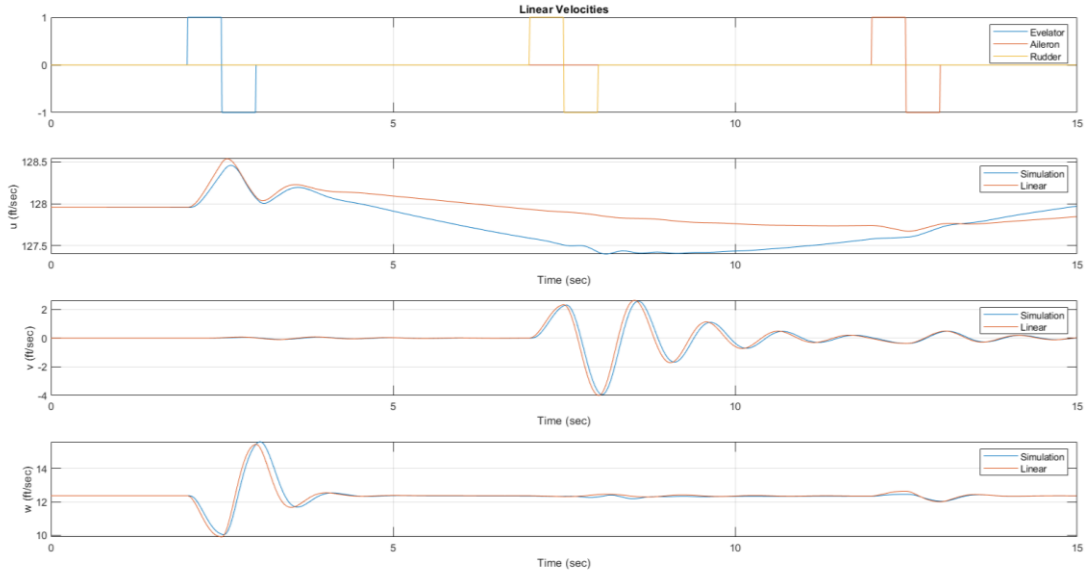

Figure 2.14 : Linear Velocities According Doublet.

2.7 Longitudinal and Lateral Modes

When the aircraft linear model is obtained, longitudinal and lateral dynamics are easily separable for fixed-wing aircraft. We can interpret the characteristics of the aircraft according to the location of the poles of the linear model of the aircraft, which is separated longitudinally and laterally in conventional aircraft traveling at subsonic speeds.

2.7.1 Longitudinal modes

Longitudinal flight modes are expressed in two separate modes:

Short period mode: It is the first mode that constitutes the longitudinal motion of the aircraft. It is the nose up and down movement that occurs as a result of the pilot's altitude rudder control. Longitudinal is generally the fastest damping mode and desired to occur. α and q directly affect V and indirectly. In the complex plane, two complex can be separated by conjugate poles.

Phugoid Mode: It is the second mode that constitutes the longitudinal motion of the aircraft. It is the nose up and down movement that occurs as a result of the pilot's altitude rudder control. It is a mode that is slowly damping and is not desired to occur. V affects h and θ directly and indirectly for α and q. In the complex plane, two complex can be separated by conjugate poles. These poles are much closer to the origin than the short-period mode. The polar characteristics of the short-period and phugoid modes for a trim point are given in Table 2.4. The variation of the polar characteristics of the short-period and phugoid modes for different trim points is given in Figure 2.15 and Figure 2.16.

Table 2.7 : Longitudinal Modes.

Mode	Pole	Damping	Frequency (rad/seconds)	Time Constant (seconds)
Phugoid Mode	-0.0229 + 0.287i	0.0796	0.288	43.6
Phugoid Mode	-0.0229 – 0.287i	0.0796	0.288	43.6
Short-Period Mode	-3.03 + 6.5i	0.422	7.17	0.330
Short-Period Mode	-3.03 + 6.5i	0.422	7.17	0.330

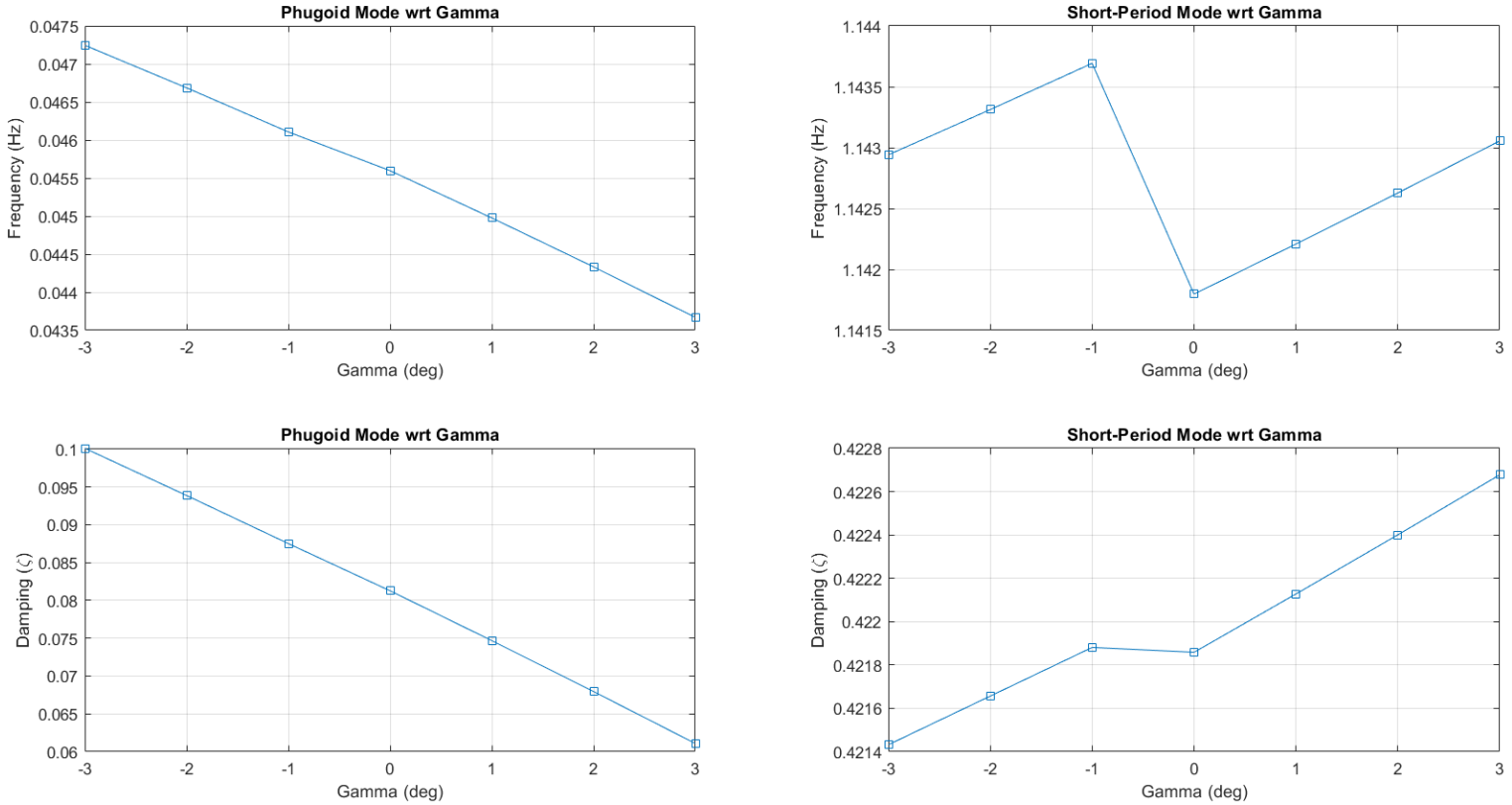

Figure 2.15 : Longitudinal Modes Frequency and Damping Change According Gamma at 80kts Estimated Airspeed.

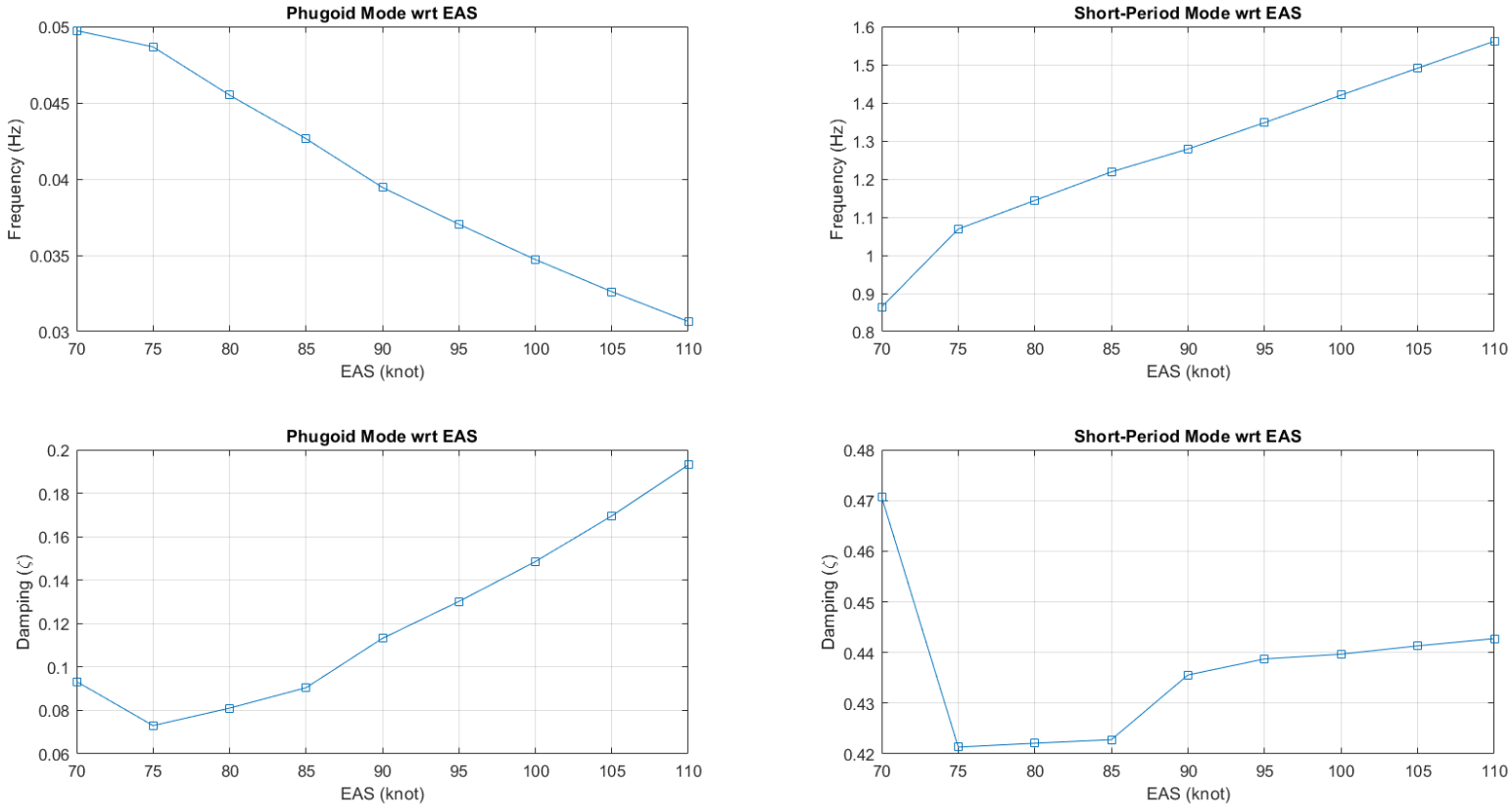

Figure 2.16 : Longitudinal Modes Frequency and Damping Change According Estimated Airspeed at 0 Degree Gamma.

2.7.2 Lateral modes

The lateral flight modes are expressed in two separate modes:

Roll mode: It is the first mode that forms the lateral-linear motion of the aircraft. It is the right and left wobbling movement that occurs as a result of the flap control of the pilot. It is a fast damping mode with lateral origin and it affects p and it is expressed by a real pole in the complex plane.

Dutch roll mode: It is the second mode that constitutes the lateral-linear motion of the aircraft. It is a lateral origin mode that is realized as a result of the pilot's aileron and / or direction rudder control, which is slower damping than the yaw mode and is undesirable to occur. It causes the plane to swing like a cradle on the lateral axis. The complex plane is expressed by two complex conjugate poles. These poles are closer to the origin than the fugoid mode poles and closer to the short period poles.

Spiral Mode: It is the third mode that forms the lateral-linear motion of the aircraft. As a result of the pilot's aileron and / or direction rudder control; lateral origin, slowest damping mode. On the complex plane, it is usually represented by a pole very close to its origin. Even its instability does not have a negative effect on the system, and its compensation does not cause any problems due to its very slow damping. The polar characteristics of the spiral, dutch-roll and roll modes for a trim point are given in Table 2.9 and Table 2.8 . The variation of the polar characteristics of the short-period and phugoid modes for different trim points is given in Figure 2.17 and Figure 2.18.

Table 2.8 : Lateral Modes.

Mode	Pole	Damping	Frequency (rad/seconds)	Time Constant (seconds)
Spiral Mode	-0.0448	1.00	0.0448	22.3
Dutch-Roll Mode	-0.857 + 6.26	0.136	6.31	1.17
Dutch-Roll Mode	-0.857 - 6.26	0.136	6.31	1.17
Roll Mode	-6.62	1.00	6.62	0.151

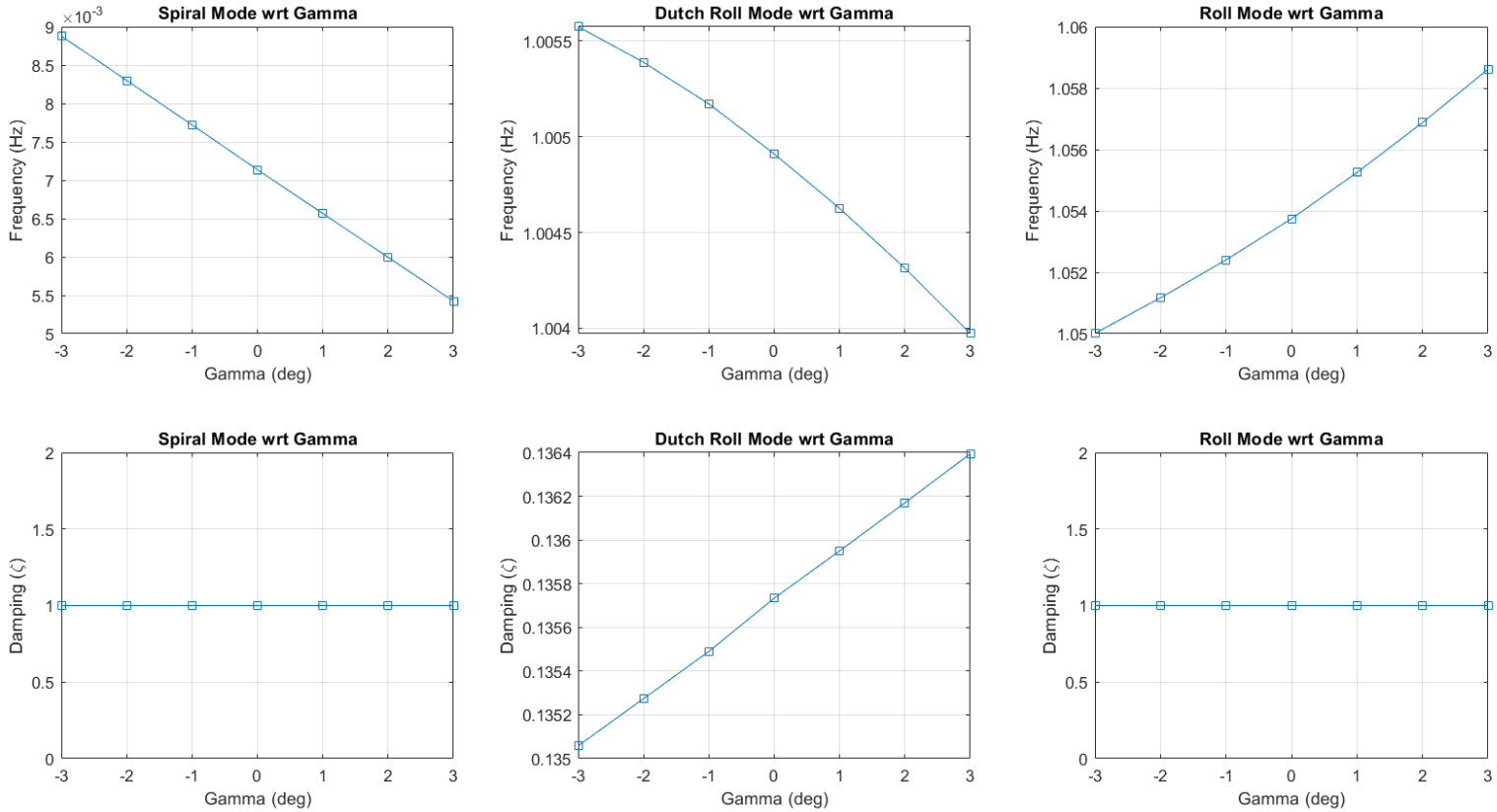

Figure 2.17 : Lateral Modes Frequency and Damping Change According Gamma at 80kts Estimated Airspeed.

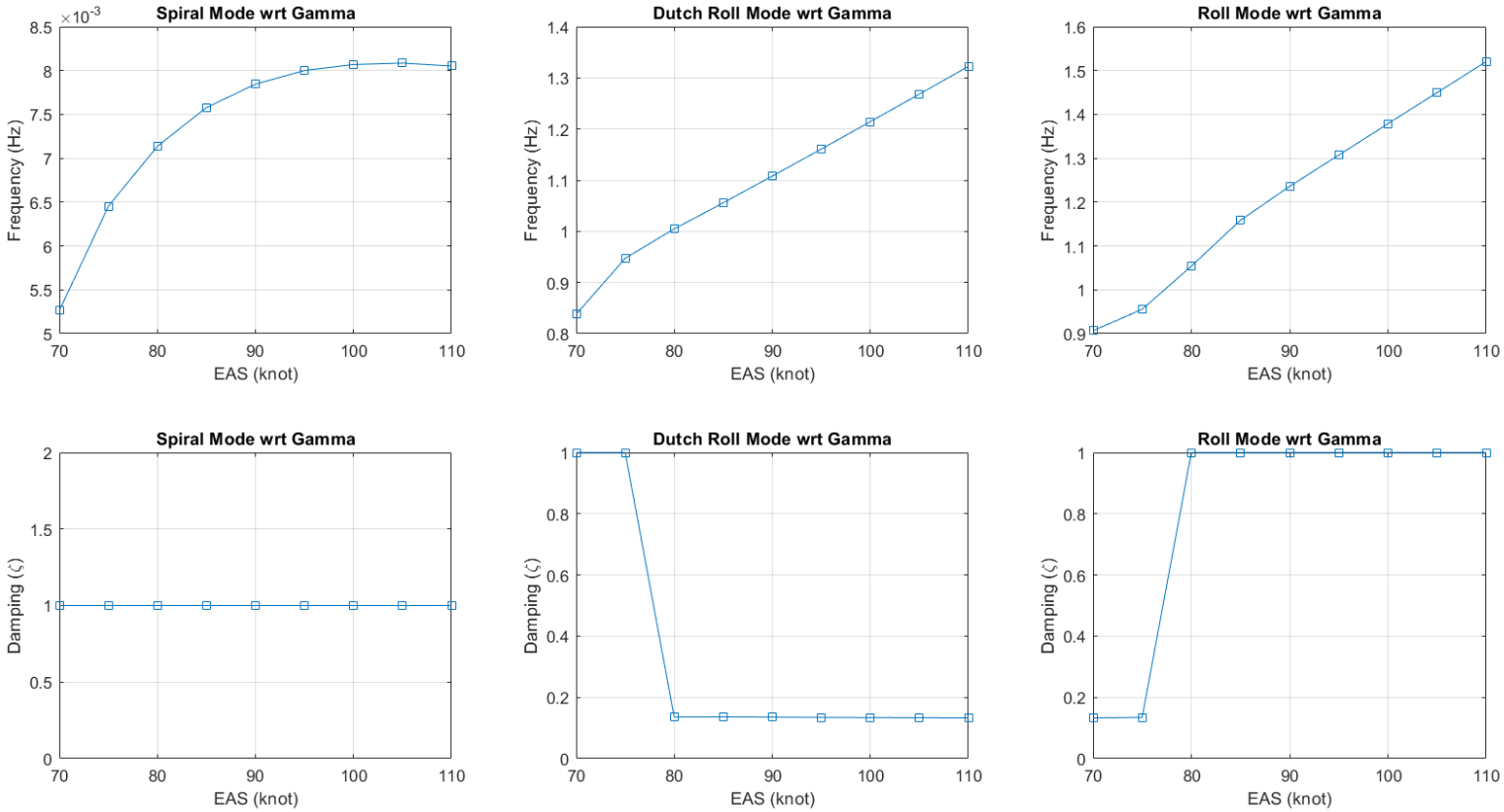

Figure 2.18 : Lateral Modes Frequency and Damping Change According Estimated Airspeed at 0 Degree Gamma.

3. AUTOMATIC LANDING

According to the MIL-F-8785C document, the moments when the aircraft is in the air and the manvera is divided into certain criteria according to the requirements of the situation. According to the standard, the flight phases are as in Table 3.1.

Table 3.1 : Flight Phases.

Category	Features
1	Those nonterminal Flight Phase that are require rapid maneuvering, precision tracking, or precise flight-path control.
2	Those nonterminal Flight Phase that are normally accomplished using gradual maneuvers and without precision tracking, although accurate flight-path control may be required.
3	Those nonterminal Flight Phase that are normally accomplished using gradual maneuvers and usually require accurate flight-path control.

According to the flight categories defined in the MIL-F-8785C document, the landing part is in the number 2 category. The automatic landing of a fixed wing aircraft consists of several phases. These phases are:

- Base Leg
- Descent / Glide
- Flare
- Touchdown
- Turning after landing

The phases listed above apply to a normal landing, where normal landing is meant: when the engine power is available, when the wind is light, or when the final approach is made directly upwind, there are no obstructions on the final approach path, the landing surface is solid and long enough to stop the aircraft gradually. [29] Depending on the characteristics of the aircraft, how the landing will take place and how the

aircraft will behave are included in the Federal Aviation Administration (FAA) approved Aircraft Flight Manual and / or the Operation Manual (AFM / POH) written for that aircraft. Position information of the vehicle is required for the landing phase of an airplane. Since 1920, landing aids have been developed to guide pilots to ascend the aircraft [30]. With these auxiliary systems, pilots realize the landing by knowing the position and direction of the plane relative to the runway.

In 1930, Diamon and Dunmore introduced a radio navigation-based landing aid similar to the Instrument Landing System (ILS) used today. [31] Automatic landing systems, with various differences, were naturally developed later than piloted landing. The first automatic landing performed by British Airways in June 1965 was made during a commercial flight using an automatic landing controller on the pitch axis. Here, lateral control is carried out by the pilot and vertical movement is controlled by the controller. Later, in 1996, a fully controlled landing was made in three axes. Due to the nature of the landing stage, it is more difficult to recover a fault, especially in unexpected situations when both speed and altitude are correspondingly low. While the transport of the aircraft decreases with the loss of speed, the air vehicle approaching the ground with the loss of altitude increases with the disruptive effects with the ground effect. There are certain limits for landing in healthy conditions for automatic landing systems. In case the wind and wind shear are within certain limits, the aircraft is expected to perform automatic landing. As a comprehensive and generally accepted study on this subject; The Federal Aviation Administration (FAA) and researchers have defined safety ranges of flight parameters for several flight phases. FAA thresholds are defined as follows: 25 knots for front winds, 10 knots for tail winds, 15 knots for cross winds; moderate turbulence, between 200 ft and 8 knots per 100 ft for wind shear. When FAA limits are exceeded, automatic landing should be canceled and the pilot should take control of the aircraft.

3.1 Base Leg

Although the base leg phase is the first phase of the descent phase, it is of great importance. At this stage, the pilot must correctly decide on the altitude and distance at which he can land. The longitudinal distance traveled during landing is related to the height of the base leg stage and the wind acting on the aircraft. In cases where strong winds will be effective on final approach, the distance at the base leg stage

should be closer than the distance in the no wind state, as flap control surfaces are used for a steep descent angle.[29] The base-leg phase continues until the aircraft is above the landing line. This turn to the descent route continues depending on the obstacles in the direction of the ground and ends at a safe altitude. At the same time, the turn that will take place in the base-leg phase must start at a certain distance from the runway where the aircraft will land, because in cases where the aircraft turns more than necessary, the wing cannot produce the required lift and the aircraft will stall. The main purpose in the base-leg phase is to bring the aircraft to the final approach at both the appropriate altitude and the appropriate speed. In cases where a steep descent angle is required to avoid traveling a long distance on the longitudinal axis during the final approach, it is recommended to stop the approach and enter the descent cycle by ascending again.

3.2 Glide

After the cruise phase is completed, it starts the descending phase. At this stage, the aircraft begins to gradually lower its altitude. At this stage, engine power is usually reduced and begins to descend while maintaining a constant flight path angle, while the wings and landing gear are used to reduce speed and provide more lift at low speeds. When the descending phase occurs under normal conditions, it has the same structure as the climb. [32] While ascending with a certain flight path angle during the climb phase, descent is achieved with a fixed flight path angle in the descending phase. The descending phase continues until the baleen phase. Under normal conditions, the landing takes place at a constant airspeed and a constant flight path angle. The pilot can change the throttle command and pitch angle to keep the airspeed constant. As the engines are usually used at a lower power setting during the landing phases, the engine noise affecting the aircraft is reduced. Towards the end of the descent phase, further acceleration and an increase in noise may be felt to make the final approach.

3.3 Flare

Flare is the last part of the aircraft in the air during the landing phase. For landing, the vertical and linear speed of the aircraft is reduced to ensure a smooth landing. This deceleration is accomplished by reducing thrust and/or using flaps, landing gear or speed brakes, thereby increasing aircraft drag. "Instrument Landing Systems"

generally available at airports assist the pilot during the landing phase. The instrument landing system (ILS) is a ground-based support system that guides the aircraft to a safe landing on the runway using a combination of radio signals and lighting devices.

This flight stage includes the following sub-stages:

• Flare: The transition from nose-low to nose-up position just before landing until it touches the ground.

• Landing Turn: From the landing runway until the airplane leaves or stops, whichever comes first.

• Landing Intercepted After Landing: An attempt to levitate after landing (whether successful or not). This does not include the take-off part of a touch gesture. [33]

Among the flight stages of the aircraft, the landing stage is the stage where accidents and errors are most common.(Figure 3.1)

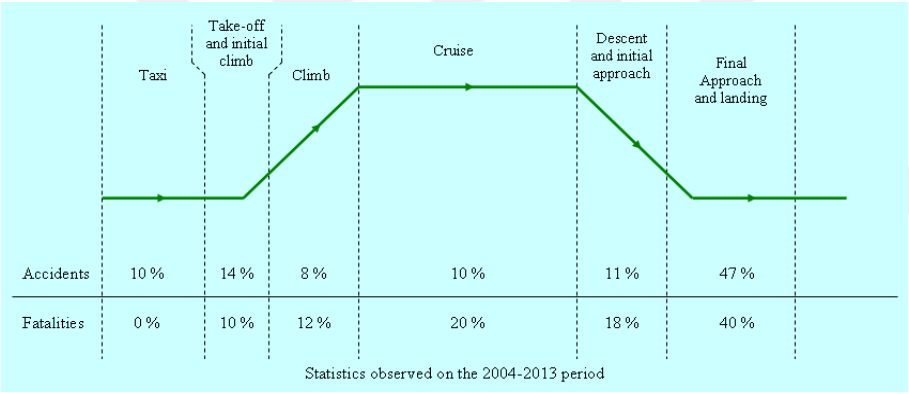

Figure 3.1 : Aircraft Accidents and Fatalities Statistics.

3.4 Touchdown

Touchdown is when the aircraft rests gently on the landing surface. Rolling and landing are normally done with the engine idling and the airplane at minimum controllable speed. Ideally, in the landing stage, as the height of the aircraft decreases, it is to reduce the vertical speed and ensure the soft landing as possible. By some pilots, the nose of the plane is lowered too much to reach the runway, which causes the aircraft to accelerate and wheel hard, and also causes the landing gear to be different from the expected order and more than the expected load. While all this is happening, it is also important at this stage that the speed of the aircraft does not go below the stall speed. [29] At this stage, since the aircraft is already close to stopping speed and has come to

a stop, a small elevator command will both slow down the aircraft and cause the aircraft to touch the ground in the appropriate landing position and lower the main wheels first, thus leaving very little weight on the nose landing gear.

4. FLIGHT CONTROL ARCHITECTURES

4.1 Stability Augmentation System

In the 1950s, the concept of "stability enhancement system" was first used by Northrop. [34] A stability enhancement system type automatic flight control system has been used to improve the incoming flight characteristics of the flying wing type YB-49 manufactured by Northrop. Since then, different stability enhancement system trials have been carried out, but the goal is the same: to bring some specific stability derivatives to the desired properties through feedback.

A stability augmentation system (SAS) is required for most high-performance commercial and military aircraft. There may be situations where the aircraft goes into instability and stability augmentation system is used to solve them. The stability augmentation system generally uses sensors that measure the angular accelerations of the aircraft's body axis, by designing a damper control system over these angular accelerations, the aircraft is prevented from going into instability. [35] The SAS structure is designed depending on the aircraft modes, there are standards defining the location of the closed loop poles of the system as a result of this design in piloted aircraft, and it is expected that the aircraft will comply with these standards with the stability augmentation system. The stability augmentation system is usually designed separately for aircraft longitudinal and lateral-directional modes. Additional feedback signals will be required if the base mode is unstable or if both damping and natural frequency are to be changed independently.

As stated earlier, stability augmentation systems control a single mode of movement of the aircraft. Aircraft movements can still be controlled by the pilot when the SAS structure is turned off, in which case the pilot commands the actuators directly. In case the SAS structure is activated, in addition to the pilot command, the actuators are driven with the corrections coming from the control structure. [1]

Figure 4.1 is a general diagram of a SAS system with longitudinal and lateral states.

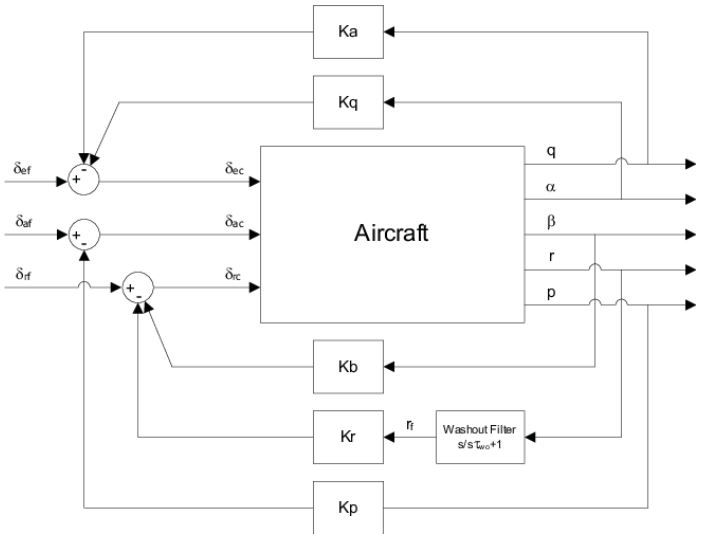

Figure 4.1 : General Stability Augmentation System Scheme.

4.1.1 Longitudinal stability augmentation system

The longitudinal SAS structure is basically the structures that provide aircraft pith rate stability, the short-period characteristic of the aircraft generally reaches the desired level.

If the short period mode is slightly damped but otherwise adequate, the pitch rate feedback is sufficient, but the angle of attack may also need to be included in the SAS if both frequency and damping are not satisfactory. If a control loop other than SAS is to be established in the aircraft, this loop should be installed outside the SAS loop. When the outer loop controller is activated, the gains of the SAS structure in the inner loop can be changed according to the need and optimal performance can be achieved.

Figure 4.2 is a general diagram of a SAS system with longitudinal states.

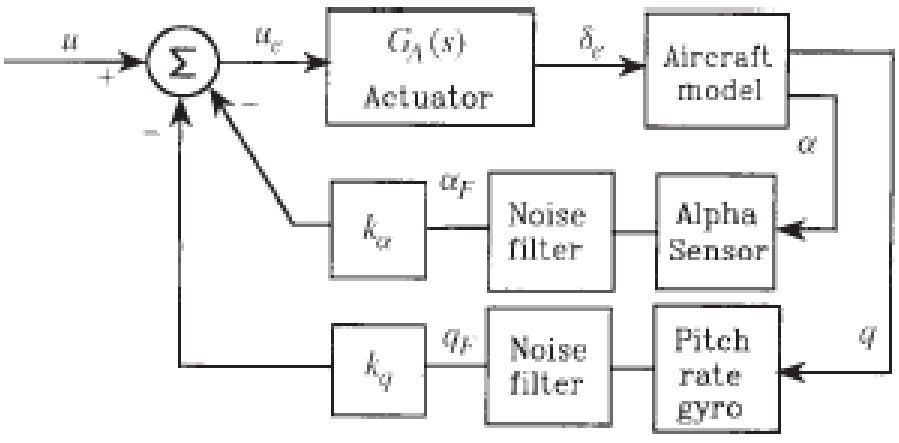

Figure 4.2 : Longitudinal Stability Augmentation System Scheme.

4.1.2 Lateral stability augmentation system

It is not possible to separate the Lateral stability augmentation system to be designed for the aircraft from Directional motion, therefore, the stability augmentation system for Lateral-Directional axes should be designed together. Roll rate feedback generates control signals to aircraft ailerons with the SAS structure designed to change the aircraft roll mode, while Yaw rate feedback generates control signals to aircraft rudders with the SAS structure (yaw damper). The SAS structure is usually set up by reducing it to a single input-single output problem. The analysis process should be done considering that it is a multi-input, multi-output system.

Figure 4.3 is a general diagram of a SAS system with lateral states.

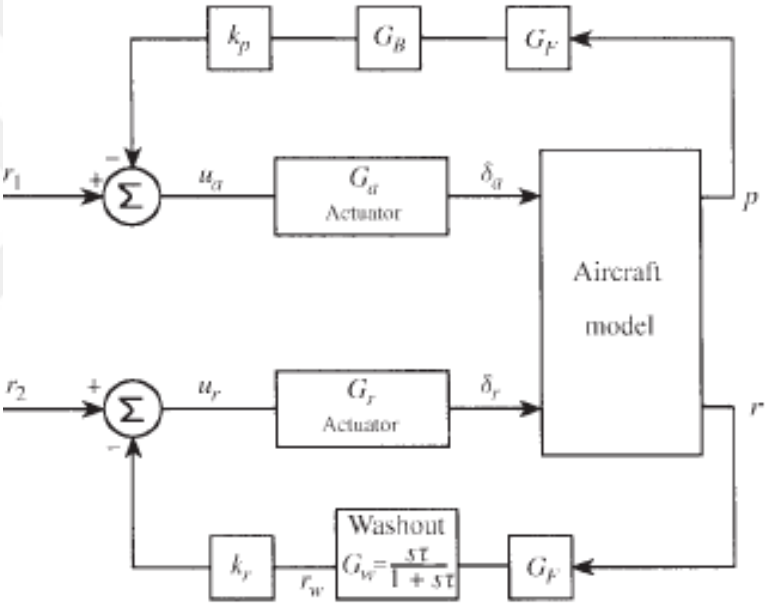

Figure 4.3 : Lateral Stability Augmentation System Scheme.

The rudder is used to create a yaw moment against the yaw movement caused by the dutch roll mode with the yaw damper. This poses a challenge for returning to coordination. During coordinated rotation, the yaw rate signal has a fixed non-zero value. For this reason, rudder use occurs, in which case the pilot uses more Rudder during the turn than he normally would. The solution to this problem is provided by the "washout filter", which is a simple high-pass filter with zero DC gain. Thanks to this filter, in cases where the feedback signal is stable, the use of yaw damper will be reduced with the feedback signals passing through this high-pass filter and the pilot's use of high rudder will be prevented.

4.2 Control Augmentation System

While the aircraft is controlled manually by the pilot, the SAS structure described in the previous section is basically sufficient. With the control augmentation system (CAS), the aircraft dynamic response is both damped and provides control signals to support the commands given by the pilot throughout the flight envelope. CAS has made significant improvements to aircraft handling characteristics; however, some military aircraft with aggressive maneuvering may require more advanced CAS structures.

Control augmentation systems are situations where the aircraft must use several control surfaces simultaneously or require the use of feedback signals that are dependent on motion variables other than those directly controlled. As a result, control enhancement systems are more complex in their operation than stability enhancement systems.

Pitch rate control is the preferred system for piloted approach and landing. Regarding lateral direction control, the most common control enhancement system is a roll rate control system.

Figure 4.4 is a general diagram of a CAS system with longitudinal and lateral states.

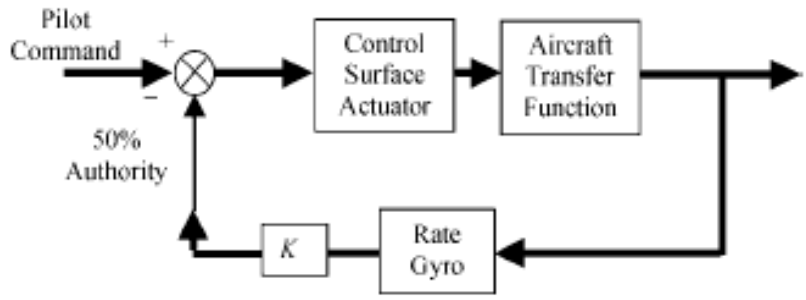

Figure 4.4 : Control Augmentation System Scheme.

4.2.1 Longitudinal control augmentation system

The systems created for the aircraft to provide grip control on the longitudinal axis are called the longitudinal control enhancing system. It is the job of the longitudinal control enhancing system to create a specific reference Pitch-rate in response to the forward and reverse commands given by the pilot with the lever and to keep it in a stable and controlled manner.

Pitch rate control systems traditionally involve using the elevator only as a control means in the system. An example structure is seen Figure 4.5.

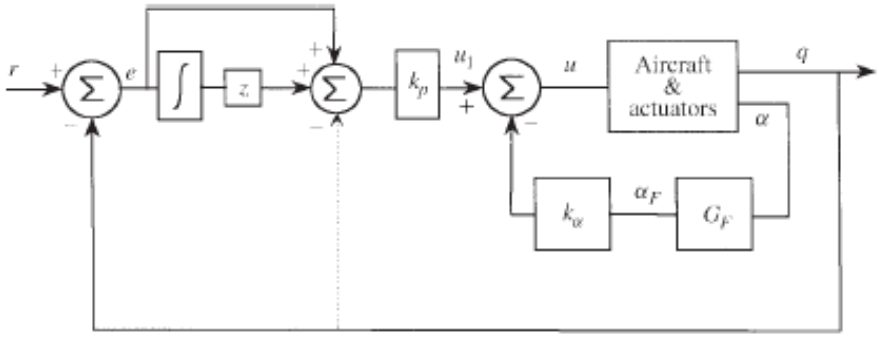

Figure 4.5 : Longitudinal Control Augmentation System Scheme.

4.2.2 Lateral control augmentation system

The systems created for the aircraft to provide grip control on the lateral-directional axis are called the lateral control enhancing system. It is the job of the side control enhancing system to create a specific reference roll-rate signal in return for the left and right commands given by the pilot with the lever and to keep it both stable and controlled.

Lateral control augmentation systems traditionally involve the use of the aileron and the rudder as control means in the system. An example structure is seen Figure 4.6.

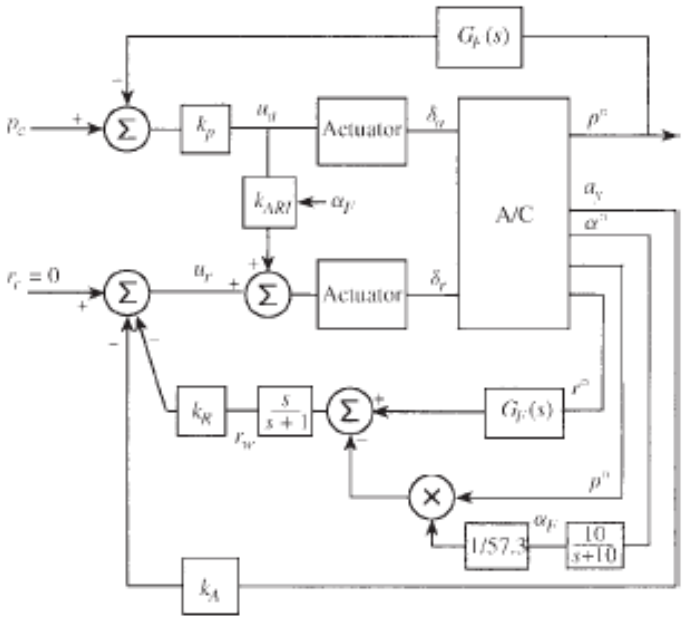

Figure 4.6 : Lateral Control Augmentation System Scheme.

4.3 Autopilot Systems

Stability enhancement and control enhancement systems are structures that operate depending on the direct commands of the pilot. In the stability enhancement system, in response to the command of the pilot, command arrangements are made by the controller to increase the stability; In control enhancement systems, there is a successful retention of the direct references given by the pilot.

In autopilot systems, although these systems may be available in inner loops, basically autopilot systems are used to follow the reference commands from the navigation modes in the higher loop. Apart from the navigation modes in the upper loop, the reference command can be given by the pilot to the autopilot, but the commands to be given by the pilot with a crowbar have no effect on the controller here.

Autopilot systems are of great importance in flight control and significantly alleviate the pilot load when activated. The definition of autopilot does not only express control of certain variables, many variables can be controlled by autopilot: hull axis angles, altitude and aircraft speed are some of them. With autopilot systems, the reference values given by the pilot are provided without the need for any other influence of the pilot, for this the autopilot generates the control surface commands itself. Autopilot systems can also be used with antecedent systems, for example: an autopilot system can be designed as the outer loop of the pitch rate CAS structure for altitude control, or a pitch autopilot can be used together with the pitch rate SAS structure. [36] The difference or error in pitch retention is used to generate proportional displacements of the elevator, thus reducing the error signal. With the designed autopilot systems, the pilot will only be able to enter the reference value in the designed autopilot and fly in a healthy way.

Most flight quality criteria are not directly applied in autopilot design. In pilot assisted semi-autonomous autopilot modes, the autopilot should be designed to meet specifications for steady-state error and distortion rejection, with less emphasis on dynamic response.

Figure 4.7 is a sample diagram for the pitch angle retention.

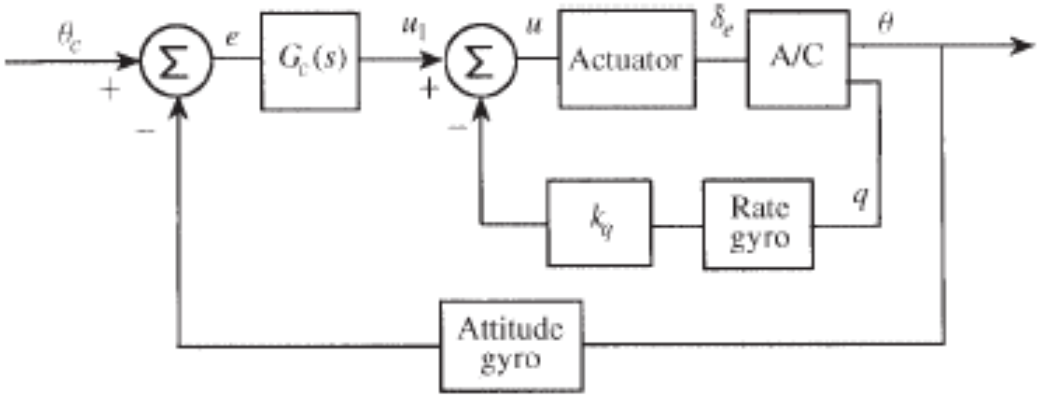

Figure 4.7 : Pitch Hold Scheme.

4.4 Flight Control System General Architecture

The fully autonomous control architecture generally used in flight control systems is as in the image below. The fast and slow modes on the lateral and longitudinal sides of the aircraft are controlled with the cascade architecture in the image. Although it is shown in the visual that the pilot command can only be given to the two outermost loops, in emergencies pilot commands can also be given to the inner loops, so the semi-autonomous modes in the inner loop can also be the savior for emergencies. (Figure 4.8)

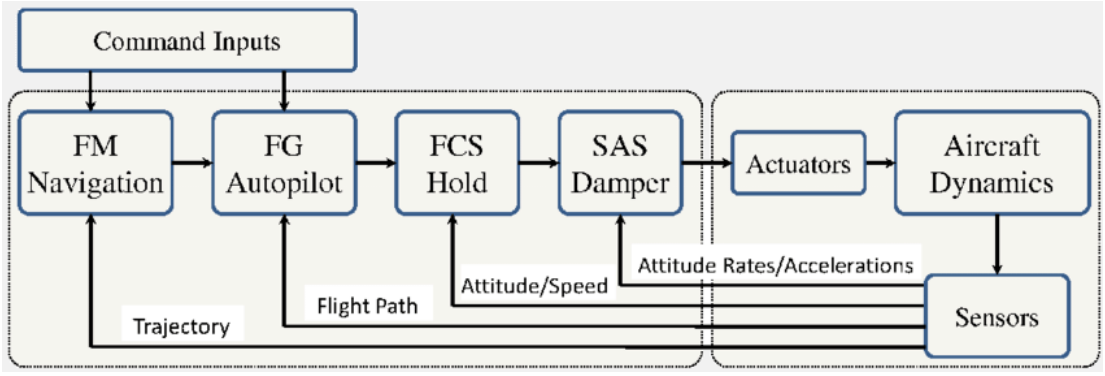

Figure 4.8 : Flight Control System Scheme.

4.5 Flight Control Robustness, Stability and Flight Quality Criterias

It is expected that the designed autopilot will be durable against degradation and delays in the feedback signals and / or control commands used in the flight control system. In the aviation field, this durability has been defined with certain definitions. As

described in [37],when designing the control system, robustness and stability analysis should be performed by loopbreaking each control and feedback loop.

While performing stability and robustness analysis, linear model should be used, sensor and actuator dynamics and delays should be included in the system. In the case of designing with a system model that does not have these, a truly remote controller design will be made, and a different result will be seen in the nonlinear model and the real world application from the linear model.

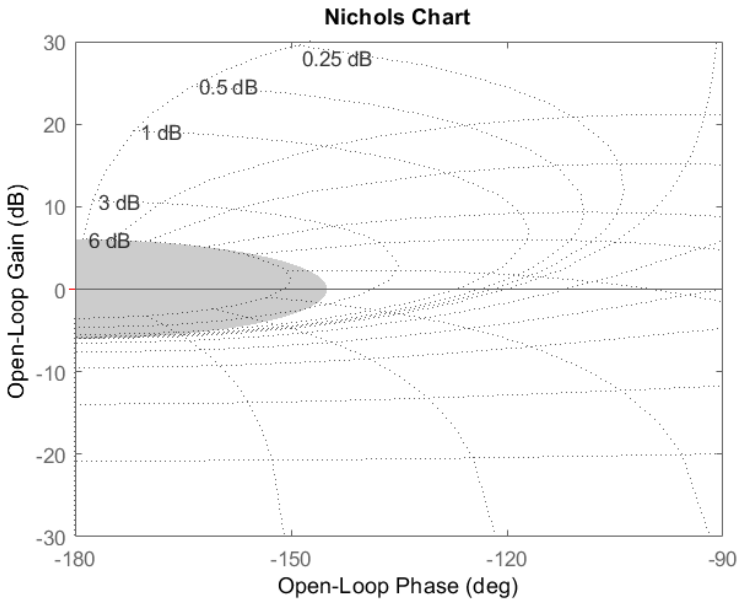

Figure 4.9 : Nichols Chart Stability Analysis.

The display of the stability analysis criteria on the Nichols chart is as in the chart given Figure 4.9. Accordingly, it is expected to have 6db gain margin in case of no phase margin and 35 degrees phase margin where there is no gain margin.

In a single-input single-output system, the stability margin will be the same no matter where the loop breaks, whereas in a multi-input multi-output system, the loop must be broken separately from each control loop.

Apart from the stability and robustness criteria, another important criterion is the quality criteria. There are important studies in the aviation industry that have been used for many years and shaped by pilot comments and gathered expressions in a mathematical equation. The study by Cooper and Harper Jr. [38] also found its way into military standards. In the MIL-F-8785C document, manned aircraft are classified according to various characteristics. This classification is given in the Table 4.1.

Table 4.1 : Aircraft Classes.

Class	Features
1	Small, light airplanes such as - Lightutility, Primary trainer, Light observation
2	Medium weight, low-to medium maneuverability airplanes such as - Heavy utility / search and rescue, Light or medium transport, Early warning / electronic countermeasures/airborne command, control, or communications relay, Antisubmarine, Assault transport, Reconnaissance, Tactical Bomber, Heavy Attack
3	Large, heavy, low-to-medium maneuverability eirplanesauohas - Heavy transport/cargo/tanker, Heavy bomber, Patrol / Early warning / electronic countermeasures/airborne command, control, or communications relay
4	High-maneuverability airplanes such as - Fighter/interceptor, Attack, Tactical Reconnaissance, Observation

Although restrictions vary depending on aircraft classes, the extent to which these restrictions are complied with is also expressed at certain levels. (Table 4.2)

Table 4.2 : Flight Quality Levels.

Level	Features
1	Flight qualities clearly adequate for the mission Flight Phase
2	Flight qualities adequate to accomplish the mission Flight Phase, but some increase in pilot workload or degradation in mission effectiveness, or both, exists
3	Flying qualities such that the airplane can be controller safely, but pilot workload is excessive or mission effectiveness is inadequate, or both. Category A Flight Phases can be terminated safely, and Category B and C Flight Phases can be completed

The MIL-F-8785C document also defines the criteria for closed-loop damping ratios and natural frequencies of longitudinal and lateral modes depending on the aircraft type, flight phase. The criteria for short-period mode, which is one of the longitudinal modes, are as Table 4.3.

Table 4.3 : Short Period Mode Damping Ratio Requirements

Level	Cat A / Cat C		Cat B	
	Min	Max	Min	Max
1	0.35	1.3	0.35	2.0
2	0.25	2	0.25	2.0
3	0.15	-	0.15	–

The criteria for phugoid mode, another of the longitudinal modes, are as Table 4.4.

Table 4.4 : Phugoid Mode Damping Ratio Requirements.

Level	Requirements
1	$\zeta_p \geq 0.04$
2	$\zeta_p \geq 0.0$
3	$T_2 \geq 55\ sec$

For Level 3, phugoid mode is predicted to be unstable, representing the time it takes to double the T_2 mode size.

The criteria for dutch-roll mode, which is one of the lateral modes, are as Table 4.5 and Table 4.3.

Table 4.5 : Dutch Roll Mode Damping Ratio and Frequency Requirements.

Level	Category	Class	$\min \zeta_d$	$\min \zeta_d\, \omega_{nd}$	$\min \omega_{nd}$
1	A	I, IV	0.19	0.35	1.0
		II, III	0.19	0.35	0.4*
	B	All	0.08	0.15	0.4*
	C	I, II – C, IV	0.08	0.15	1
		II – I,III	0.08	0.15	0.4*
2	All	All	0.02	0.05	0.4*
3	All	All	0.02	-	0.4*

*Class III airplanes may be excepted from the minimum ζ_d requirement, subject to approval by the procuring activity.

The criteria for roll mode, which is one of the lateral modes, are as Table 4.6 and Table 4.3

Table 4.6 : Roll Mode Requirements.

Category	Class	Roll Time Constant T_R		
		Level 1	Level 2	Level 3
A	I, IV	1.0	1.4	-
	II, III	1.4	3.0	-
B	All	1.4	3.0	10
C	I, II	1.0	1.4	-
	II, III	1.4	3.0	-

5. AUTOMATIC LANDING ARCHITECTURES

Trajectory control of an aircraft is very difficult to be performed by the pilot, and autopilot systems are usually designed for this. As an important sub-problem of trajectory control, we can count descent in difficult weather conditions and limited visibility. Tracking of the trajectory in such a situation by the pilot can be carried out by obtaining position information according to the external equipment in the square, but the necessity of fully autonomous landing does not decrease in this case.

5.1 Longitudinal Automatic Landing Architectures

For automatic landing, it is necessary to control various variables in longitudinal control; speed, altitude and flight path angle. Transition to the flight path angle designed in terms of fixed flight path is important for flare maneuver.(Figure 5.1) The glide path deviation ratio, i.e. the component of velocity perpendicular to the glide path, is defined as:

$$\dot{d} = V_T \sin(\gamma - \gamma_d) \approx V_T(\gamma - \gamma_d) \tag{5.1}$$

A reference is given where the altitude reference decreases exponentially after the transition from the glide stage to the flare stage. The descent trajectory is defined as an exponential decreasing function as follows. [35,39–42]

$$\dot{h} = \frac{1}{\tau}h + r, h(0) = h_0 \tag{5.2}$$

Here r is the reference input and h is the altitude of the aircraft. In case of reference $r = 0$, we can write the above expression as:

$$h(t) = h_0 e^{(-t/\tau)} \tag{5.3}$$

The altitude at which the aircraft begins the glide phase is expressed by h_0, and the reference trajectory γ_R provided by a transmitter to guide the aircraft for the glide

slope. τ is the time constant used for the flare phase and can be found by linear distance (D).

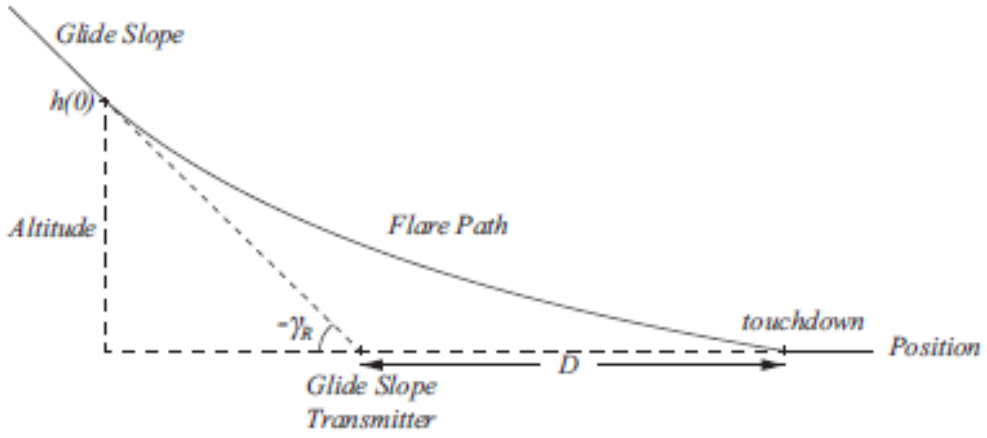

Figure 5.1 : Desired Altitude Reference at Flare.

The control scheme designed in [39]is as follows. In this control scheme, the controller between the speed reference and speed feedback is controlled by the throttle control channel; The desired glide-path deviation and desired pitch-rate control are also controlled by the elevator channel, the command of which is created by two different controllers.(Figure 5.2)

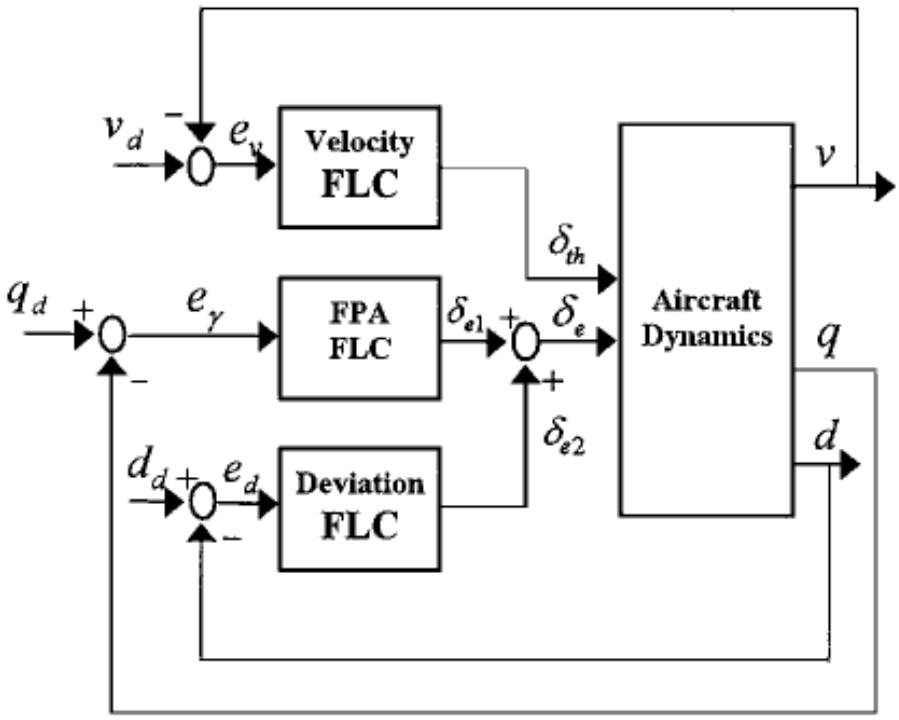

Figure 5.2 : Desired Longitudinal Trajectory Scheme.

In [40],speed and altitude feedbacks are extracted from reference speed and reference altitude and commands are generated by passing these differences through a command generator. The altitude and speed values coming from the feedback and the control commands are passed through a filter system. Here, there is a controller in the feedback channel after the filter system.(Figure 5.3)

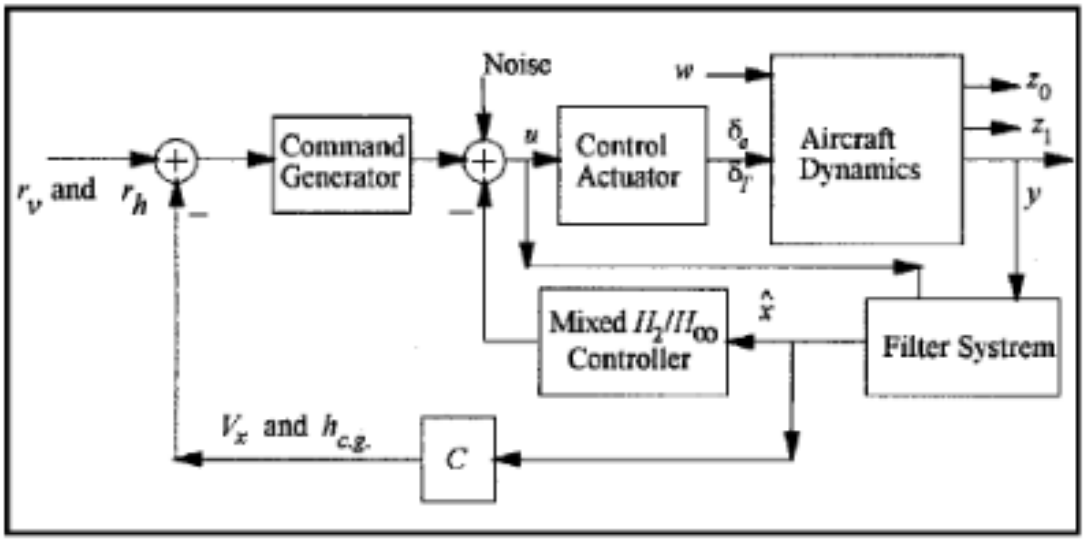

Figure 5.3 : Desired Longitudinal Trajectory Scheme.

In [41], all states except altitude in the longitudinal channel are used in feedback and these are tried to be regulated, besides the altitude variable is used together with the integrator in the feedback channel, so a control system is designed that includes tracking for altitude and a regulator for other states.

In [42] an altitude reference for the altitude reference based on the tangent of the negative of the ground range to the predicted touchdown point and the angle of the desired flight path angle; An altitude derivative reference is created depending on the ground speed and the tangent of the desired flight path angle angle. The altitude error is controlled by the integrator and the altitude derivative error is controlled with a proportional multiplier and the Pitch reference is established. In addition to these, with the transition to the flare phase, the pitchup reference is fed as a feed-forward. (Figure 5.4) Pitch reference from all these channels is controlled by a Pitch controller located in the inner loop. (Figure 5.5)

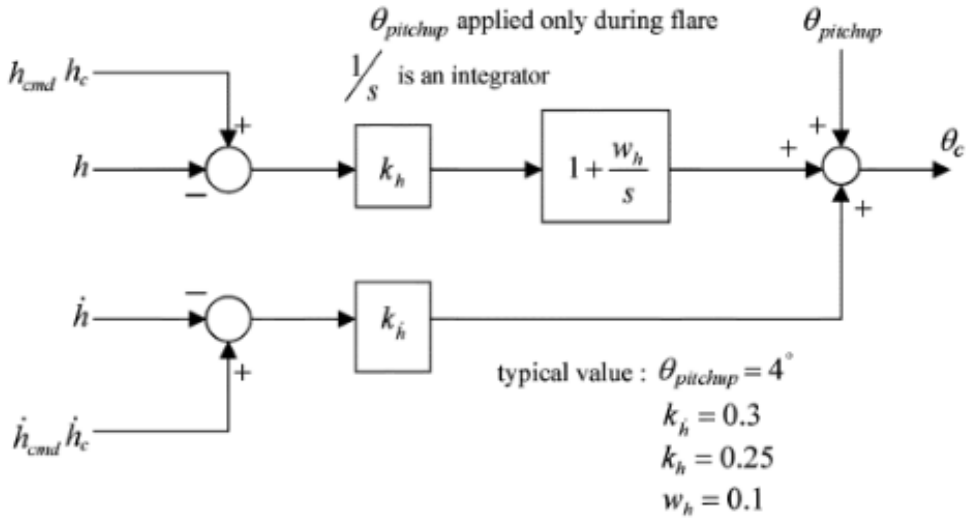

Figure 5.4 : Pitch Reference Generator Outer Loop.

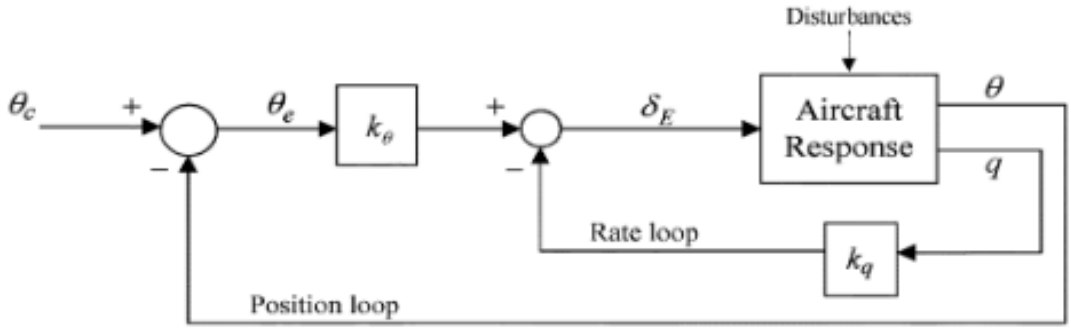

Figure 5.5 : Pitch Loop Controller.

In [43], the difference between the altitude reference and altitude feedback is multiplied by a gain and the flight path angle reference is obtained by using the speed. If the error between the flight path angle reference and flight path obtained is passed through a PI type controller, the Alpha reference is obtained. The alpha error is multiplied by a constant gain, and the nonlinear B block is summed up with the compensation value of the rotational speed (q) measured by the IMU around the Y axis of the plane pointing right when the airplane is not in horizontal flight. This sum is subtracted from the feedback q and multiplied by a speed dependent value to generate the elevator command. (Figure 5.6)

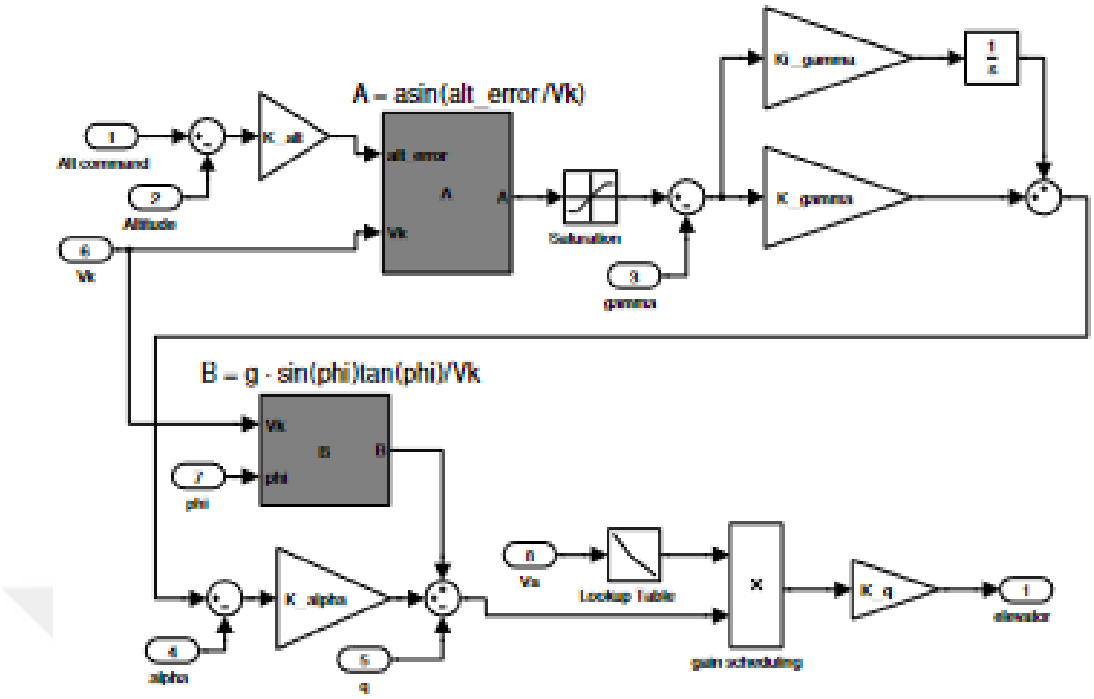

Figure 5.6 : Altitude Controller Architecture.

5.2 Lateral Automatic Landing Architectures

The two main control surfaces used in lateral automatic landing autopilot systems are aileron and rudder. While the rudder control surface enables the aircraft to yaw; The aileron control surface allows the aircraft to make a roll movement. Different types of controllers can be used in landing phases during auto landing.

In [41], two signals are used in the lateral descent controller; beta (lateral slip angle) and lateral error. For these two variables, the value zero is commanded directly, their errors are passed through the integrator and multiplied by a factor. Thus, it is aimed to keep these two variables around the reference without any steady-state error.

In [44] the deviation of the aircraft with respect to the runway direction variable has been filtered through a third order command filter, while the beta variable has been filtered through a quadratic command filter and used. The command filtered versions of these two references are used as new reference values. In addition, optimal observer was used to predict crosswind and sensor errors. (Figure 5.7)

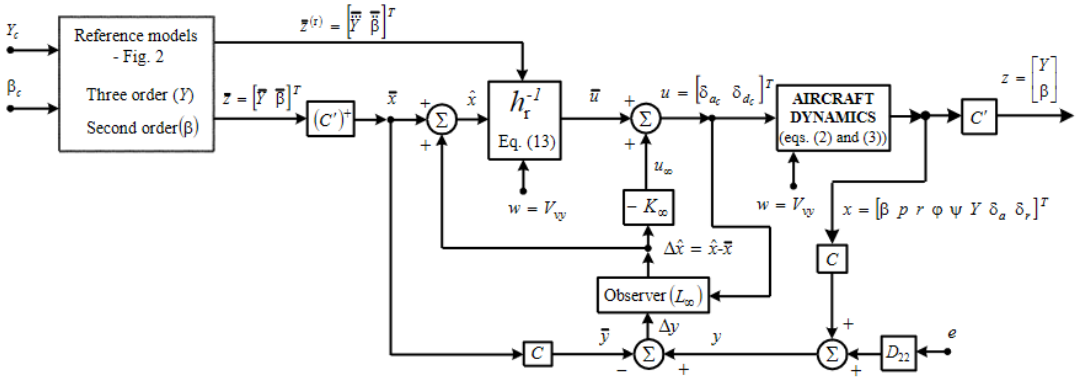

Figure 5.7 : Landing (Lateral Part) General Scheme.

In [43], the heading error is multiplied by a coefficient and entered into a block where the speed dependent roll reference is created. From the roll reference extracting from this block, the roll feedback is removed and the roll rate reference is obtained with the PI controller. The roll rate error also generates the aileron control surface command multiplied by a gain depending on the speed.(Figure 5.8)

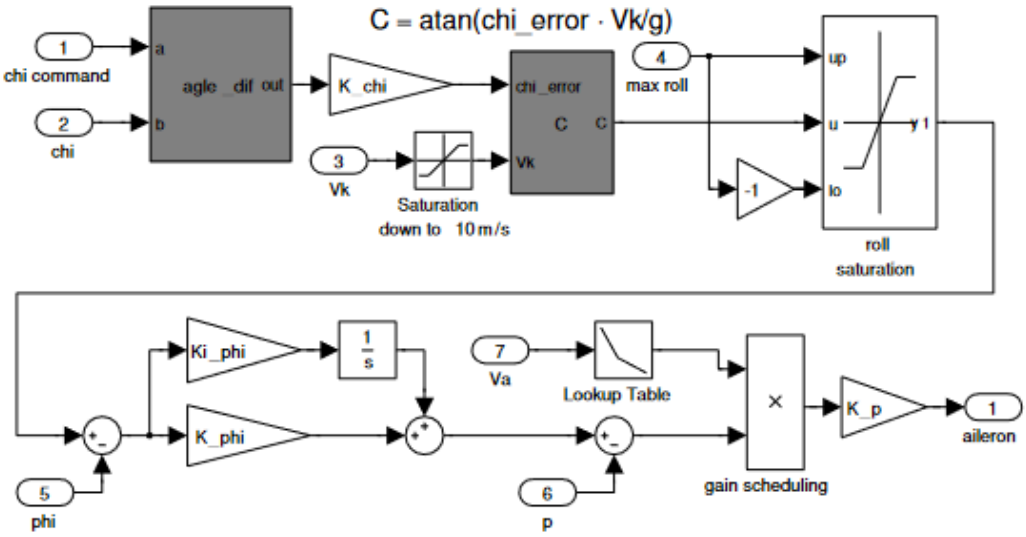

Figure 5.8 : Landing (Lateral Part) General Scheme.

There is another lateral landing autopilot scheme based on the heading angle reference. (Figure 5.9) Here, too, a roll reference is created based on the heading angle error. [45]

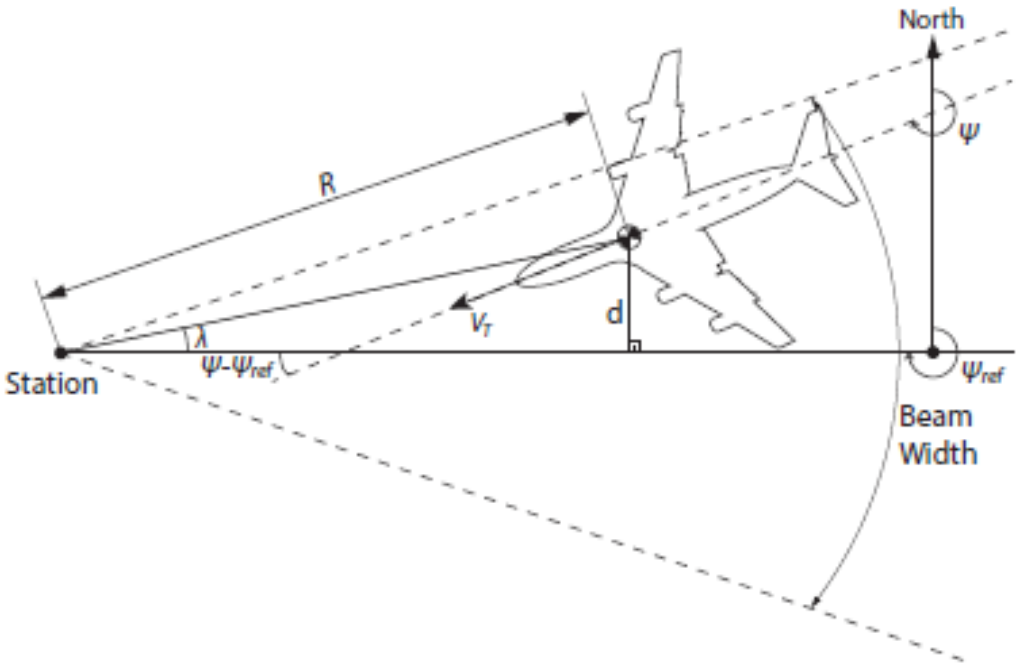

Figure 5.9 : Landing (Lateral Part) General Scheme.

If λ is desired to be in degree form and for the small angles, λ becomes

$$\lambda \simeq \frac{57.3d}{R} \tag{5.4}$$

And

$$\dot{\mathrm{d}} = V_{\mathrm{T}}\left(\sin\left(\psi - \psi_{ref}\right) \simeq V_{\mathrm{T}}\left(\psi - \psi_{ref}\right)\right. \tag{5.4}$$

$$\dot{d} \simeq \left(\frac{V_T}{57.3}\right)\left(\left(\psi - \psi_{ref}\right)\right. \tag{5.5}$$

$$sd(s) = \left(\frac{V_T}{57.3}\right)\left(\psi(s) - \psi_{ref}\right) \tag{5.6}$$

$$\lambda(s) = \frac{V_T}{R}\left(\frac{\psi(s) - \psi_{r\epsilon f}}{s}\right) \tag{5.7}$$

The purpose here for the automatic tracking system is to force λ to be zero to align the aircraft at the center of the runway for landing.

6. AUTOMATIC LANDING CONTROLLER DESIGN

Within the scope of the thesis, a control architecture in which the pitch reference due to altitude error is generated in the longitudinal plane [35] will be preferred for automatic landing. The first order command generator structure, in which the altitude reference is reduced exponentially, will be used for the speed reference in the same way. A value of 0 will be fed as the altitude reference, while $1.25 * V_{stall}$ will be fed for the speed reference as in the [29]. V_{stall} for the respective aircraft has been calculated as follows:

$$V_{STALL} = \sqrt{\frac{2W * g}{\rho A C_{L_{MAX}}}} \tag{6.1}$$

Where

$$\mathrm{W} = \mathrm{Weight}$$

$$\rho = \mathrm{Air\ \ Density}$$

$$\mathrm{A} = \mathrm{Wing\ Area}$$

$$C_{L_{MAX}} = Maximum\ Lift\ Coefficient$$

For GTM-T2 Aircraft

$$\mathrm{W} = 57.75\ \mathrm{lb} \tag{6.2}$$

$$\rho = 0.0765 \frac{\mathrm{lb}}{\mathrm{ft}^3} \tag{6.3}$$

$$\mathrm{A} = 5.9018\ \mathrm{ft}^2 \tag{6.4}$$

$$C_{L_{MAX}} = 1.3541, \mathrm{g} = 32.17404855643 \frac{\mathrm{ft}}{\mathrm{s}^2} \tag{6.5}$$

$$V_{STALL} = \sqrt{\frac{2 * 57.75\ \text{lb}\ * 32.17404855643\,\frac{\text{ft}}{\text{s}^2}}{0.0765\,\frac{\text{lb}}{\text{ft}^3} * 5.9018\ \text{ft}^2 * 1.3541}} \tag{6.6}$$

$$V_{STALL} = 84.2349\frac{ft}{s} = 42.9598\ kts \tag{6.7}$$

$$Landing\ Speed = V_{STALL} * 1.3 = 60.1283\ kts \cong 60kts \tag{6.8}$$

In the glide phase, the aircraft should approach the landing with a gamma angle of about -3 degrees, depending on the aircraft characteristics. [37] Within the scope of the thesis, a ramp-like approach is carried out for the glide phase and transferred to the flare phase.

With the onset of the flare phase (approximately the last 50 feet), the aircraft begins to descend for a soft kickback towards the landing point, the descent acceleration at the touchdown point should be less than $-2\frac{feet}{sec}$. In order to meet the required requirements, the required τ should be selected in the equation below.

$$\dot{h} = \frac{1}{\tau}h + r, h(0) = h_0 \tag{6.9}$$

$$h(t) = h_0 e^{(-t/\tau_{alt})} \tag{6.10}$$

According to this:

$$\tau_{alt} = 25 \tag{6.11}$$

will be selected.

The following equation is used to convert the altitude error to theta reference:

$$(h_{cmd} - h) * K_{hdot} = \dot{h}_{ref} \tag{6.12}$$

$$\text{atan}\left(\frac{\dot{h}_{ref}}{Speed}\right) = \gamma_{ref} \tag{6.13}$$

$$\gamma_{ref} + \propto_{actual} = \theta_{ref} \tag{6.14}$$

The reference of velocity, which is another variable in the longitudinal plane, is created in a similar way to the altitude reference. While the speed reference is commanded to ramp down to $V_{STALL} * 1.2$ during the glide-flare transition, there is an exponential speed reference to descend to $V_{STALL} * 1.05$ with the flare. The reason for the $V_{STALL} * 1.05$ command of the flare moment is for the aircraft to descend to the maximum speed that will provide lift during wheel landing and not to take off again after wheel landing.

In the lateral-linear plane, an outer loop controller that generates a roll reference due to head angle error like [45] will be preferred. The heading reference of the aircraft will be obtained from the angle at which the aircraft will land and the distance it takes on the lateral axis. Before the flare phase, the heading control is done with the Roll control, and with the flare phase, zero is commanded as a roll reference so that the wings of the aircraft are straight and the wheel is not placed with the bank angle. Along with Flare, beta is used to follow the heading reference. Reference models to be used for lateral control before flare phase are as follows:

$$\Psi_{ref} = \lambda * K_{\lambda}, \lambda = -\left(\frac{d}{R}\right), d = \frac{V_t * sin\left(\Psi - \Psi_{ref}\right)}{s} \tag{6.15}$$

R is distance to landing point

$$\varphi_{cmd} = \left(\Psi_{ref} - \Psi\right) * \frac{Speed}{\tau_{heading} * g}, \beta_{cmd} = 0 \tag{6.16}$$

Reference models to be used for lateral control after flare phase are as follows:

$$\varphi_{cmd} = 0, \beta_{cmd} = \left(\Psi_{ref} - \Psi\right) * K_{heading2beta} \tag{6.17}$$

$$\beta_{ref}(t) = (\beta_{trim} - \beta_{cmd}) * e^{\left(-\frac{t}{\tau_{sideslip}}\right)} + \beta_{cmd} \tag{6.18}$$

And

$$\tau_{heading} = 30, K_{heading2beta} = -1, K_{\lambda} = 1 \quad (6.19)$$

In architectures where yaw rate (r) signal is used as feedback in lateral autopilot design, washout filtered version of r signal is used as feedback. This is because noises during lateral movement in the pilot assist systems will over-manipulate the pilot's commands. What needs to be done in the washout filter is to make sure that the spiral mode does not move further to the left half plane after the control loop is closed. The filter places a zero at the origin and this forces the spiral mode pole to stay close to the origin.

$$wo_{filter} = K * \frac{s}{s + \alpha} \quad (6.20)$$

First, a time constant α is chosen. α for a time constant of five seconds.

$$\alpha = 0.2 \quad (6.21)$$

For K selection, the system's open-loop root locus graph should be examined. The gain that provides maximum damping in the open-loop root locus should be chosen as K. The K gain for this aircraft can be selected as 0.4293. As a result, the washout filter is obtained as follows:

$$wo_{filter} = 0.4293 * \frac{s}{s + 0.2} \quad (6.22)$$

6.1 Automatic Landing with PID Controller

6.1.1 Mathematical background

PID is a controller that includes the terms Proportional, Integral and Derivative. Each term has a different effect on the system.

Proportional control is one of the most common and logically simplest control methods in practice. In this structure, the feedback signal is extracted from the reference signal and the error obtained is multiplied by a constant multiplier to obtain the control command.

Integral, as a concept, expresses the sum of the area under a curve. In integral control, the error obtained from the reference and feedback difference of the system is added continuously and multiplied by a gain and the control command is obtained. Integral control, unlike proportional control, naturally avoids steady-state error because it is based on the continuous accumulation of error.

Derivative control is a structure that affects the control signal through the change on the related signal of the system. Depending on the rate of change of the signal, its effect on the control signal changes, however, it cannot be used alone as it only focuses on the change in error, because in case of fixed error it will not contribute to the control signal. Noisy feedback or reference signals can cause problems for derivative control, because of the noises on the sensor, the derivative term will always want to generate the control signal.

PID control is obtained by using Proportional, Integral and Derivative control together. The gain of each structure varies depending on the performance expected from the system. PID control works on the difference between the feedback and reference signal coming from the system, it has high industrial usage due to its easy application. General scheme of PID controller as Figure 6.1.

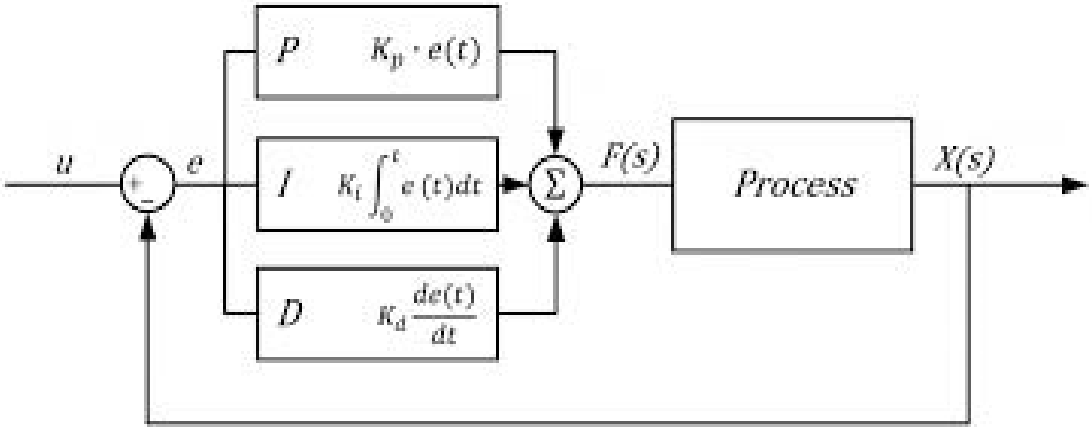

Figure 6.1 : PID Controller Scheme.

6.1.2 Automatic landing with PID controller

PID type controllers provide the generation of control signals between an input and an output due to their structure. The aircraft is modeled with a state-space model with 2 inputs and 4 outputs on the longitudinal side and 2 inputs and 4 outputs laterally. However, it is also possible to reduce a system with multiple-input multiple-output to

a single-input single-output solution. In order to analyze the relationship between inputs and outputs in the system with a mathematical background, it is necessary to use the Relative Gain Array method[46].

At 300ft, -3 degree Gamma and 80kts condition,

Longitudinal RGA matrix is

$$\begin{bmatrix} KIAS \\ Alpha \\ q \\ Theta \end{bmatrix} = \begin{pmatrix} -0.3592 & 1.3592 \\ 0.0057 & 0.0065 \\ 0 & 0 \\ 1.3649 & -0.3849 \end{pmatrix} \begin{matrix} \\ \\ \\ \\ [Elevator & Throttle] \end{matrix}$$

Lateral RGA matrix is

$$\begin{bmatrix} Beta \\ p \\ r \\ Phi \end{bmatrix} = \begin{pmatrix} 11.7666 & 1.8234 \\ -0.0521 & 0.0526 \\ -2.8487 & 2.9695 \\ 2.1342 & -8.1988 \end{pmatrix} \begin{matrix} \\ \\ \\ \\ [Aileron & Rudder] \end{matrix}$$

According to the relative gain array matrix, it is seen that the elevator control surface should be used for the throttle control signal, pitch, alpha and q for speed control on the longitudinal autopilot side; On the lateral autopilot side, rudder in beta control and aileron in phi control should be used. In the case of controlling the aircraft with PID and similar single-input, single-output controllers, the distribution of control surfaces and feedback signals is similarly given in the literature.

Although the relative gain array method gives a relative gain array at zero frequency, the effectiveness of the control surfaces at different frequencies can be variable for different outputs, depending on the internal dynamics of the system. In the PID controller design made in this thesis, only the relative gain array at zero frequency is considered, and it is assumed that similar responses will be obtained for all frequencies.

6.1.2.1 Longitudinal autopilot

The method in 5.1 will be used in the longitudinal autopilot design. This method specifies an exponential reference as the altitude reference; likewise for the speed reference, a reference will be commanded in which the speed decreases

exponentially with the start of the descent. In order to provide this structure, a control scheme has been created as Figure 6.2.

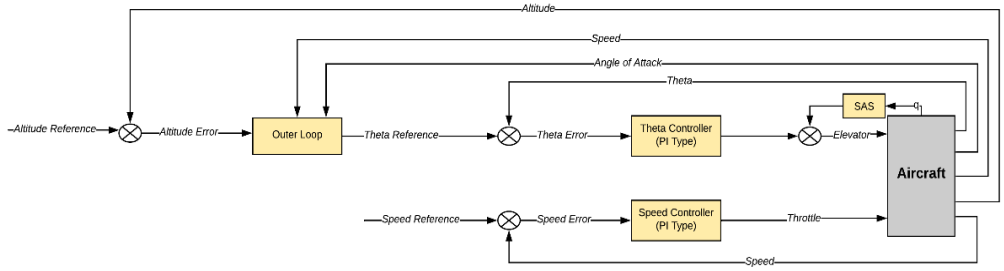

Figure 6.2 : Longitudinal Controller Scheme.

In the control scheme, the value consisting of the altitude error is fed as Theta reference, however, a stability augmentation system has been designed for the q signal; the sum of control signals from the ThetaHold and q-SAS signal is also fed into the system as an elevator command. Speed error is controlled by PI controller and fed as Throttle command.

The gains used for the PID type controller are as Table 6.1:

Table 6.1 : Longitudinal PID Gains.

Controller	Gain
Speed PI Controller - Proportional	5.9416
Speed PI Controller - Integral	0.8355
Theta PI Controller - Proportional	-79.7643
Theta PI Controller - Integral	-20.0701
q-SAS	34.9278

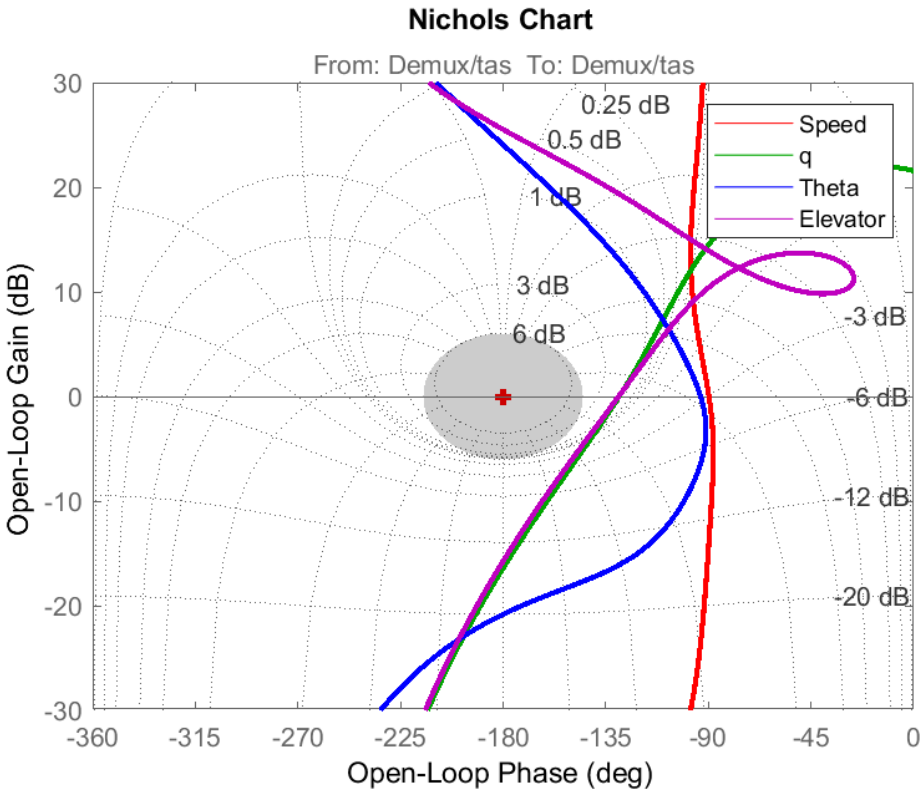

Figure 6.3 : Longitudinal Stability Margins (PID Controller).

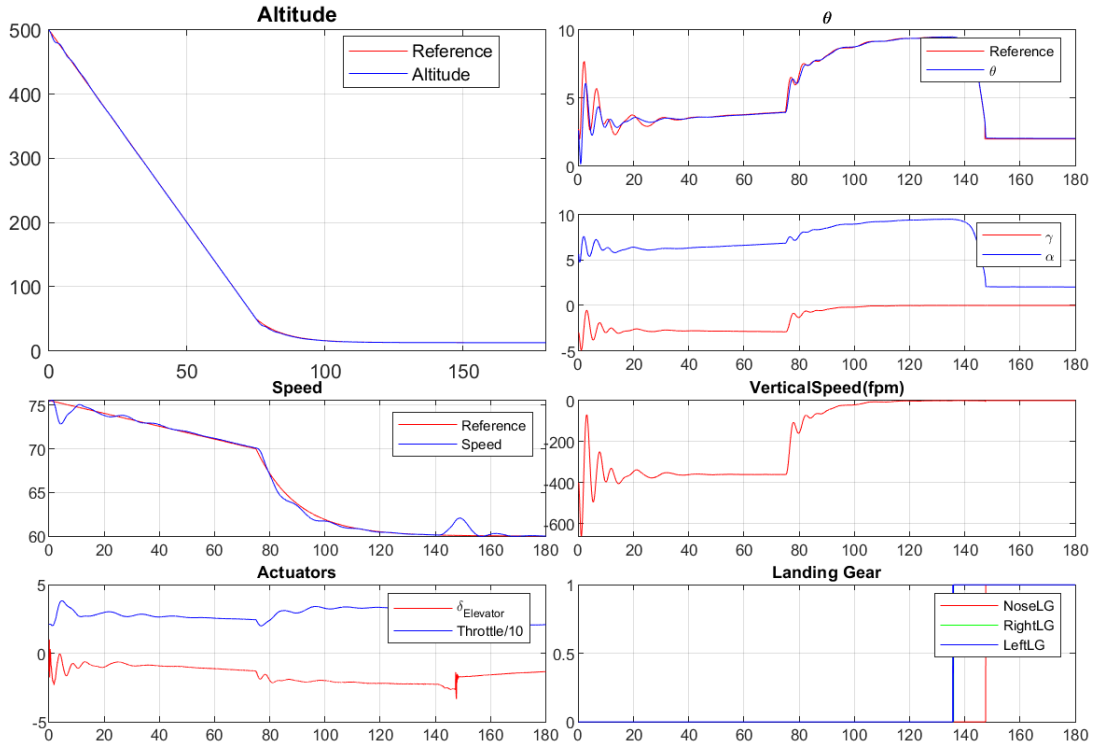

Figure 6.4 : Longitudinal Performance (PID Controller).

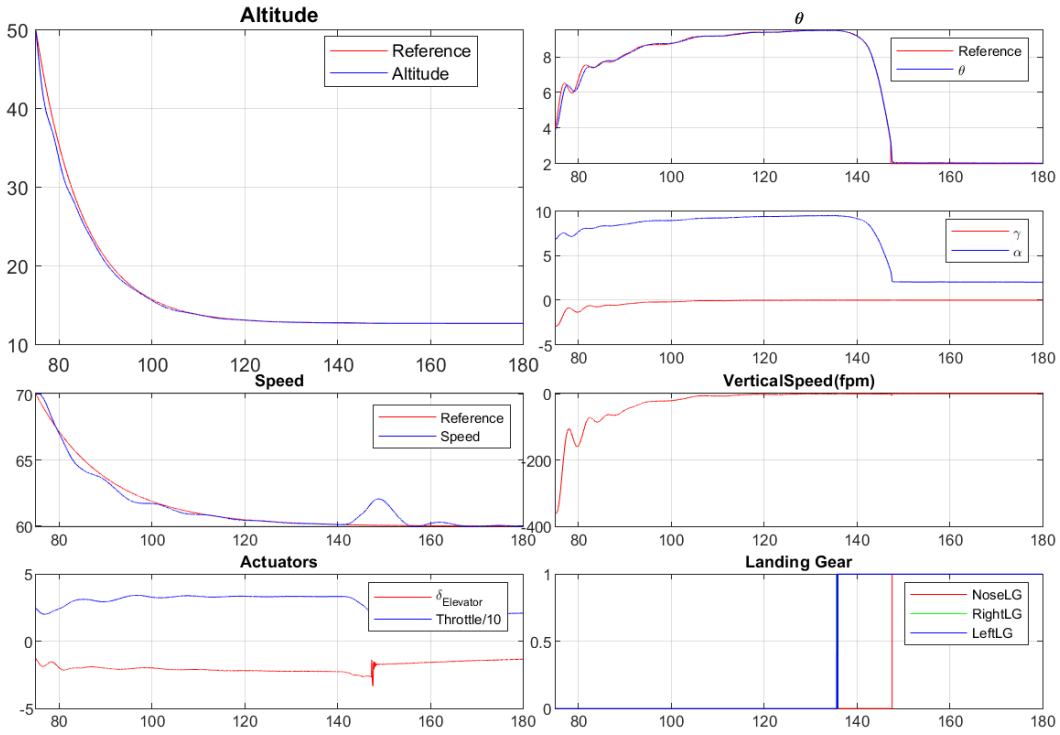

Figure 6.5 : Longitudinal Performance at Flare (PID Controller).

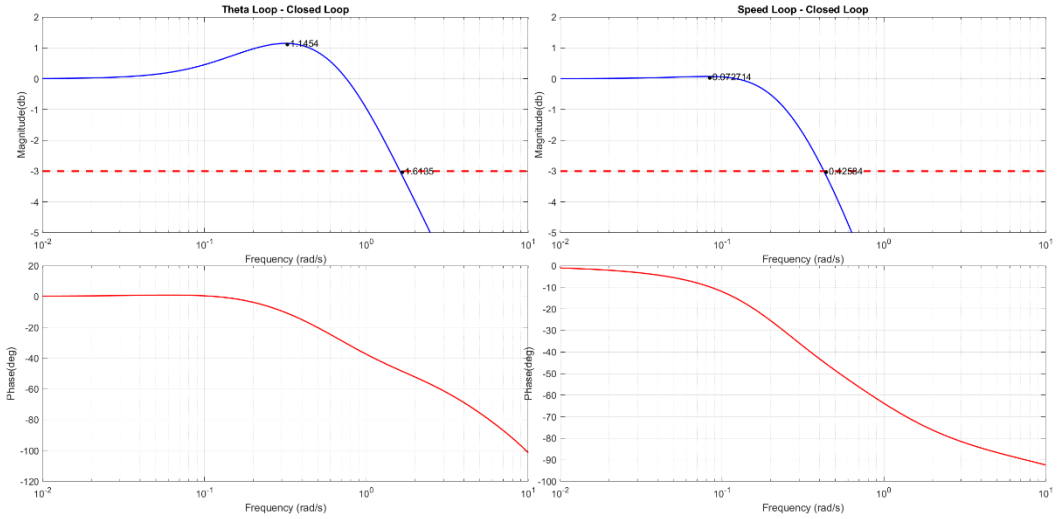

Figure 6.6 : Longitudinal Closed Loop Frequncy Analysis (PID Controller).

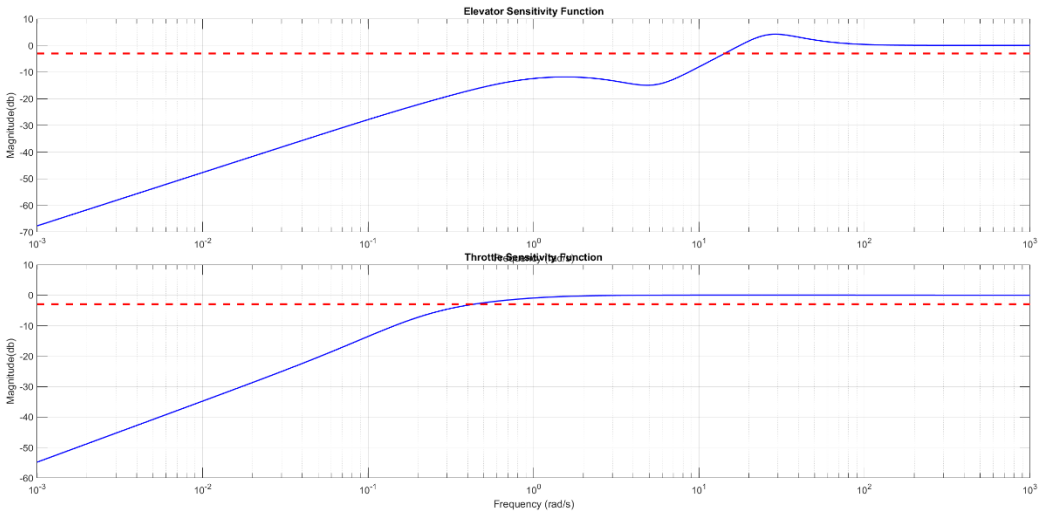

Figure 6.7 : Sensitivity Bode Diagrams of Longitudinal Actuators (PID Controller).

Looking at the longitudinal autopilot performance results and stability analysis results, it can be said that the landing with the PID controller both provides the stability limits and successfully follows the landing horizon in terms of performance. (Table 6.2)

Table 6.2 : Longitudinal Stability Margins.

Loop	Gain Margin	Gain Crossover Frequeny	Phase Margin	Phase Crossover Frequeny
Speed	Inf	Inf	90.2543	0.4286
q	16.4	59.4676	50.8692	20.6598
Theta	20.8	24.7645	86.56008	1.5239
Elevator	15.7	57.3	50.6	19.5443

Looking at the open-loop stability margins in the longitudinal plane (Figure 6.3, Figure 6.6, Figure 6.7), we see that it meets the stability margins in MIL-F-8785C, which are clearly defined in Section 4.5. When the closed-loop sensitivity Bode diagrams are examined, it is seen that the interference suppression bandwidth frequency of the elevator loop is 14.33 rad/s and the disturbance suppression resonance value is 4.208 dB. When the closed-loop sensitivity Bode diagrams are examined, it is seen that the interference suppression bandwidth frequency of the throttle loop is 0.4272 rad/s and the interference suppression resonance value is 0.0367 db.

If we examine the performance of the longitudinal part of the automatic landing autopilot designed with PID; In Figure 6.4 altitude hold, pitch(theta) hold and speed hold are important during the entire descent. With the transition to the flare part, which takes place around the 75th second, the aircraft makes a nose lift. With this movement, the vario decreases, and before the wheel put, the 2 degree theta command, which is the stance theta angle on the track, comes, it is seen that the controller follows these references successfully. In speed hold, the throttle control signal is used, here again with the transition to the flare phase, the speed command starts to decrease not linearly but exponentially, it is seen that the controller successfully keeps the speed reference.

Figure 6.5 shows the controller performances in the flare phase; There is no loss in theta grip of the aircraft, accordingly the altitude grip is also seen to be successful. In altitude hold, although it stays below the altitude line during the transition, the altitude hold of the aircraft decreases to a distance of six meters as it approaches the runway. Although there is fluctuation in speed holding with the flare transition, the performance improves as it gets closer to the track. If the behavior of the control surfaces during the landing is examined; There is no situation that occurs to the limit, only hard movements are seen in the elevator at the moment of contact with the wheel. This situation is negligible since ground controller is not designed within the scope of the thesis.

6.1.2.2 Lateral autopilot

With the PID controller, a lateral landing autopilot was designed using the method in 5.2. For the lateral landing autopilot, a point on the runway, the direction of the runway, the position of the aircraft, and the sideshift of the aircraft are used. The angle between the aircraft and the runway is fed as the heading reference, this heading reference is controlled with roll before flare and controlled with beta after flare. Before the flare phase, the beta reference is taken as 0. With this logic, while the heading angle of the aircraft is aimed to be the same as the runway, since the heading control is made with beta in the flare phase, side wheel placement may occur on the runway, and this situation can be corrected after wheel placement in a landing autopilot design where the ground controller is designed. (Figure 6.8)

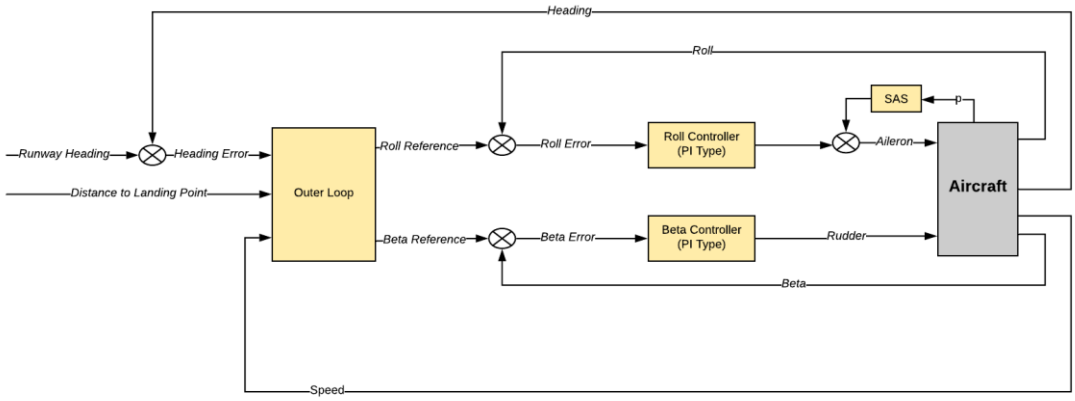

Figure 6.8 : Lateral Controller Scheme.

Looking at the lateral conditions of the system, it can be seen that there are 2 inputs. The first of these is the aileron control surface, the second control surface is the rudder.

The gains used for the PID type controller are as Table 6.3.

Table 6.3 : Lateral PID Gains.

Controller	Gain
Beta PI Controller - Proportional	17.8776
Beta PI Controller - Integral	50.4756
Roll PI Controller - Proportional	-50.9205
Roll PI Controller - Integral	-5.3916
p-SAS	4.5362

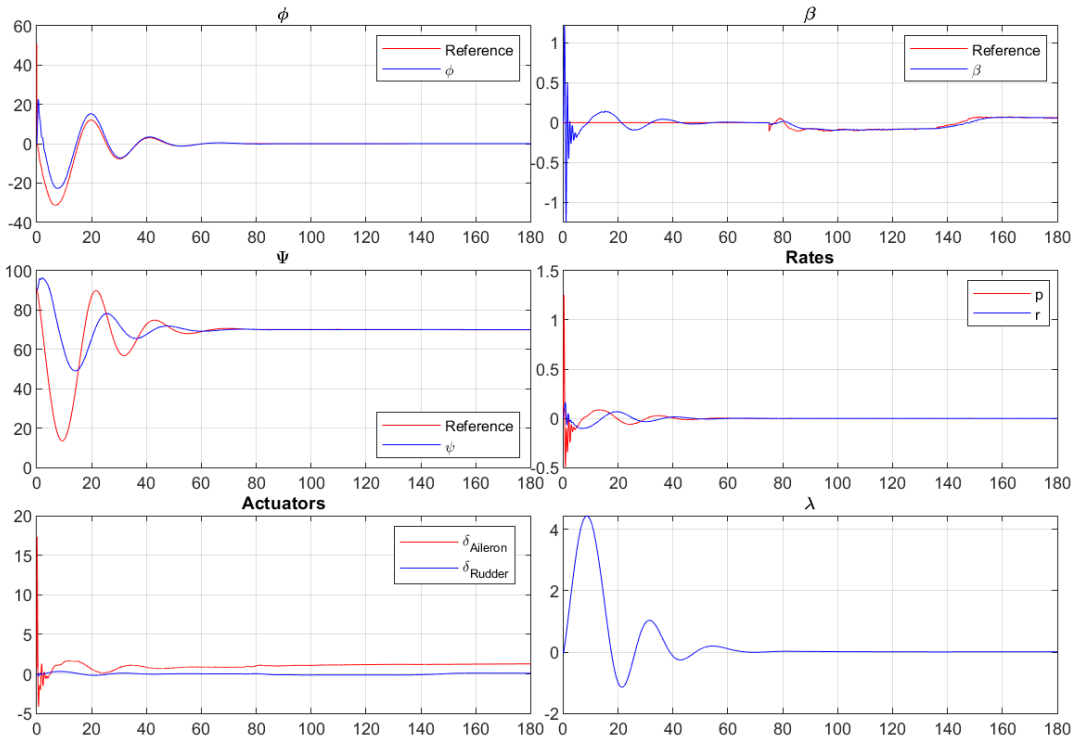

Figure 6.9 : Lateral Performance (PID Controller).

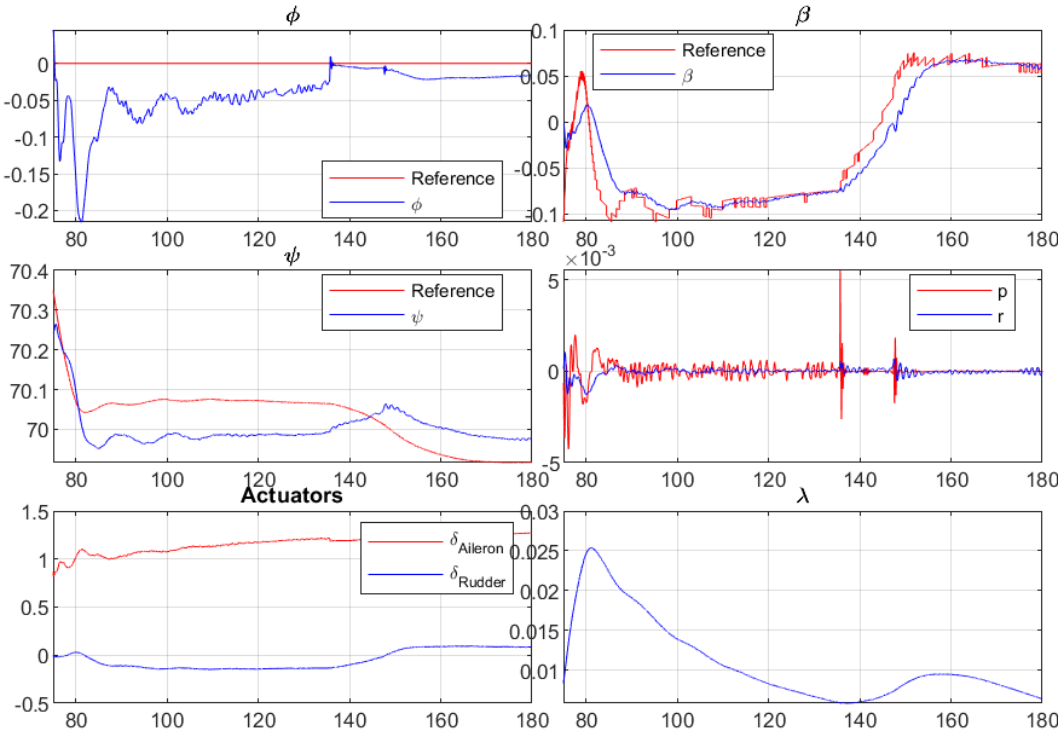

Figure 6.10 : Lateral Performance at Flare (PID Controller).

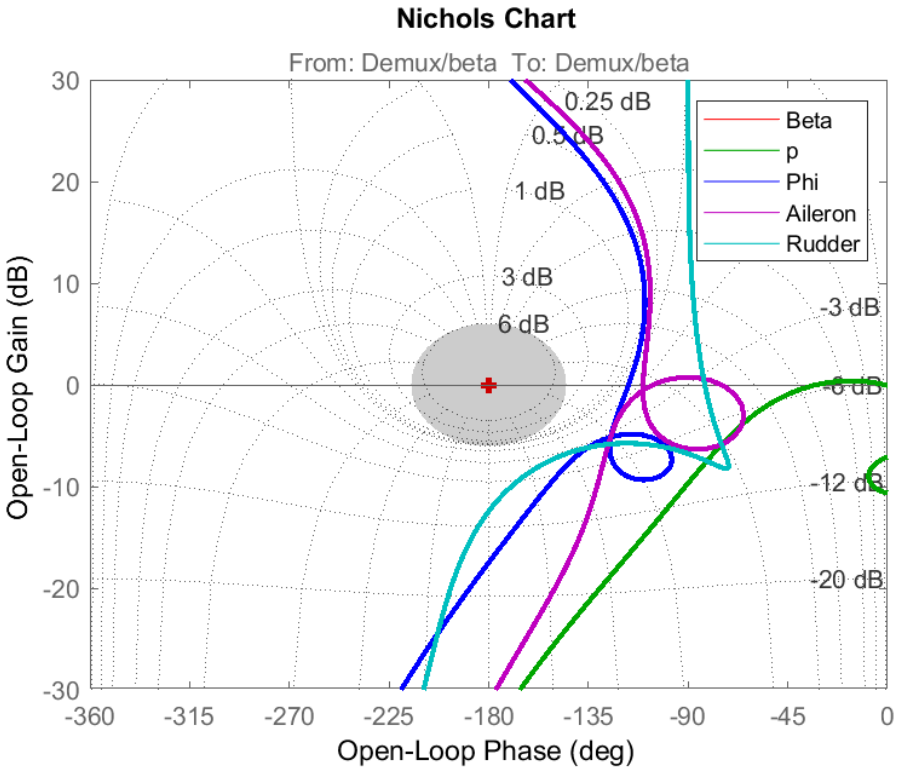

Figure 6.11 : Lateral Stability Margins (PID Controller).

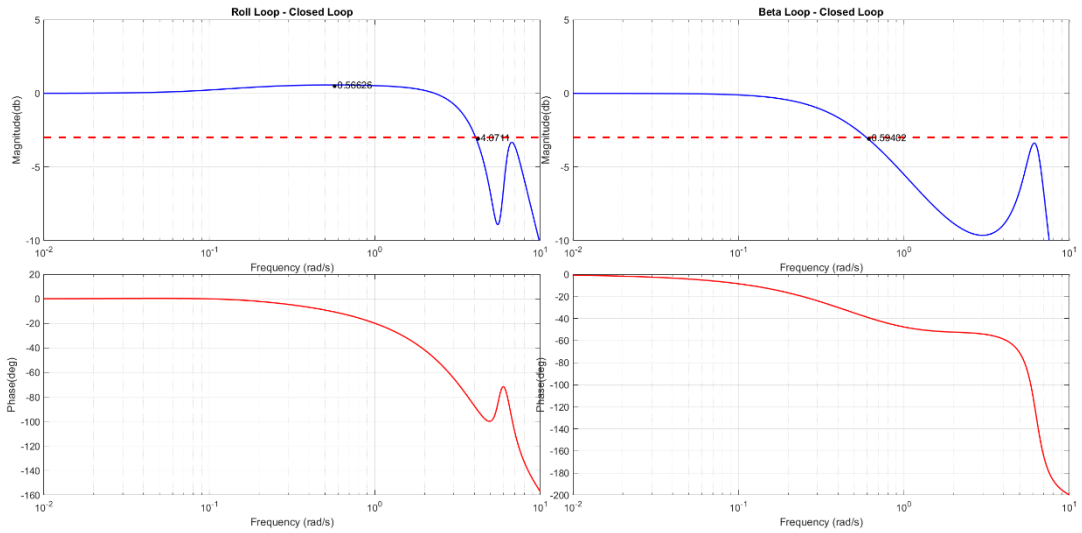

Figure 6.12 : Lateral Closed Loop Frequncy Analysis (PID Controller).

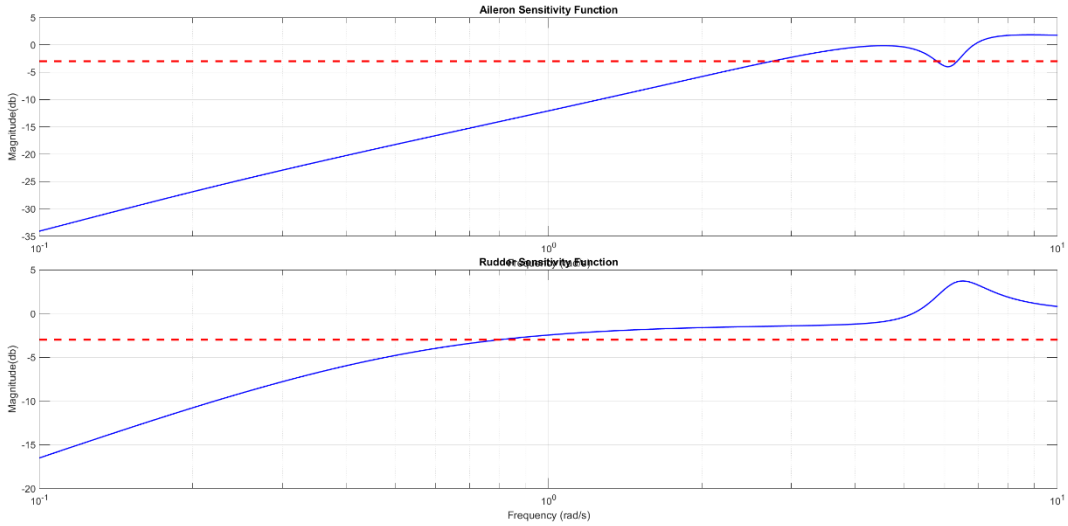

Figure 6.13 : Sensitivity Bode Diagrams of Lateral Actuators (PID Controller).

Considering the performance results of the lateral autopilot design and the results of the stability analysis (Table 6.4), a controller has been designed that provides the necessary constraints in the stability analysis and provides the desired performance in terms of performance.

Table 6.4 : Lateral Stablity Margins.

Loop	Gain Margin	Gain Crossover Frequeny	Phase Margin	Phase Crossover Frequeny
Beta	12.4	7.5612	97.526	0.6737
p	53.2442	61.5865	147.6681	6.9603
Phi	7.4813	13.515	63.1042	2.7247
Aileron	36.3518	51.249	69.6942	3.5023
Rudder	12.4	7.5612	97.526	7.56

Looking at the open-loop stability margins in the lateral plane (Figure 6.11), we see that it meets the stability margins in MIL-F-8785C, which are clearly defined in Section 4.5. When the closed-loop sensitivity Bode diagrams are examined (Figure 6.12), it is seen that the disturbance rejection bandwidth frequency of the elevator loop is 2.802 rad/s and the disturbance rejection resonance value is 1.576 dB. When the closed-loop sensitivity Bode diagrams are examined, it is seen that the disturbance

rejection bandwidth frequency of the throttle loop is 0.796 rad/s and the disturbance rejection resonance value is 3.695 db. (Figure 6.13)

If we examine the performance of the lateral part of the landing autopilot (Figure 6.9, Figure 6.10); Heading with roll before the flare phase is seen to be successful and it is seen that the heading reference is approximately settled before the flare phase is completed, it is seen that it can keep heading with low beta commands in keeping the heading with beta after flare, what low beta references bring to the landing autopilot is that the nose of the aircraft is on the runway at the time of landing. being in the same direction. It also successfully keeps the 0 degree beta reference before the flare. It successfully maintains the 0 degree roll reference after flare, which is important for the aircraft to contact the rear landing gear at the same time with the runway and not to overturn.

6.2 Automatic Landing with Linear Quadratic Integrator (LQI)

6.2.1 Mathematical background

LQR control structure is an optimal control method with state feedback designed to minimize a determined cost function. LQR controller, which is actively used in many fields such as industry, manufacturing, automotive and robotics, stands out in MIMO systems in matters such as its stability and successful noise rejection. LQR controller, a method of modern control theory, uses the state-space representation in the analysis of the system. State-space representation provides a successful analysis and control opportunity for MIMO and complex systems. The main purpose of the LQR controller is to calculate the K gain matrix that will minimize the cost function from the system parameters.

The state-space representation of the system to be controlled is as follows:

$$\dot{x} = Ax + Bu, y = Cx \tag{6.23}$$

and the cost function to be minimized with the state feedback controller u = −Kx in the LQR control system is as follows:

$$J = \frac{1}{2}\int_0^\infty [x^T Q x + u^T R u]dt \tag{6.24}$$

The Q and R matrices in the J cost function are called weight matrices. These matrices allow the control designer to adjust the weight values acting on the control inputs and state variables, ie the extent to which these matrices have an impact on the performance of the system. The Q and R matrices here are positively defined Hermitian or real symmetric matrices. If the R matrix is chosen large with respect to Q, the optimal regulator will bring the state vector to zero by consuming a small control power. However, the residence time of the system will be longer. When the R matrix is chosen small compared to the Q matrix, a greater control power will be consumed and the state vector will rapidly move to zero, reducing the settling time.

LQI control architecture has a different side than LQR. In the LQI control architecture, an integral is added between the selected or all channels and their references and it is expected that there will be no steady-state error against the reference command given in the system.[47]

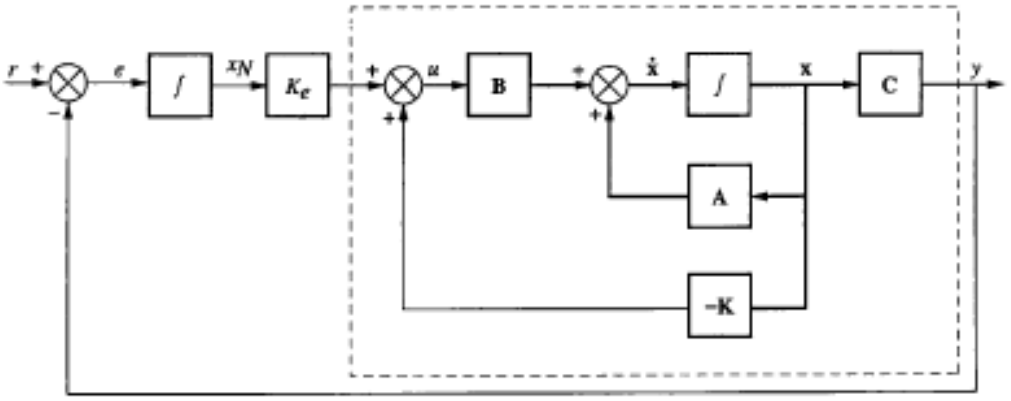

Figure 6.14 : LQI Controller Scheme.

If we write the state equations on the diagram Figure 6.14.

$$\dot{x_N} = r - Cx \tag{6.25}$$

$$\dot{x} = Ax + Bu \tag{6.26}$$

$$\dot{x_N} = -Cx + r \tag{6.27}$$

$$y = Cx \tag{6.28}$$

$$\begin{bmatrix} \dot{x} \\ \dot{x}_N \end{bmatrix} = \begin{bmatrix} A & 0 \\ -C & 0 \end{bmatrix} \begin{bmatrix} x \\ x_N \end{bmatrix} + \begin{bmatrix} B \\ 0 \end{bmatrix} u + \begin{bmatrix} 0 \\ 1 \end{bmatrix} r \tag{6.29}$$

$$y = [C \quad 0] \begin{bmatrix} x \\ x_N \end{bmatrix} \tag{6.30}$$

But

$$u = -Kx + K_e x_N = [K \; -K_e] \begin{bmatrix} x \\ x_N \end{bmatrix} \tag{6.31}$$

Here K matrix is the gain matrix of state feedback signals and K_e matrix is the gain matrix of integrator part.

In LQI control, a quaadratic function solution is aimed as in LQR control, however, since there is an integrator effect on certain states and augmented matrices are formed as seen in the above equations, the size of the Q and R matrices changes. Accordingly, the Q and R matrices should be selected in accordance with the size of the new augmented matrices.

6.2.2 Automatic landing with LQI controller

The LQI type controller structure allows the creation of a multi-input multi-output control architecture unlike PID. Accordingly, a multi-input multi-output architecture was preferred in both the longitudinal autopilot structure and the lateral autopilot structure.

6.2.2.1 Longitudinal autopilot

In the longitudinal autopilot architecture (Figure 6.15), a Theta reference is created from altitude and altitude error. For this, the PI controller is used as the outer loop controller, the coefficients of this controller are chosen the same as in the PID descent controller. Tracking is provided by adding the integral effect to the Theta and velocity retention part. Apart from that, feedback coefficients were found for 4 states (Speed, Alpha, q, Theta) as in the LQR structure.

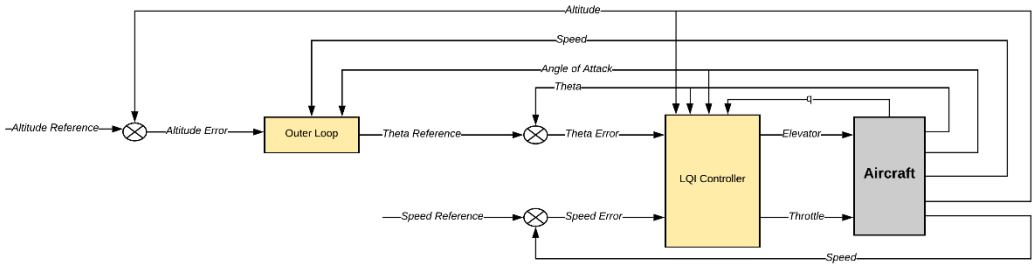

Figure 6.15 : Longitudinal Controller Scheme.

$$J = \frac{1}{2}\int_0^\infty [x^T Q x + u^T R u]\, dt \tag{6.32}$$

For the above quadratic optimization problem, the Q and R weight matrices are chosen as follows.

$$Q = \begin{bmatrix} 1 & 0 & 0 & 0 & 0 & 0 \\ 0 & 0 & 0 & 0 & 0 & 0 \\ 0 & 0 & 0 & 0 & 0 & 0 \\ 0 & 0 & 0 & 1 & 0 & 0 \\ 0 & 0 & 0 & 0 & 2 & 0 \\ 0 & 0 & 0 & 0 & 0 & 100 \end{bmatrix} R = \begin{bmatrix} 1 & 0 \\ 0 & 5 \end{bmatrix} \tag{6.33}$$

The state space matrices of the state space model and Q, R matrices obtained as a result of Algebraic Riccati Equation are as follows.

$$Kx_{lon} = \begin{bmatrix} 1.5348 & 42.7226 & -11.4447 & -115.8236 \\ 2.0775 & 12.119 & -0.1166 & -12.1533 \\ 2.0775 & 12.119 & -0.1166 & -12.1533 \end{bmatrix} \tag{6.34}$$

$$Ki_{Speed} = \begin{bmatrix} -0.5389 \\ -0.4133 \\ -0.4136 \end{bmatrix} \tag{6.35}$$

$$Ki_{Theta} = \begin{bmatrix} 292.369 \\ -38.0935 \\ -38.1178 \end{bmatrix} \tag{6.36}$$

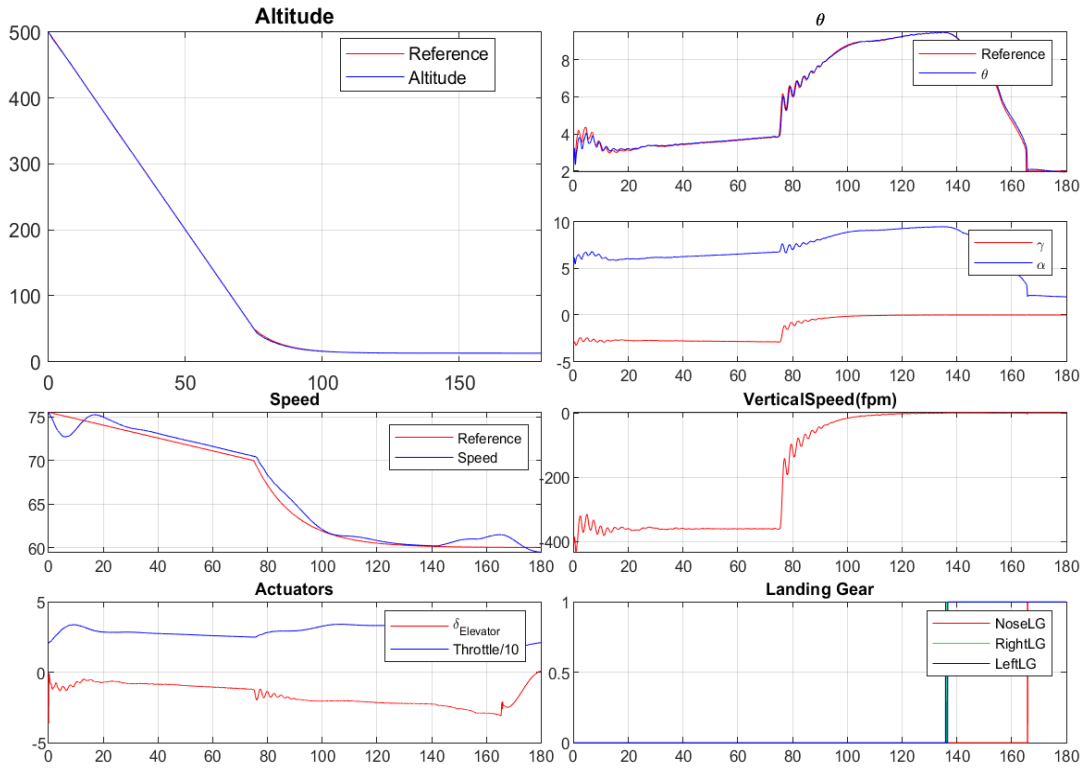

Figure 6.16 : Longitudinal Performance (LQI Controller).

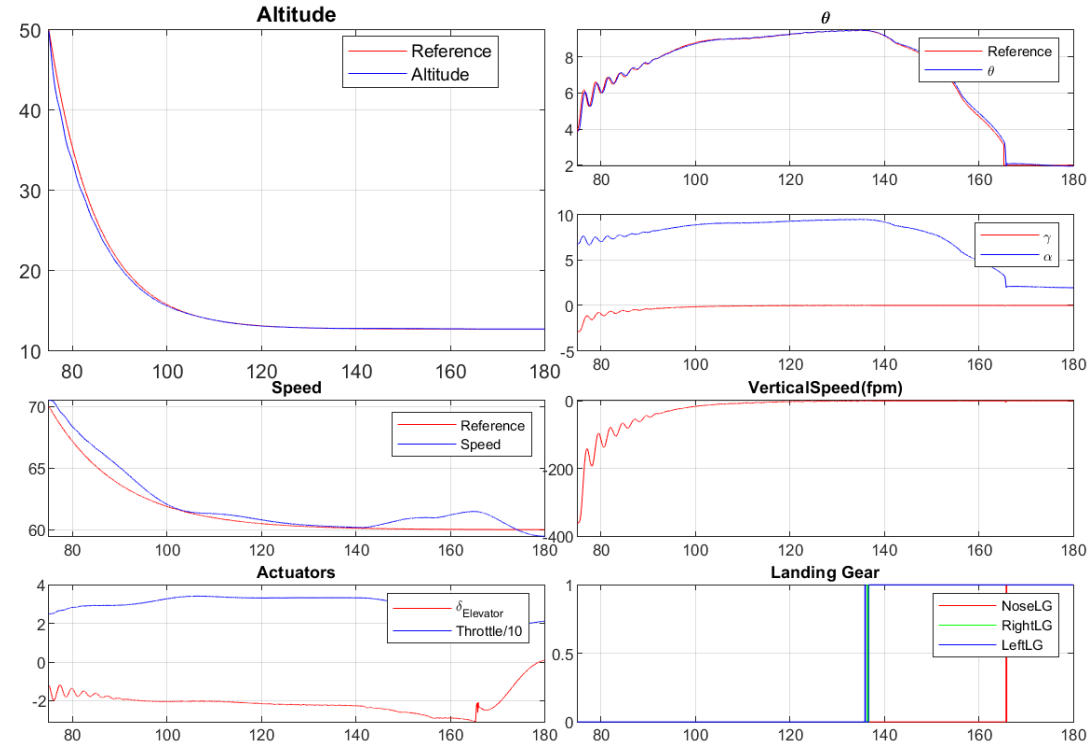

Figure 6.17 : Longitudinal Performance at Flare (LQI Controller).

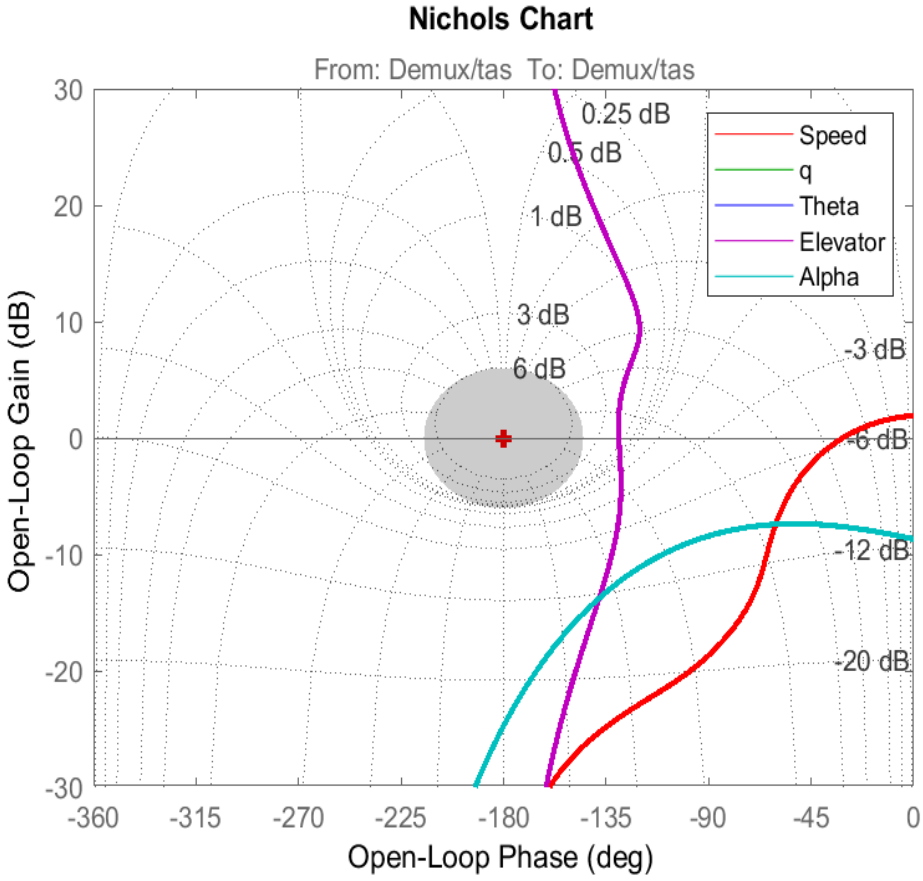

Figure 6.18 : Longitudinal Stability Margins (LQI Controller).

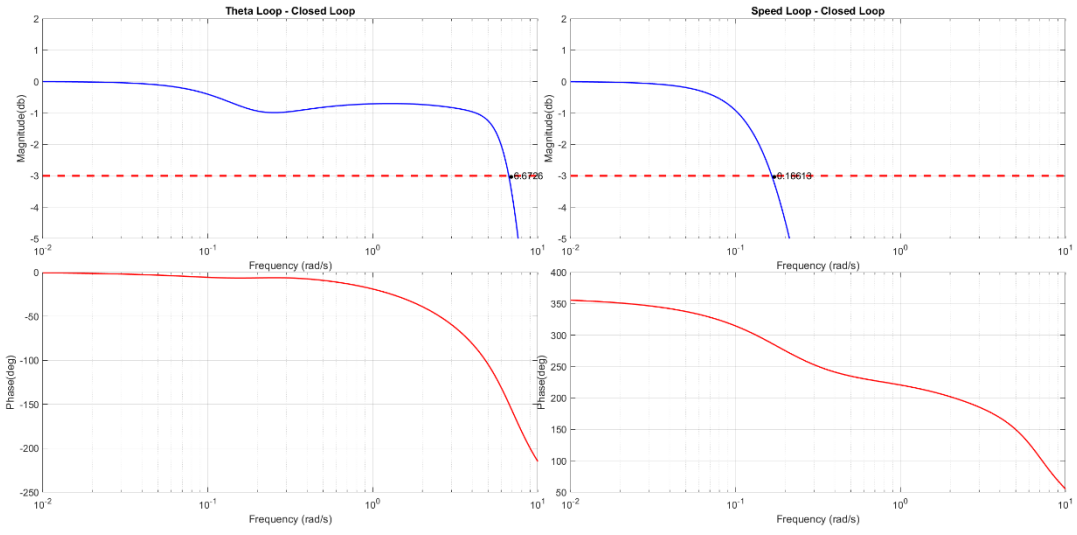

Figure 6.19 : Longitudinal Closed Loop Frequncy Analysis (LQI Controller).

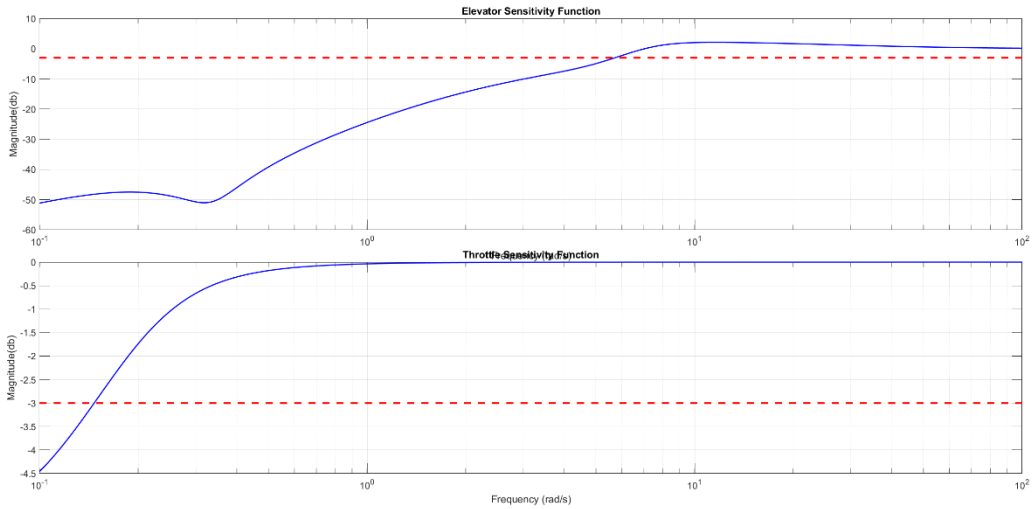

Figure 6.20 : Sensitivity Bode Diagrams of Longitudinal Actuators (LQI Controller).

Table 6.5 : Longitudinal Stablity Margins

Loop	Gain Margin	Gain Crossover Frequeny	Phase Margin	Phase Crossover Frequeny
Speed	Inf	0	139.8178	0.1507
q	13.9	7.9476	73.1	11.7
Theta	13.9	18.1	32.8517	7.2448
Alpha	17.24	21.9637	Inf	Inf
Elevator	Inf	Inf	50.5967	8.1958

Looking at the open-loop stability margins in the longitudinal plane (Figure 6.18), we see that it meets the stability margins in MIL-F-8785C, which are clearly defined in Section 4.5. When the closed-loop sensitivity Bode diagrams are examined (Figure 6.19), it is seen that the disturbance rejection bandwidth frequency of the elevator loop is 5.672 rad/s and the disturbance rejection bandwidth value is 2.124 dB. When the closed-loop sensitivity Bode diagrams are examined (Figure 6.20), it is seen that the disturbance rejection bandwidth frequency of the throttle loop is 0.1473 rad/s and the disturbance rejection value is -0.001176 db.

If we examine the performance of the longitudinal part of the automatic landing autopilot designed with LQI; Figure 6.16 shows altitude hold, pitch hold, and speed hold throughout the entire descent. Although the altitude hold of the aircraft is seen to

be quite successful in the pre-flare part, the speed hold does not follow the reference exactly and the speed of the aircraft is seen as higher than the reference. The vertical speed of the aircraft decreases with the nose lift directional pitch reference provided with the flare transition, which is important for smooth wheeling on the runway. To examine the performance after flare transition, it is necessary to look at Figure 6.17. After the flare transition, although the LQI controller stays below the altitude reference at the first moment, as in the PID controller, the error is reset as it approaches the runway, and a similar behavior is in question when holding the speed. In addition, if the control surfaces are examined, sudden movements are not seen in any part of the descent. As the advantage of multi-input multi-output control, it is seen that the feedbacks in the states are damped and the states that receive feedback with integral are more successful reference tracking. In particular, the couple effects in the pitch hold and, accordingly, the altitude hold are seen to be considerably reduced in the LQI controller.

6.2.2.2 Lateral autopilot

In the lateral autopilot architecture (Figure 6.21), a Roll reference is created from the head angle error. For this, the P controller is used as the outer loop controller, the coefficients of this controller are chosen the same as in the PID descent controller. Tracking is provided by adding the integral effect to the roll and beta grip part. Apart from that, feedback coefficients were found for 4 states (Beta, p, r, Roll) as in the LQR structure.

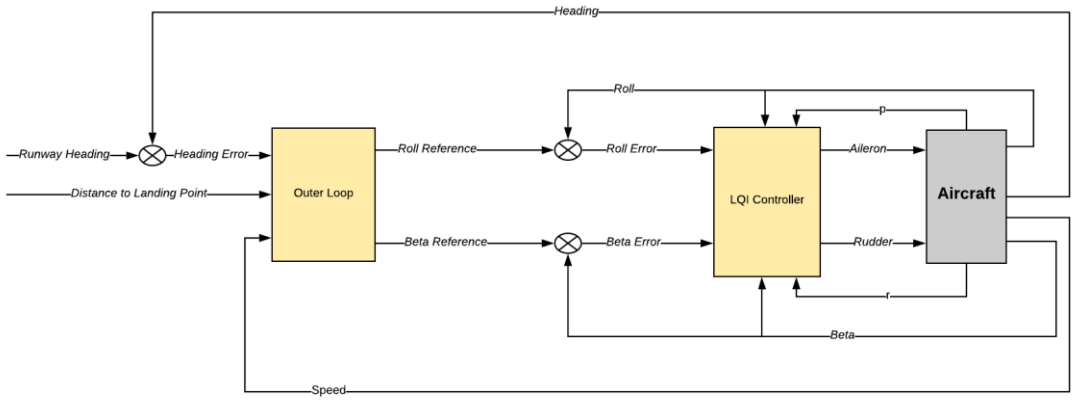

Figure 6.21 : Lateral Controller Scheme.

$$J = \frac{1}{2}\int_0^{\infty} [x^T Q x + u^T R u] dt \tag{6.37}$$

For the above quadratic optimization problem, the Q and R weight matrices are chosen as follows.

$$Q = \begin{bmatrix} 10 & 0 & 0 & 0 & 0 & 0 \\ 0 & 0 & 0 & 0 & 0 & 0 \\ 0 & 0 & 0 & 0 & 0 & 0 \\ 0 & 0 & 0 & 10 & 0 & 0 \\ 0 & 0 & 0 & 0 & 500 & 0 \\ 0 & 0 & 0 & 0 & 0 & 200 \end{bmatrix} R = \begin{bmatrix} 0.2 & 0 \\ 0 & 0.2 \end{bmatrix} \tag{6.38}$$

The state space matrices of the state space model and Q, R matrices obtained as a result of Algebraic Riccati Equation are as follows.

$$Kx_{lon} = \begin{bmatrix} 11.6835 & -2.3593 & -5.0849 & -18.8631 \\ 15.9491 & -1.6504 & -7.4479 & -15.8387 \end{bmatrix} \tag{6.39}$$

$$Ki_{Beta} = \begin{bmatrix} 32.8471 \\ -37.6971 \end{bmatrix} \tag{6.40}$$

$$Ki_{Speed} = \begin{bmatrix} 23.8417 \\ 20.7743 \end{bmatrix} \tag{6.41}$$

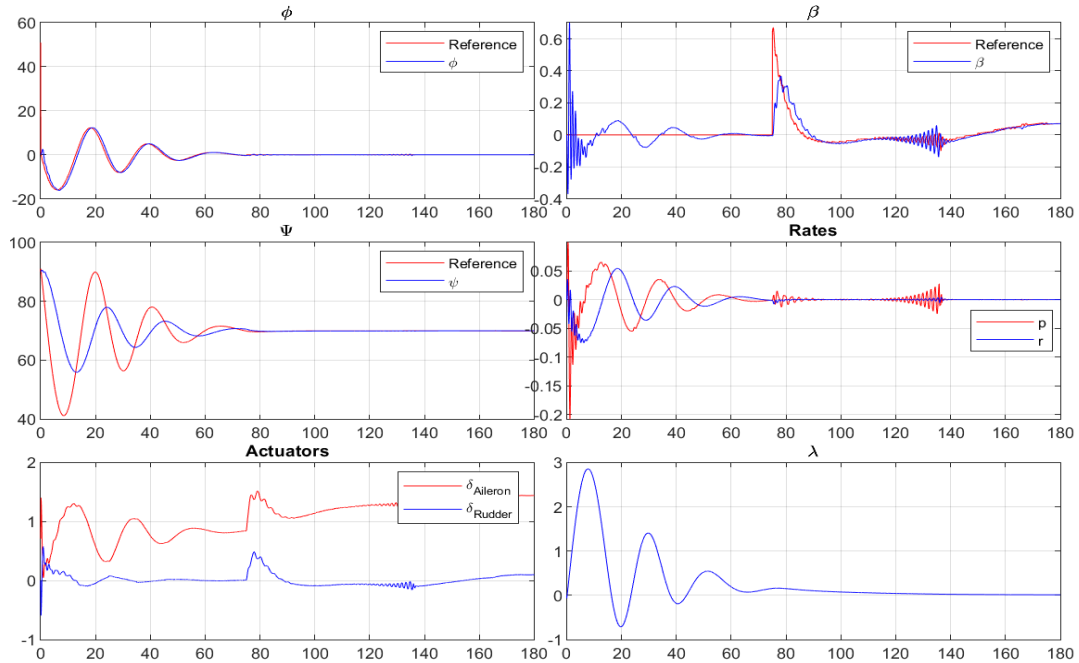

Figure 6.22 : Lateral Performance (LQI Controller).

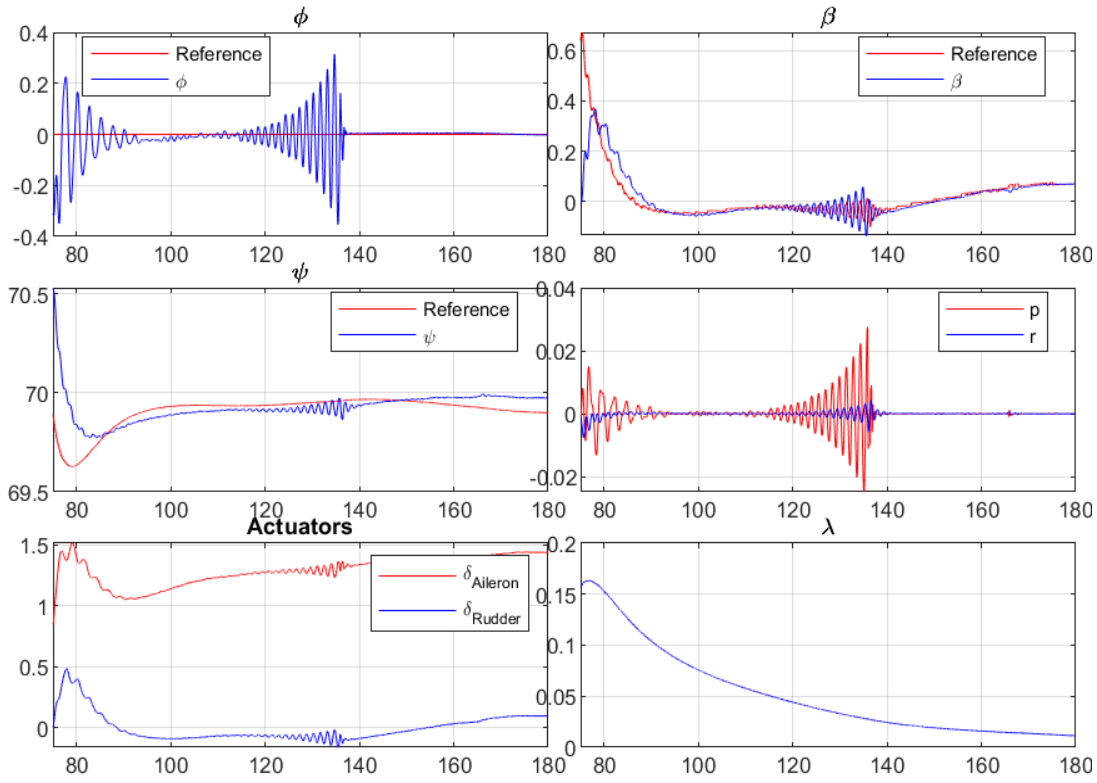

Figure 6.23 : Lateral Performance at Flare (LQI Controller).

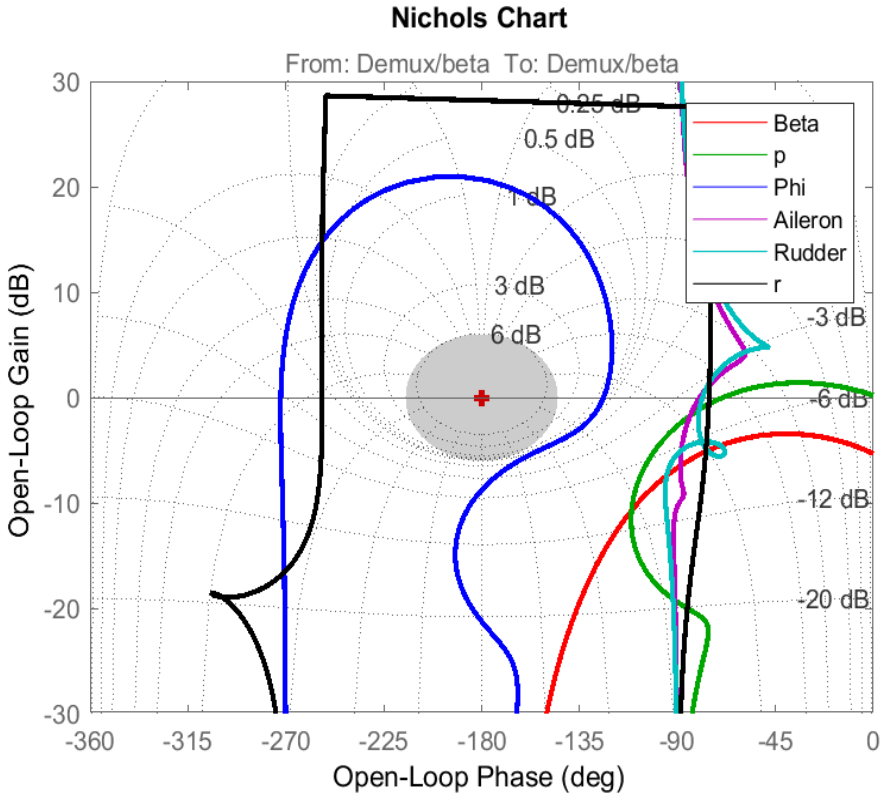

Figure 6.24 : Lateral Stability Margins (LQI Controller).

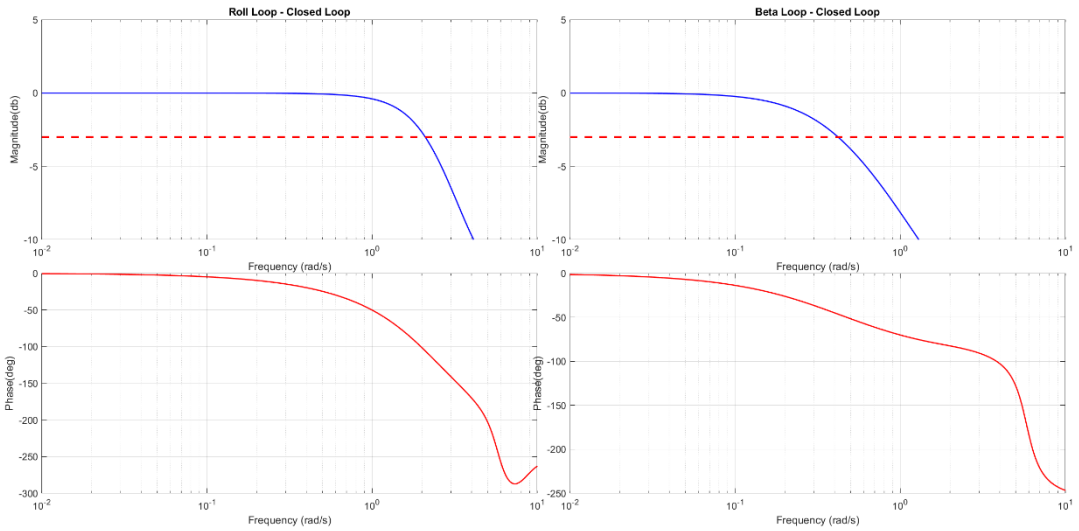

Figure 6.25 : Lateral Closed Loop Frequncy Analysis (LQI Controller).

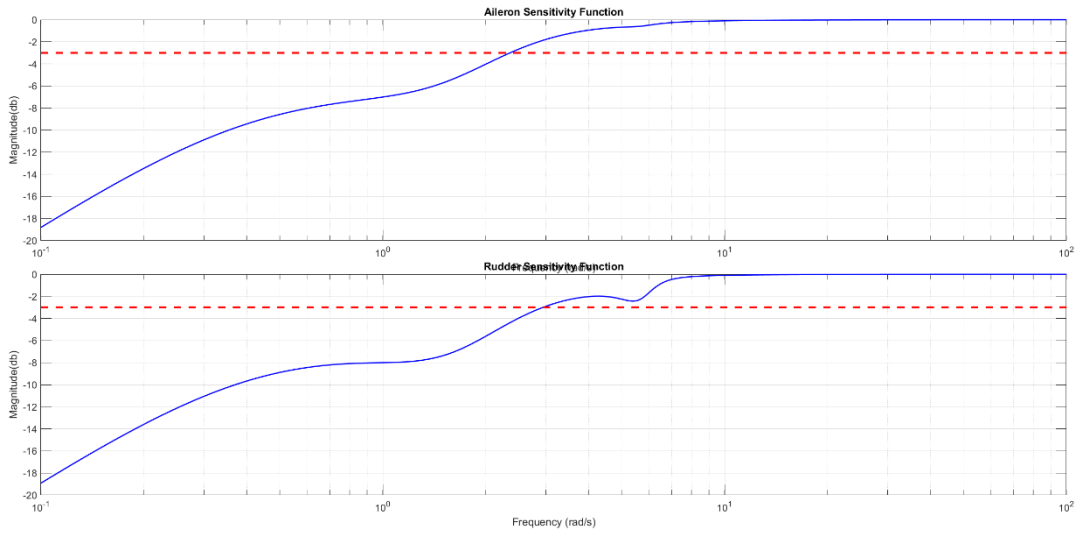

Figure 6.26 : Sensitivity Bode Diagrams of Lateral Actuators (LQI Controller).

Table 6.6 : Lateral Stablity Margins.

Loop	Gain Margin	Gain Crossover Frequeny	Phase Margin	Phase Crossover Frequeny
Beta	Inf	Inf	Inf	Inf
p	381.7802	0.1701	110.7815	5.3313
r	10.4	6.2024	73.2562	5.2866
Phi	8.77	6.3273	55.956	3.3691
Aileron	Inf	Inf	100.2159	2.0996
Rudder	Inf	Inf	101.4409	2.5666

Looking at the open-loop stability margins in the lateral plane (Figure 6.24, Table 6.6), we see that it meets the stability margins in MIL-F-8785C, which are clearly defined in Section 4.5. When the closed-loop sensitivity Bode diagrams are examined (Figure 6.25), it is seen that the disturbance rejection bandwidth frequency of the elevator loop is 2.341 rad/s and the disturbance rejection resonance value is -0.02362 dB. When the closed-loop sensitivity Bode diagrams are examined (Figure 6.26), it is seen that the disturbance rejection bandwidth frequency of the throttle loop is 2.961 rad/s and the disturbance rejection resonance value is -0.02462 db.

If we examine the performance of the lateral part of the landing autopilot designed with the LQI controller (Figure 6.22, Figure 6.23); Keeping the beta angle at 0 degrees before the flare and tracking the roll reference produced from the heading error are seen as successful. It is seen that the heading reference is followed successfully with the low beta commands after the controller change (keeping the roll angle of 0 degrees and controlling the heading reference with beta) with the flare phase. High-frequency commands on the control surfaces are only seen at the time of the flare transition, where the controller change is experienced, and this is considered normal, however, the fact that the control surfaces are far from saturation shows that the control of the aircraft can be made without forcing the limits.

6.3 Automatic Landing with Model Predictive Control (MPC)

6.3.1 Mathematical background

Basically, Model Predictive Control calculates the next output value of the system using the current and previous input signal of the system. (Figure 6.27) In order to minimize the error between the output of the system and the reference value, the most appropriate control (input) signal sequence is calculated and applied to the system. That is, a Model Predictive Controller is a controller that calculates the necessary control sequence to optimize the future behavior of a system. The reciding horizon control method is used to predict future output. Model Predictive Control began to be used in industry in the 1980s and was initially used in slow processes such as petroleum, chemistry, petro-chemistry. With the development of microprocessor technology, it started to be used in fast systems such as robotic systems and power systems in the following years. The main advantage of MPC are:

• With linear and non-linear systems or systems with one variable and multiple variables, the problem is solved without changing the controller formula.

• An optimal control law is used.

• Constraints are included during the design of the controller.

• The process model captures dynamic and static interactions between inputs, outputs and disturbances.

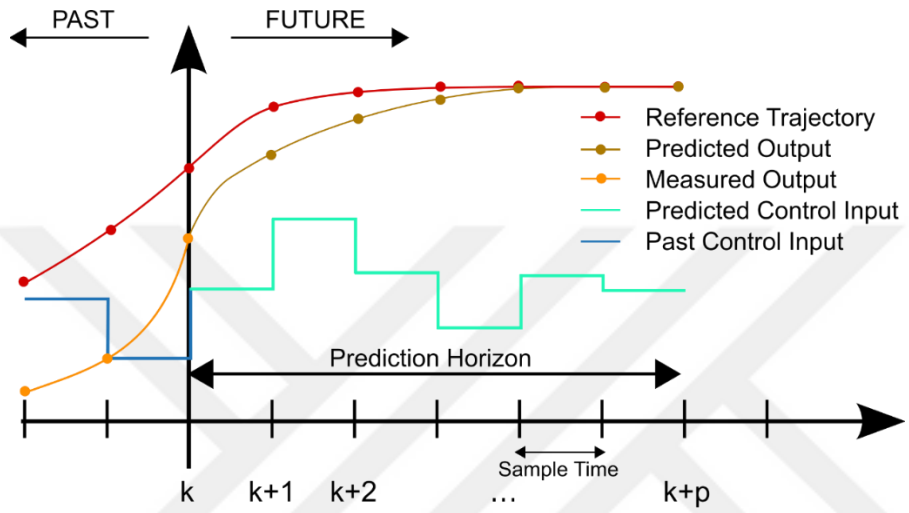

Figure 6.27 : Model Predictive Control Approximation Scheme.

Let the expression of a linear time-invariant system in discrete time space be as follows:

$$x_{k+1} = A \cdot x_k + B \cdot u_k, y_k = C \cdot x_k \tag{6.42}$$

Here x_k denotes the states of the system and u_k denotes the inputs of the system. In the model predictive control method, obtaining the optimal control sign of the system at a certain horizon can be expressed with a quadratic function.

$$J_0(x_0, U) = \sum_{k=0}^{Np-1} (ref - y_k^T) * Q * (ref - y_k) + \sum_{k=0}^{Nc-1} u_k^T * R * u_k \tag{6.43}$$

In quadratic function; Np denotes the predict horizon of the system, Nc denotes the control horizon of the system, while x_0 denotes the state vector. The main purpose in model predictive control is to calculate the U vector that will minimize this quadratic function. Q, P and R weighting matrices are also important in the calculation of this

vector. While the Q matrix expresses the weighting between the states of the system, the R matrix expresses the weighting between the inputs of the system.

It may be necessary to add an integrator effect to the system in order to avoid disturbances that may affect the system and/or to enable the system to follow the reference without a steady-state error. For this, we need to manipulate the matrices of the system and make them augmented.[9,48]

$$\begin{aligned} \overbrace{\begin{bmatrix}\Delta x(k+1)\\ y(k+1)\end{bmatrix}}^{x(k+1)} &= \overbrace{\begin{bmatrix}A & o^T\\ CA & 1\end{bmatrix}}^{A_{aug}}\overbrace{\begin{bmatrix}\Delta x(k)\\ y(k)\end{bmatrix}}^{x(k)} + \overbrace{\begin{bmatrix}B\\ CB\end{bmatrix}}^{B_{aug}}\Delta u(k) \\ y(k) &= \overbrace{[o\ 1]}^{C_{aug}}\begin{bmatrix}\Delta x(k)\\ y(k)\end{bmatrix}, \end{aligned} \tag{6.44}$$

The augmented models obtained after this manipulation contain an internal integrator and prevent the system from having a steady-state error.

Based on the state-space form, the future state variables of the system can be expressed as follows:

$$x(k+1) = A\,x(k) + B\big(\Delta u(k) + u(k-1)\big) \tag{6.45}$$

$$\begin{aligned} x(k+2) &= A^2\,x(k) + AB\big(\Delta u(k) + u(k-1)\big) + B\Delta u(k+1) \\ &\quad + B\,\Delta u(k) + Bu(k-1) \\ &= A^2\,x(k) + (AB+B)\Delta u(k) + B\Delta u(k+1) \\ &\quad + (AB+B)u(k-1) \end{aligned} \tag{6.46}$$

$$\begin{aligned} x(k+3) &= A^3\,x(k) + (A^2B + AB + B)\Delta u(k) \\ &\quad + (AB+B)\Delta u(k+1) + B\Delta u(k+2) \\ &\quad + (A^2B + AB + B)u(k-1) \\ &\quad \dots \end{aligned} \tag{6.47}$$

$$
\begin{aligned}
x(k+\mathrm{Np}) = {} & A^{\mathrm{Np}}\, x(k) \\
& + (A^{\mathrm{Np}-1}B + A^{\mathrm{Np}-2}B + \cdots + A^2B + AB \\
& + B)\Delta u(k) \\
& + (A^{\mathrm{Np}-2}B + A^{\mathrm{Np}-3}B + \cdots + AB + B)\Delta u(k+1) \\
& + (A^{\mathrm{Np}-3}B + A^{\mathrm{Np}-4}B + A^{\mathrm{Np}-5}B + \cdots \\
& + B)\Delta u(k+2) \\
& + (A^{\mathrm{Np}-1}B + A^{\mathrm{Np}-2}B + \cdots + A^{\mathrm{Np}-\mathrm{Nc}}B + AB \\
& + B)u(k-1)
\end{aligned}
\tag{6.48}
$$

Based on the state-space form, the future output variables of the system can be expressed as follows:

$$
y(k+1) = CAx(k) + CB\big(\Delta u(k) + u(k-1)\big) \tag{6.49}
$$

$$
\begin{aligned}
y(k+2) = {} & CA^2\, x(k) + (CAB + CB)\Delta u(k) + CB\Delta u(k+1) \\
& + (CAB + CB)u(k-1)
\end{aligned}
\tag{6.50}
$$

$$
\begin{aligned}
y(k+3) = {} & CA^3\, x(k) + (CA^2B + CAB + CB)\Delta u(k) \\
& + (CAB + CB)\Delta u(k+1) + CB\Delta u(k+2) \\
& + (CA^2B + CAB + CB)u(k-1)
\end{aligned}
\tag{6.51}
$$

$$
\begin{aligned}
y(k+4) = {} & CA^4\, x(k) + (CA^3B + CA^2B + CAB + CB)\Delta u(k) \\
& + (CA^2B + CAB + CB)\Delta u(k+1) \\
& + (CAB + CB)\Delta u(k+2) \\
& + (CA^3B + CA^2B + CAB + CB)u(k-1))
\end{aligned}
\tag{6.52}
$$

(6.53)

$$
\begin{aligned}
y(k+\mathrm{Np}) = {} & CA^{\mathrm{Np}}\,x(k) \\
& + (CA^{\mathrm{Np}-1}B + CA^{\mathrm{Np}-2}B + \cdots + CA^{2}B + CAB \\
& + CB)\Delta u(k) \\
& + (CA^{\mathrm{Np}-2}B + CA^{\mathrm{Np}-3}B + \cdots + CAB + CB)\Delta u(k \\
& + 1) \\
& + (CA^{\mathrm{Np}-3}B + CA^{\mathrm{Np}-4}B + CA^{\mathrm{Np}-5}B + \cdots \\
& + CB)\Delta u(k+2) \\
& + (CA^{\mathrm{Np}-1}B + CA^{\mathrm{Np}-2}B + \cdots + CA^{\mathrm{Np}-\mathrm{Nc}}B)u(k \\
& - 1)
\end{aligned}
$$

Note that all variables can be expressed in terms of previous outputs of the system and future control signals. If the output variables are expressed as a vector:

$$Y = \left[y(k_i+1 \mid k_i)y(k_i+2 \mid k_i)y(k_i+3 \mid k_i) \ldots y\left(k_i+N_p \mid k_i\right)\right]^T \tag{6.54}$$

$$\Delta U = [\Delta u(k_i)\Delta u(k_i+1)\Delta u(k_i+2) \ldots \Delta u(k_i+N_c-1)]^T \tag{6.55}$$

With these vectors, we can express the prediction horizon of the system in a simpler way.

$$Y = Fx(k_i) + \mathrm{H}\Delta U \tag{6.56}$$

where

$$F = \begin{bmatrix} CA \\ CA^2 \\ CA^3 \\ \vdots \\ CA^{N_p} \end{bmatrix}; \mathrm{H} = \begin{bmatrix} CB & 0 & 0 & \ldots & 0 \\ CAB & CB & 0 & \ldots & 0 \\ CA^2B & CAB & CB & \ldots & 0 \\ \vdots & & & & \\ CA^{N_p-1}B & CA^{N_p-2}B & CA^{N_p-3}B & \ldots CA^{N_p-N_cB} & \end{bmatrix} \tag{6.57}$$

Let ref_s the reference value given to the system be extended along the forecast horizon. Accordingly, we can also revise the quadratic function equation.

$$J = (ref_s - Y)^T(ref_s - Y) + \Delta U^T\mathrm{R}\Delta U \tag{6.58}$$

The place where a quadratic function is the minimum for the unconstrained solution is located where its first derivative is 0, accordingly:

$$\frac{\partial J}{\partial \Delta U} = -2\Phi^T\left(ref_s - Fx(k_i)\right) + 2(\Phi^T\Phi + \bar{R})\Delta U = 0 \quad (6.59)$$

and the control sign for the unconstrained solution can be expressed with the prediction matrices F and H:

$$\Delta U = (\mathrm{H}^T\mathrm{H} + \bar{R})^{-1}\Phi^T\left(ref_s - Fx(k_i)\right) \quad (6.60)$$

For the constrained solution of the quadratic function, the first derivative of the objective function will not be sufficient, here the control command that minimizes the objective function can be calculated with different optimization solution methods.

Another thing as important as performance in control system design is the stability of the system. Since the control coefficients of control loops are certain in Explicit solutions, open loop and closed loop stability analyzes can be made by breaking the loops from various places. In the Model Predictive Control method, where the online control signal is obtained, it is not possible to do this analysis with classical methods.

[16] made some recommendations for stability analysis for MPC. For this, all eigenvalues of the A matrix of the state-space model are in the unit-circle, the weighting matrix $Q \geq 0$ and the Lyapunov matrix $\bar{Q} \geq 0$ ensure the stability of the system.

6.3.2 Automatic landing with MPC controller

The Model Predictive Control method is a multi-input multi-output control method. For the reasons explained in chapter 6.3.1 , an integrator has been added to the system and control is provided over the obtained augmented matrices. In addition, the system was divided into two parts longitudinally and laterally, as in the previous sections and general aviation applications, and a separate controller design was made for these two parts. The continuous time state-space model of the system is discrete according to the operating frequency of the system.

In the controller design, constraints were added on the control signals, while the constraints were added, the boundaries of the system inputs (control surfaces) were taken as limits and the MATLAB $quadprog$ function was used for the constrained solution.

One of the most important performance criteria of the Online Model Predictive Control method is the speed of solution of the problem. Within the scope of automatic descent control problem, control signals created continuously by the state-space Model Predictive Control method were used. While the system is running for 0.0005s, the sampling time of the control structure is chosen as 0.02s. In the Model Predictive Control problem, the prediction horizon is 40 steps and the control horizon is 1 step. However, the average solution speed of the problem was 0.0013s. It is seen that the solution speed of the MPC problem is 14.9324 times the sampling time of the controller.

6.3.2.1 Longitudinal autopilot

In the longitudinal autopilot design, altitude and speed hold autopilot are designed. Theta reference was obtained by passing the altitude error PI control, the Model Predictive Control structure was used for Theta and Speed holding as the inner loop controller. (Figure 6.28)

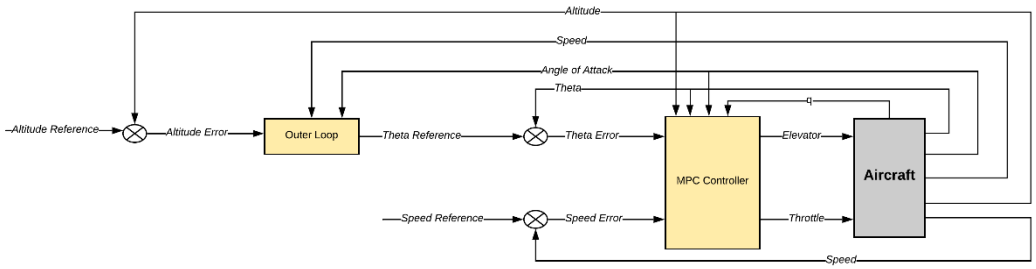

Figure 6.28 : Longitudinal Model Predictive Control Scheme.

The Q and R weighting matrices for the Model Predictive Control are defined as follows.

$$Q = \begin{bmatrix} 0.00443 & 0 \\ 0 & 684.7243 \end{bmatrix} R = \begin{bmatrix} 68.889 & 0 \\ 0 & 0.04 \end{bmatrix} \quad (6.61)$$

When the weighting matrices used for longitudinal autopilot are examined with Lyapunov Theorem:

$$\bar{Q} = \begin{bmatrix} 314.2895 & -3382.3 & 222.6021 & 3346 \\ -3382.3 & 839540 & -72299 & -992840 \\ 222.6021 & -72299 & 6689.7 & 879710 \\ 3346 & -99284 & 87971 & 120110 \end{bmatrix} \quad (6.62)$$

$$\lambda(\bar{Q}) = [234.1146 \quad 285.607 \quad 11256 \quad 2035900] \tag{6.63}$$

However, in the controller designed discrete linear model of the system, the eigenvalues of the system are in the unit circle, their locations:

$$[0.986 + 0.023i \quad 0.986 - 0.023i \quad 0.9995 + 0.0016i \quad 0.9995 - 0.0016i]$$

Along with these proofs, the system provides stability in closed loop as stated in 6.3.1

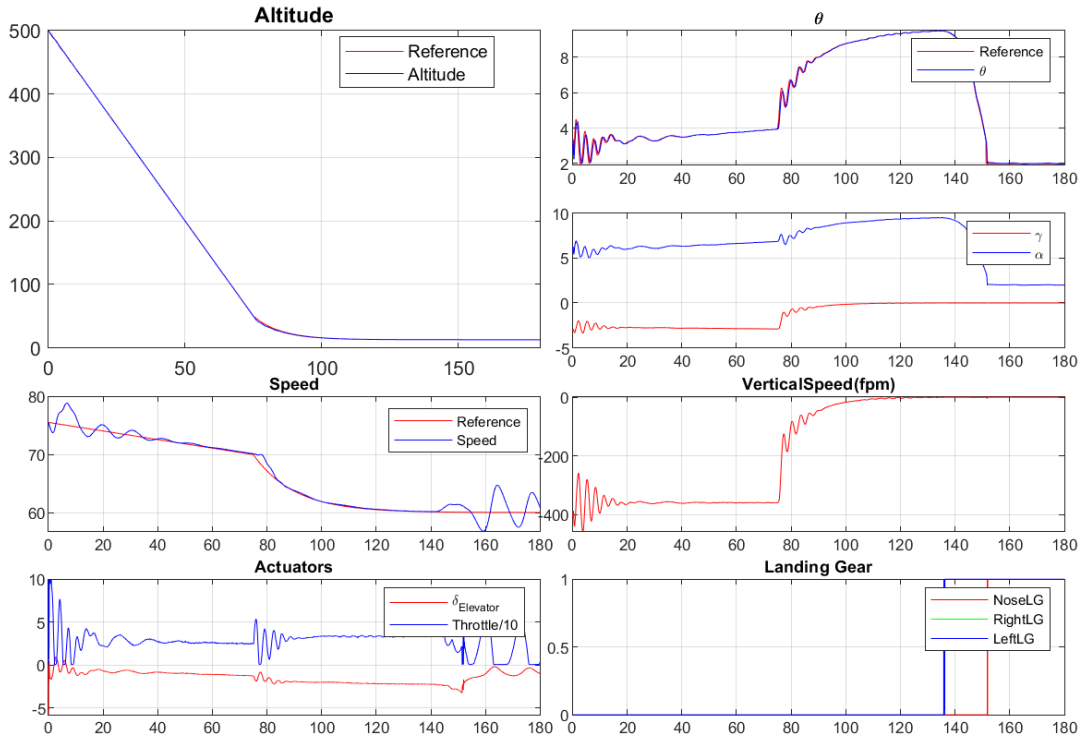

Figure 6.29 : Longitudinal Performance (MPC Controller).

If we examine the performance of the longitudinal part of the automatic landing autopilot designed with MPC; Figure 6.29 shows altitude hold, pitch hold, and speed hold throughout the entire descent. If we examine the speed holding before the flare phase; With the start of landing, the speed of the aircraft hovers around the speed reference and successfully follows the speed reference after about 20 seconds. Roaming around the reference here is one of the initial conditions of the simulation, and such a situation will not be seen in case of a rollover from another autopilot structure before the landing autopilot. After the flare transition (Figure 6.30), the speed hold is seen to be very successful. If we examine the control surface commands, there is no such thing as limiting in the commands and it is seen that the control is achieved

with a successful one. If the altitude hold of the aircraft is examined; Altitude hold is seen as successful before the flare phase and there is no loss in theta grip. With the flare transition, the altitude reference comes exponentially rather than linearly, altitude hold is also very successful here, and the performance of the altitude tracking increases as the wheel approaches the put-down phase.

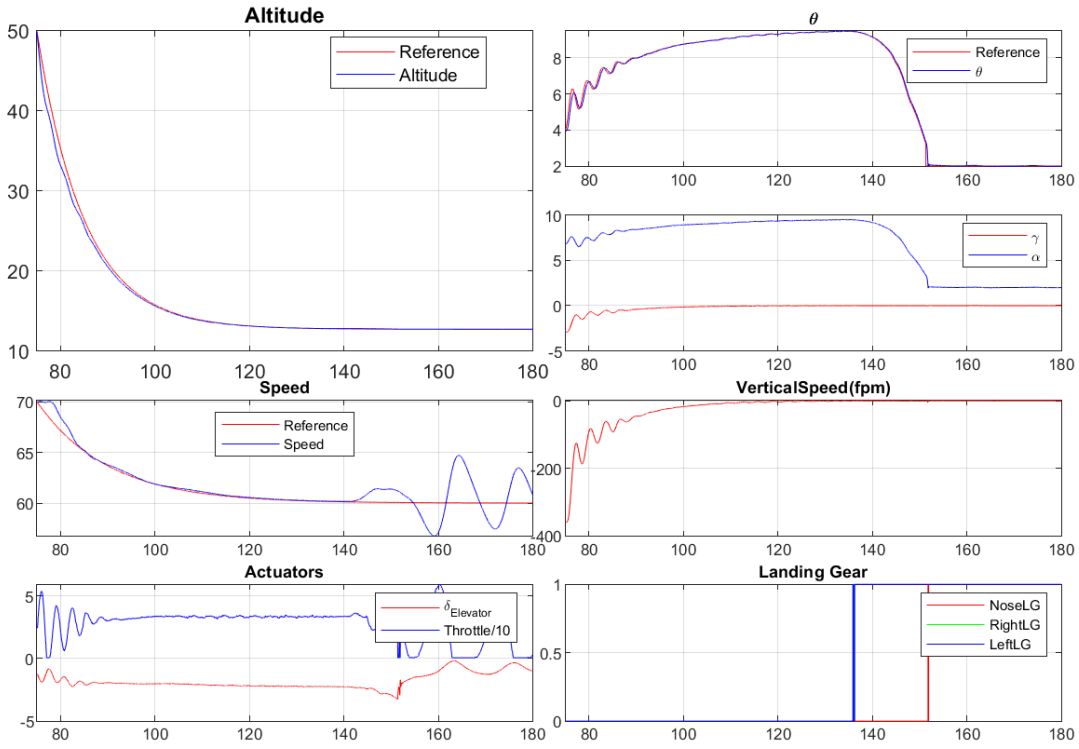

Figure 6.30 : Longitudinal Performance at Flare (MPC Controller).

6.3.2.2 Lateral autopilot

In the lateral autopilot design, heading angle and sideslip(beta) hold autopilot are designed. Roll reference was obtained by passing the heading error, the Model Predictive Control structure was used for Roll and Beta holding as the inner loop controller. (Figure 6.31)

The Q and R weighting matrices for the Model Predictive Control are defined as follows.

$$Q = \begin{bmatrix} 4 & 0 \\ 0 & 1 \end{bmatrix} R = \begin{bmatrix} 500 & 0 \\ 0 & 500 \end{bmatrix} \quad (6.64)$$

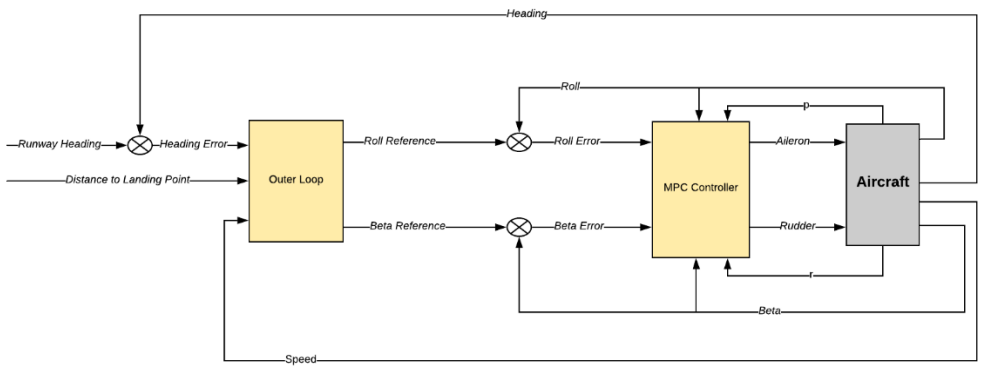

Figure 6.31 : Lateral Model Predictive Control Scheme.

When the weighting matrices used for longitudinal autopilot are examined with Lyapunov Theorem:

$$\bar{Q} = \begin{bmatrix} 165520 & -364010 & -20155 & -25375 \\ -36401 & 32380 & 10433 & 21907 \\ -11502 & 10433 & 34284 & 70547 \\ -2575 & 21907 & 70547 & 14930 \end{bmatrix} \tag{6.65}$$

$$\lambda(\bar{Q}) = [161.219 \quad 7552.5 \quad 120390 \quad 190570] \tag{6.66}$$

However, in the controller designed discrete linear model of the system, the eigenvalues of the system are in the unit circle, their locations:

$$[0.9739 \quad 0.9878 - 0.0301i \quad 0.9878 + 0.0301i \quad 0.9988]$$

Along with these proofs, the system provides stability in closed loop as stated in chapter 6.3.1

If we examine the performance of the lateral part of the landing autopilot (Figure 6.32) designed with the MPC controller; Before the flare phase, the tracking of the heading reference with the roll cycle is quite successful, and it is seen that it converges to the required heading reference before the flare transition. With the flare phase transition (Figure 6.33), it successfully follows the 0 degree reference of the roll angle. After the phase transition, a structure in which the heading reference tracking is made with beta is passed, it is seen that the beta reference tracking is followed successfully, at the end of the flare phase, there is a heading holding error of 0.1 degrees during wheel placement, this shows that the aircraft put the wheels in the same direction with the runway.

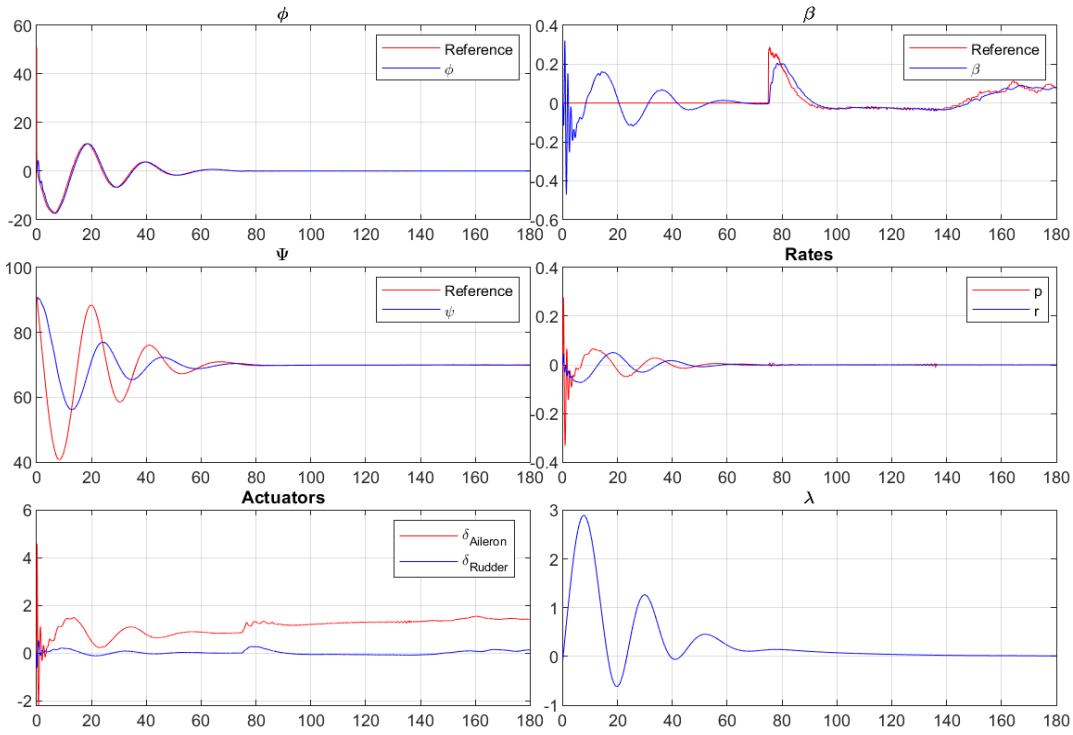

Figure 6.32 : Lateral Performance (MPC Controller).

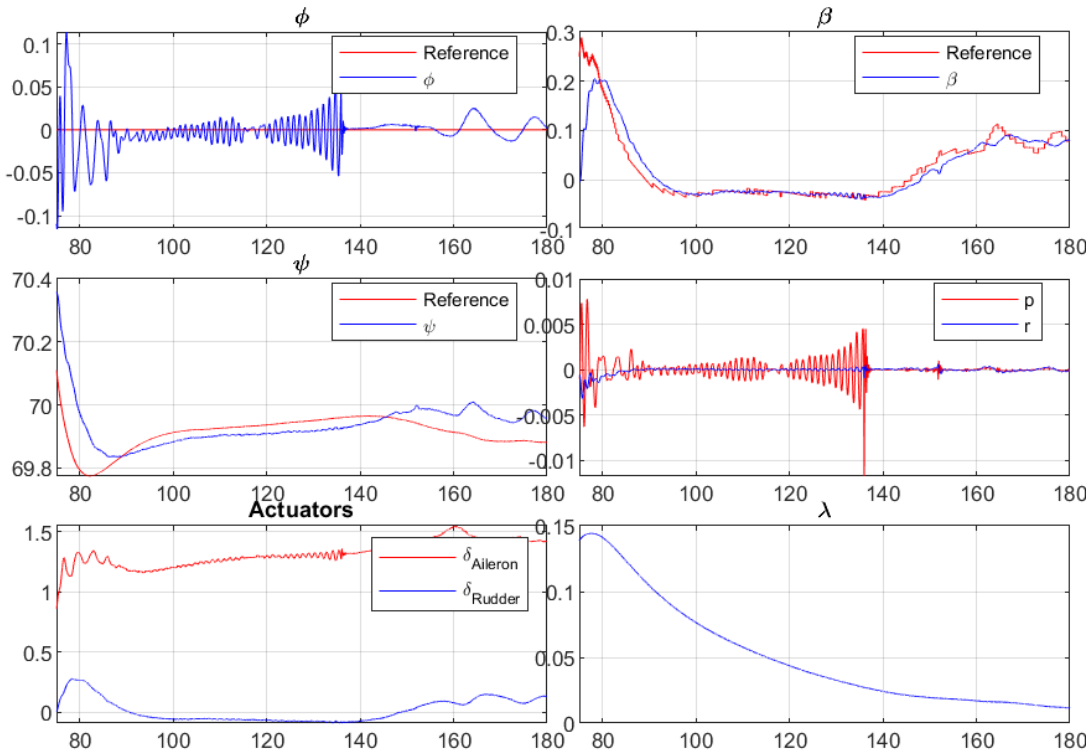

Figure 6.33 : Lateral Performance at Flare (MPC Controller).

6.4 Automatic Landing with Algebraic Model Predictive Control (A-MPC)

6.4.1 Mathematical background

Many different methods have been proposed to increase the solution speed of the Model Predictive Control method. The Algebraic Model Predictive Control method is one of the recommended methods to increase the solution speed. [49] In this method, the constrained model predictive control problem is reduced to an unconstrained mpc problem by using the tangent hyperbolic function. Tanh, as a continuous and differentiable saturation-like function, allows system constraints to be expressed in dynamic equations. The tanh function definition for inputs, states and outputs can be done as follows:

$$\varphi(x) = \tilde{x}_c \cdot \tanh(\tilde{x}_c^{-1} \cdot x) \tag{6.67}$$

$$\varphi(u) = \tilde{u}_c \cdot \tanh(\tilde{u}_c^{-1} \cdot u) \tag{6.68}$$

$$\varphi(y) = \tilde{y}_c \cdot \tanh\,(\tilde{y}_c^{-1} \cdot y) \tag{6.69}$$

The vector form of the equations obtained as a result of advancing the MPC problem passed through the tanh function along the control horizon:

$$\varphi\left(\begin{bmatrix} x_1 \\ \vdots \\ x_N \end{bmatrix}\right) = \tilde{X}_c \cdot \tanh\left[\tilde{X}_c^{-1}\left(\tilde{A} \cdot \begin{bmatrix} x_0 \\ \vdots \\ x_{N-1} \end{bmatrix} + \tilde{B} \cdot \tilde{U}_c \cdot \tanh\left[\tilde{U}_c^{-1} \cdot \begin{bmatrix} u_0 \\ \vdots \\ u_{N-1} \end{bmatrix}\right]\right)\right] \tag{6.70}$$

Here

$$\begin{gathered} \tilde{X}_c = blkdiag\{\tilde{x}_c, \dots, \tilde{x}_c\}, \tilde{U}_c = blkdiag\{\tilde{u}_c, \dots, \tilde{u}_c\} \\ \tilde{A} = blkdiag\{\mathrm{A}, \dots, \mathrm{A}\}, \tilde{B} = blkdiag\{\mathrm{B}, \dots, \mathrm{B}\} \end{gathered} \tag{6.71}$$

In the Algebraic Model Predictive Control method, the signal coming out of the control system is passed through the following structure to be a precaution to limit the control signal.

$$\varphi(u^*) = \tilde{u}_c \cdot \tanh(\tilde{u}_c^{-1} \cdot u^*) \tag{6.72}$$

6.4.1.1 Input constraints handling

The algebraic MPC problem with input constraints can be expressed as:

$$J_0(x_0, U) = x_N^T \cdot P \cdot x_N + \sum_{k=0}^{N-1} x_k^T \cdot Q \cdot x_k + \varphi(u_k)^T \cdot R \cdot \varphi(u_k) \tag{6.73}$$

The state equations along the prediction horizon can be written as follows.

$$X = S_x * x_0 + S_U * \varphi(u) \tag{6.74}$$

$$X = \begin{bmatrix} x_0 \\ \vdots \\ x_N \end{bmatrix}, U = \begin{bmatrix} u_0 \\ \vdots \\ u_N \end{bmatrix} \tag{6.75}$$

$$S_x = \begin{bmatrix} I \\ A \\ . \\ . \\ . \\ A^N \end{bmatrix}, S_U = \begin{bmatrix} 0 & 0 & . & 0 \\ B & 0 & . & 0 \\ AB & . & . & . \\ . & . & . & . \\ A^{N-1}B & . & . & B \end{bmatrix} \tag{6.76}$$

Accordingly, the cost function can be written as follows.

$$J_0(x_0, U) = \varphi(U)^T H \varphi(U) + 2x_0^T F \varphi(U) + x_0^T Y x_0 \tag{6.77}$$

Where

$$H = S_U^T * \bar{Q} * S_U + R, F = S_X^T * \bar{Q} * S_U, Y = S_X^T * \bar{Q} * S_X \tag{6.78}$$

By taking the gradient (slope) of the cost function, the equation to obtain the control sign is obtained:

$$\begin{aligned} &\nabla_u J(x_0) = 2H \cdot \left[\tilde{U}_c \tilde{U}_c^{-1} \text{sech}^2\left(\tilde{U}_c^{-1} U\right)\right] \cdot \left[\tilde{U}_c \tanh\left(\tilde{U}_c^{-1} U\right)\right] \\ &+2x_0^T F \cdot \left[\tilde{U}_c \tilde{U}_c^{-1} \text{sech}^2\left(\tilde{U}_c^{-1} U\right)\right] = 0 \end{aligned} \tag{6.79}$$

The control sign can be obtained by factoring the equation:

$$\nabla_u J(x_0) = \text{sech}^2\left(\tilde{U}_c^{-1} U\right) \cdot \left(2H\left[\tilde{U}_c \tanh\left(\tilde{U}_c^{-1} U\right)\right] + 2x_0^T F\right) = 0 \tag{6.80}$$

$$\tanh\left(\widetilde{U}_c^{-1}U\right) = -\widetilde{U}_c^{-1}H^{-1}F^T x_0 \tag{6.81}$$

Tanh is applied to both sides of the equation:

$$\tanh\left[\alpha_1 \cdot \tanh\left(\widetilde{U}_c^{-1}U\right)\right] = \tanh\left[-\alpha_1 \cdot \widetilde{U}_c^{-1}H^{-1}F^T x_0\right] \tag{6.82}$$

In this equation, α_1 is an adjustable coefficient matrix. In this way, it is guaranteed that both sides of the equation are in the range $(-1,1)$.

$$\widetilde{U}_c^{-1}U = \tanh^{-1}\left(\tanh\left[-\alpha_1 \cdot \widetilde{U}_c^{-1}H^{-1}F^T x_0\right]\right) \tag{6.83}$$

Leaving U alone, the suboptimal solution for MPC is obtained under input constraint.

$$U_u^* = K_U \cdot x_0, K_U = -\alpha_1 H^{-1}F^T \tag{6.84}$$

Where K_U is adjustable parameter.

The proposed method provides adjustable parameters for the designer. By using α_1, the designer can use it for performance tuning in different applications.

Input constraints handling tracking revision for augmented matrices

If we replace the S_x and S_U matrices in Equation 6.56 with the matrices in Augmented Model Predictive Control, we get the following matrices.

$$S_E = \begin{bmatrix} C \\ CA \\ . \\ . \\ . \\ CA^N \end{bmatrix}, S_{UE} = \begin{bmatrix} 0 & 0 & . & 0 \\ CB & 0 & . & 0 \\ CAB & . & . & . \\ . & . & . & . \\ CA^{N-1}B & . & . & CB \end{bmatrix} \tag{6.85}$$

After revising the S_x and S_U matrices, it is necessary to turn the X matrix into error regulation (tracking). For this reason, it is necessary to arrange the X matrix in 6.55 as follows.

$$E = \begin{bmatrix} ref - x_0 \\ \vdots \\ ref - x_N \end{bmatrix} \tag{6.86}$$

When we put the state equation matrix in 6.54 into the tracking form with the augmented matrix, we get the equation in 6.66.

$$Y = S_E * (ref - y_0) + S_{UE} * \varphi(u) \tag{6.87}$$

In this case, the control signal for the algebraic model predictive control expressed with augmented matrices is as follows.

$$\Delta U_u^* = K_{UE} \cdot (ref - y_0), K_{UE} = -\alpha_1 H_E^{-1} F_E^T \tag{6.88}$$

Here

$$H_E = S_{UE}^T * \bar{Q} * S_{UE} + R, F_E = S_E^T * \bar{Q} * S_{UE} \tag{6.89}$$

6.4.1.2 State constraints handling

If we write the state equations expressed along the prediction horizon by restricting it to the tanh operation and if we put U* as control signal, we get the following equation.

$$X = \tilde{X}_c * tanh\left(\tilde{X}_c^{-1} * [S_x * x_0 + S_U * \varphi(U_u^*)]\right) \tag{6.90}$$

If we insert U^* as the control signal in equation 6.54 and write this equation together with equation 6.64, we get equation 6.65.

$$S_x * x_0 + S_U * \varphi(U^*) = \tilde{X}_c * tanh\left(\tilde{X}_c^{-1} * [S_x * x_0 + S_U * \varphi(U_u^*)]\right) \tag{6.91}$$

At this point U^*can be written as a function of U_u^*.

$$tanh\left(\tilde{U}_c^{-1} * U\right) = \tilde{U}_c^{-1} * S_U^+ \left[\tilde{X}_c{}^T * tanh\left(\tilde{X}_c^T * [S_x * x_0 + S_U * \varphi(U_u^*)]\right) - S_x * x_0\right] \tag{6.92}$$

Where S_U^+ is Moore-Penrose pseudoinverse of nonsquare S_U matrix.

$$U^* = \tilde{U}_c \tanh^{-1}\left(tanh\left(\propto_2 \tilde{U}_c^{-1} * S_U^+ \left[\tilde{X}_c{}^T * tanh\left(\tilde{X}_c^T * [S_x * x_0 + S_U * \varphi(U_u^*)]\right) - S_x * x_0\right]\right)\right) \tag{6.93}$$

State constraints handling tracking revision for augmented matrices

In order to revise the State Constraint approach according to the Augmented Model Predictive method, the revisions made in the Input Constraint approach should be made first. For this, the matrices must be changed as in 6.67. After these operations are done, the State Constraint solution is obtained as follows.

$$\begin{aligned} tanh\left(\tilde{U}_c^{-1} * U\right) = \tilde{U}_c^{-1} \\ * S_U^+ \left[\tilde{E}_c{}^T * tanh\left(\tilde{E}_c^T * [S_E * (ref - y_0) + S_{UE} * \varphi(U_u^*)]\right)\right. \\ \left. - (ref - y_0)\right] \end{aligned} \tag{6.94}$$

Here

$$\tilde{E}_c = blkdiag\{\tilde{e}_c, \dots, \tilde{e}_c\}, \tilde{e}_c = diag\{(ref - x_{c_1}), \dots, (ref - x_{c_n})\} \tag{6.95}$$

If Equation 6.76 is written together with 6.77, the control signal for the Algebraic Augmented Model Predictive can be expressed by the following equation.

$$\begin{aligned} \Delta U^* = \tilde{U}_c \tanh^{-1}\Big(tanh\Big(\propto_2 \tilde{U}_c^{-1} \\ * S_{UE}^+ \left[\tilde{E}_c{}^T * tanh\left(\tilde{E}_c{}^T * [S_E * e + S_{UE} * \varphi(U_u^*)]\right) - S_E * e\right]\Big)\Big) \end{aligned} \tag{6.96}$$

Here

$$e = ref - y_0 \tag{6.97}$$

6.4.2 Automatic landing with input constraint AMPC controller

Algebraic Model Predictive Control is a solution method that numerically solves the Model Predictive Control problem with an algebraic approach. This method, which uses the system's state-space matrices, uses the saturation-like and differentiable tanh function to handle the constraints. Within the scope of the thesis, for a solution that follows the reference and does not have a steady state error, the system matrices are replaced with augmented matrices and integral action is added to the system. In the input constraint solution, a control signal is determined by assuming that the system has only input constraints, and the calculation of this signal can be calculated completely offline.

6.4.2.1 Longitudinal autopilot

In order for the Algebraic Model Predictive Control response to be comparable to the Model Predictive Control response, the weighting matrices are taken the same as the Model Predictive Control. In the longitudinal autopilot design, altitude and speed hold autopilot are designed. Theta reference was obtained by passing the altitude error PI control, the Algebraic Model Predictive Control structure was used for Theta and Speed holding as the inner loop controller. (Figure 6.34)

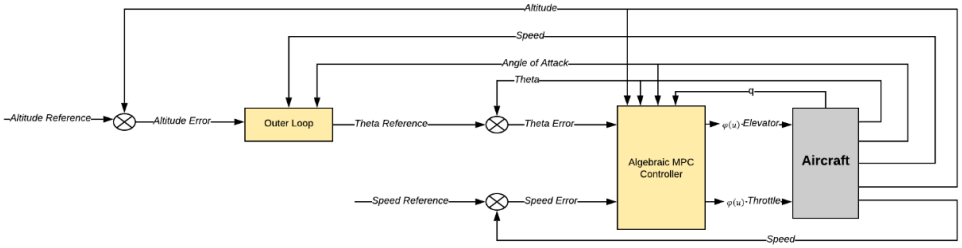

Figure 6.34 : Longitudinal Algebraic Model Predictive Control Scheme.

The Q and R weighting matrices for the Algebraic Model Predictive Control are defined as follows.

$$Q = \begin{bmatrix} 0.00443 & 0 \\ 0 & 684.7243 \end{bmatrix} R = \begin{bmatrix} 68.889 & 0 \\ 0 & 0.04 \end{bmatrix} \quad (6.98)$$

If we examine the performance of the longitudinal part of the automatic landing autopilot designed with algebraic MPC; Figure 6.35 shows altitude hold, pitch hold, and speed hold throughout the entire descent. The performance is expected to be basically similar as the weighting matrices of the algebraic MPC are chosen to be the same as the MPC controller. When the altitude hold is examined in general, although it is seen as similar, the performance in speed holding is seen to be lower than MPC. The reason for this is thought to be the offline calculation of the gain in the input constraint solution, unlike MPC. The performance in altitude grip is seen as similar to the classical solution and the performance of the altitude grip is considered sufficient after the flare transition and there is no loss in theta grip. It is seen that the vertical speed converges around 0 fpm until the moment of landing, which is important for the aircraft to put wheels on the runway smoothly. With the flare, there is an error of the order of 2 knots in holding the speed, although this speed is higher than the reference, it is sufficient for the aircraft not to rise after landing. (Figure 6.36) During the design,

the speed commanded here is at the speed at which the lift will not stay, ensuring that it does not rise again in this situation.

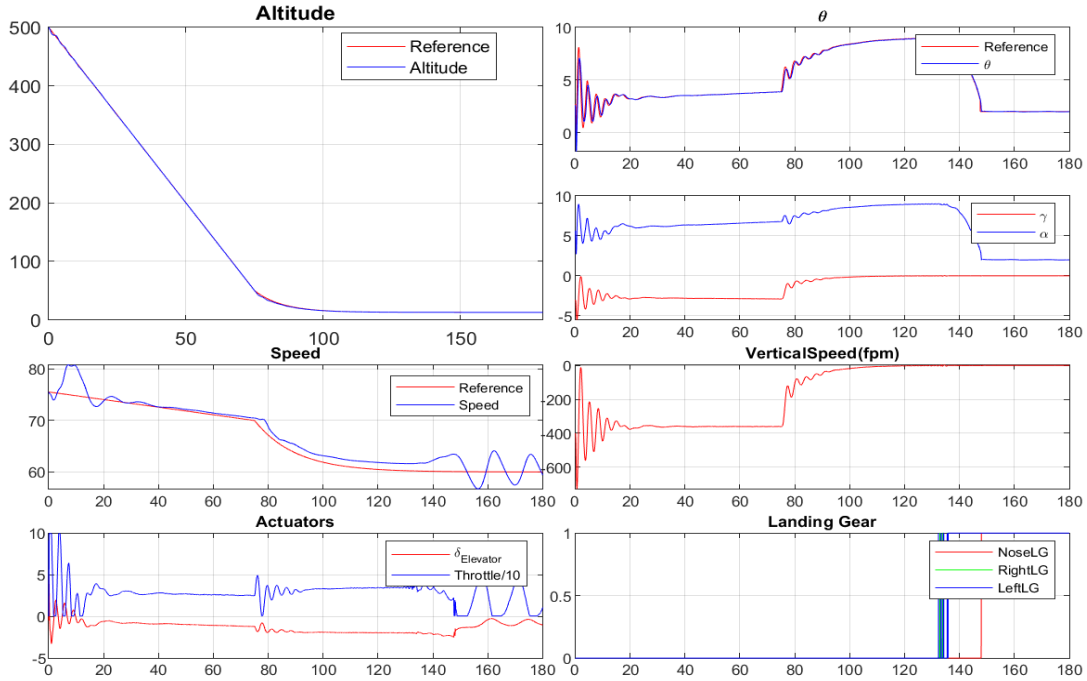

Figure 6.35 : Longitudinal Performance (Input Constraint AMPC Controller).

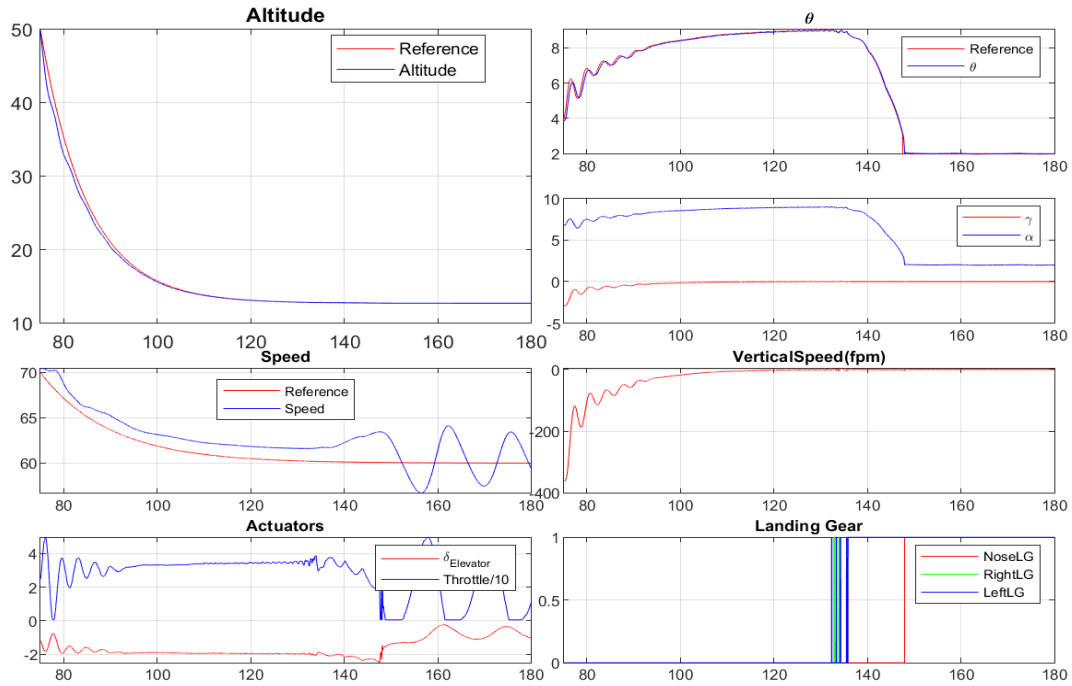

Figure 6.36 : Longitudinal Performance at Flare (Input Constraint AMPC Controller).

6.4.2.2 Lateral autopilot

In order for the Algebraic Model Predictive Control response to be comparable to the Model Predictive Control response, the weighting matrices are taken the same as the Model Predictive Control. In the lateral autopilot design, heading angle and sideslip(beta) hold autopilot are designed. Roll reference was obtained by passing the heading error, the Algebraic Model Predictive Control structure was used for Roll and Beta holding as the inner loop controller. (Figure 6.37)

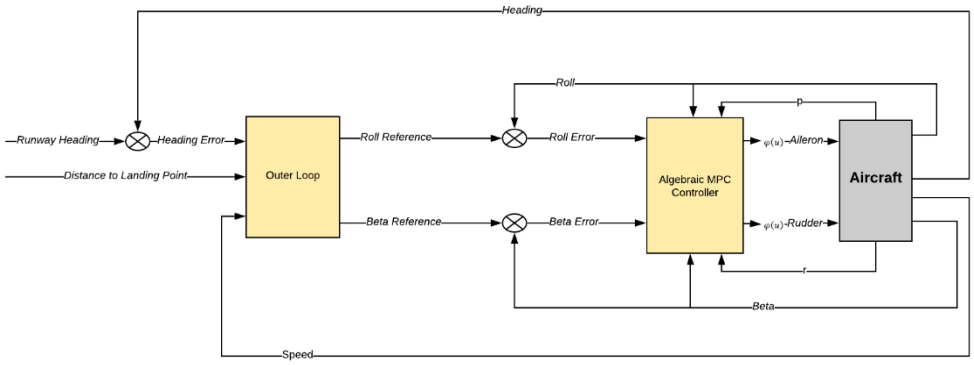

Figure 6.37 : Lateral Algebraic Model Predictive Control Scheme.

The Q and R weighting matrices for the Model Predictive Control are defined as follows.

$$Q = \begin{bmatrix} 4 & 0 \\ 0 & 1 \end{bmatrix} R = \begin{bmatrix} 500 & 0 \\ 0 & 500 \end{bmatrix} \quad (6.99)$$

If we examine the performance of the lateral part of the landing autopilot designed with an algebraic MPC controller; The performance of the outer loop structure, which ensures that the aircraft is in the same direction with the runway, is seen when the difference is around 0 degrees at the time of landing. In this structure, it is provided by the roll tracking of the heading angle reference before the flare, and it is provided by the beta tracking after the flare. It is seen that the beta reference grows as it approaches the landing moment, where the beta tracking is in accordance with the reference and there is no phase shift that would cause a loss or oscillation. This increase in the beta reference is thought to be due to the ground effect, which increases with approaching the ground. The performance in roll holding is considered sufficient both before and

after flare, and there is no loss between the reference roll and the feedback. (Figure 6.38, Figure 6.39)

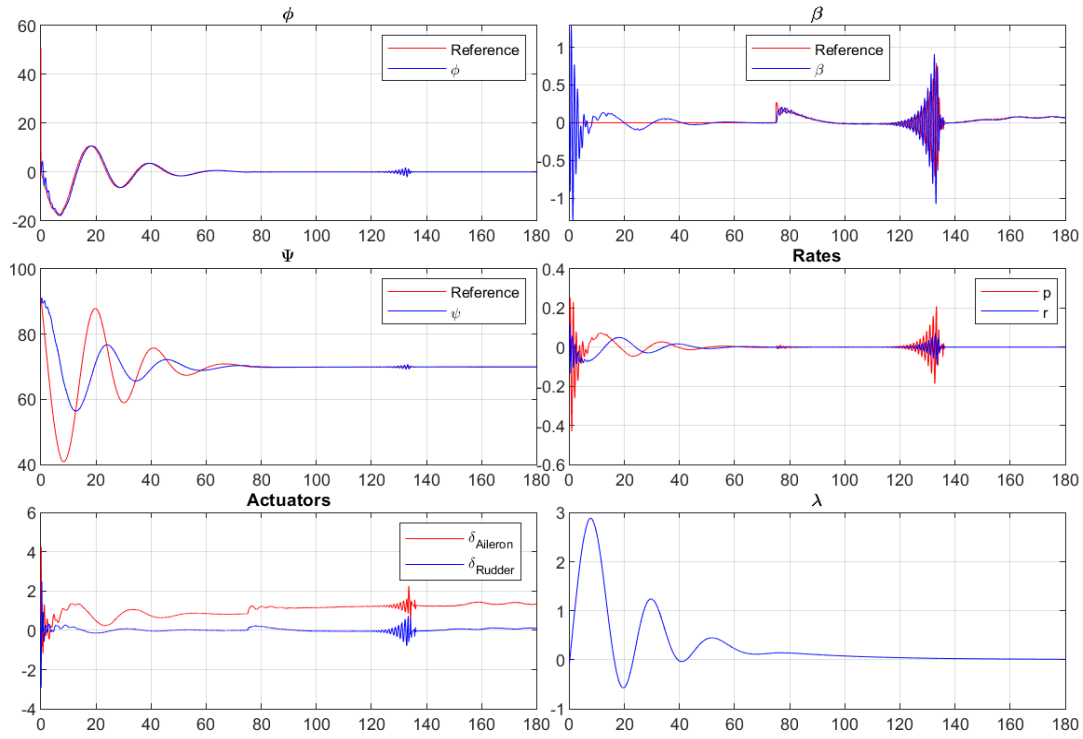

Figure 6.38 : Lateral Performance (Input Constraint AMPC Controller).

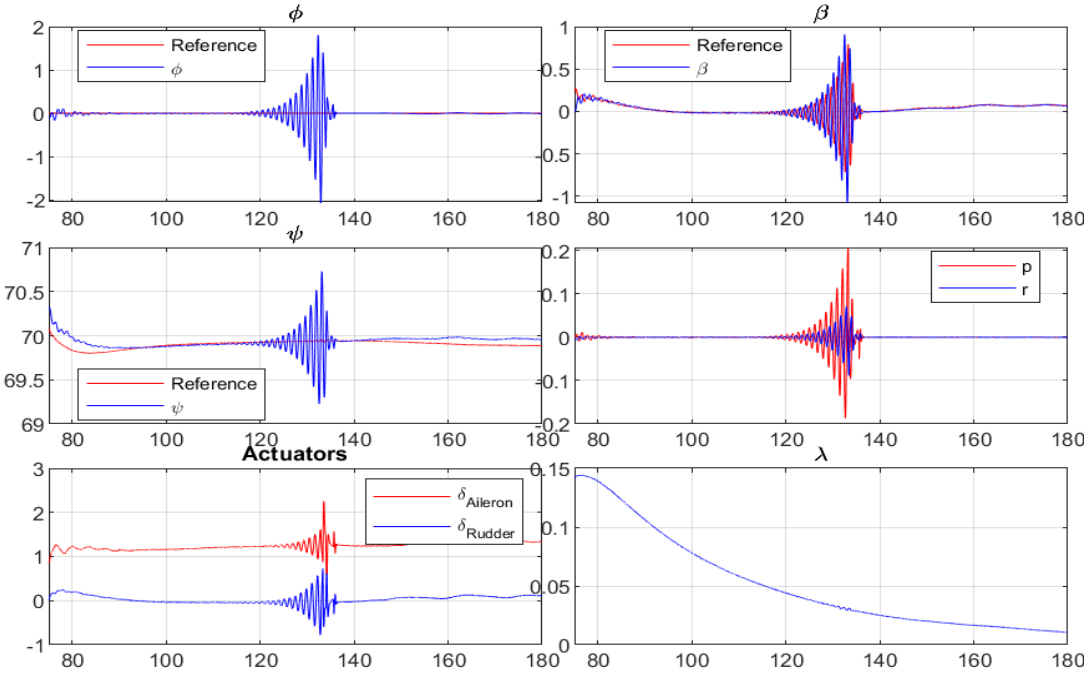

Figure 6.39 : Lateral Performance at Flare (Input Constraint AMPC Controller).

6.4.3 Automatic landing with state constraint AMPC controller

In the State Constraint approach of the Algebraic Model Predictive Control method, unlike the Input Constraint approach, the constraints for the states of the system are used to determine the control signal. In Section 0, a revision of the State Constraint solution with augmented state space matrices was made and this revision was also used in the automatic descent algorithm. In this case, the constraints are not added directly to the states, but to the difference (error) of the states by reference. Another factor that distinguishes the State Constraint Algebraic Model Predictive Control method from the Input Constraint method is that online calculation is effective in determining the control signal. Here, although some of the parameters can be determined offline, the final control signal is obtained with the online solution.

While the system is running for $0.0005s$, the sampling time of the control structure is chosen as $0.02s$. In the Model Predictive Control problem, the prediction horizon is 40 steps and the control horizon is 1 step. However, the average solution speed of the problem was $9.07177535829346 * 10^{-6}s$. It is seen that the solution speed of the AMPC problem is 2204.64 times the sampling time of the controller.

In the state constraint MPC structure, the weighting matrices are taken the same as the MPC, and it is considered sufficient that the main gain is the increase in the solution speed of the problem. Although an improvement in performance is not expected due to its basic structure, an increase in performance when the control surfaces reach saturation has been observed in the previous study on this subject [50].

6.4.3.1 Longitudinal autopilot

In order for the Algebraic Model Predictive Control response to be comparable to the Model Predictive Control response, the weighting matrices are taken the same as the Model Predictive Control. In the longitudinal autopilot design, altitude and speed hold autopilot are designed. In this control structure, fixed gains are used in the outer loop and these gains are taken in the same way in the previous control structures, the values are given in Figure 6.40.

The Q and R weighting matrices for the Algebraic Model Predictive Control are defined as follows.

$$Q = \begin{bmatrix} 0.00443 & 0 \\ 0 & 684.7243 \end{bmatrix}, R = \begin{bmatrix} 68.889 & 0 \\ 0 & 0.04 \end{bmatrix} \quad (6.100)$$

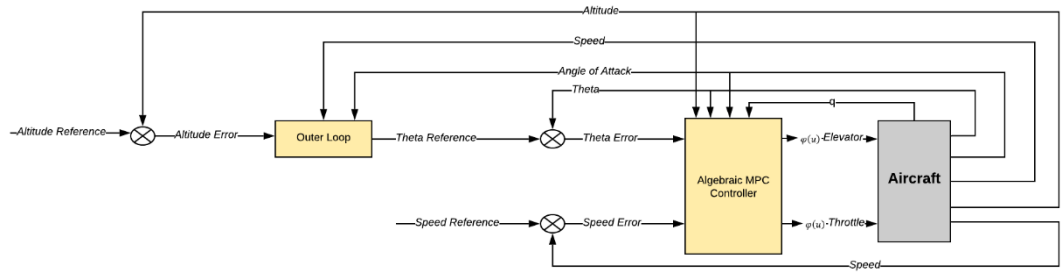

Figure 6.40 : Longitudinal Algebraic Model Predictive Control Scheme.

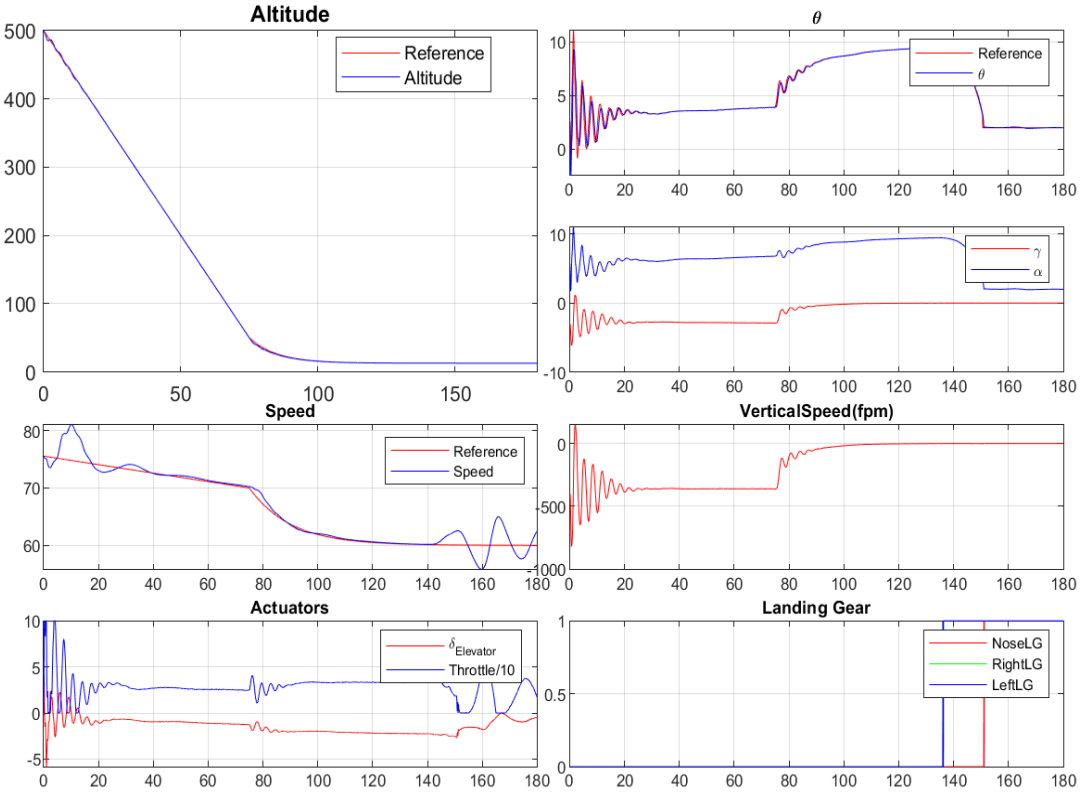

Figure 6.41 : Longitudinal Performance (State Constraint AMPC Controller).

If we examine the performance of the longitudinal part of the automatic landing autopilot designed with the State Constarint Algebraic MPC; Figure 6.41 shows altitude hold, pitch hold, and speed hold throughout the entire descent. With the start of the landing simulation, there is a damped oscillation as can be seen in the aircraft control surface behavior, this is because the control surfaces are not in the trim condition at the start of the simulation. In a purely autopilot design, this will not occur

as the initial conditions for the control surfaces will be the conditions prior to the descent transition. Until the transition to the flare phase, a successful performance is observed in both speed hold and altitude hold, with the transition, the theta reference is given so that the vertical speed of the aircraft is 0 and the aircraft successfully follows this reference. However, it is seen that the exponential decrease in the speed reference during the transition is also followed successfully, here with the advantage of being a multi-input multi-output controller structure, the couple effects do not predominantly affect the behavior of the system. With the vertical velocity (vario) reference coming around 0 before landing, it appears that wheeling can be accomplished with low fpms. (Figure 6.42)

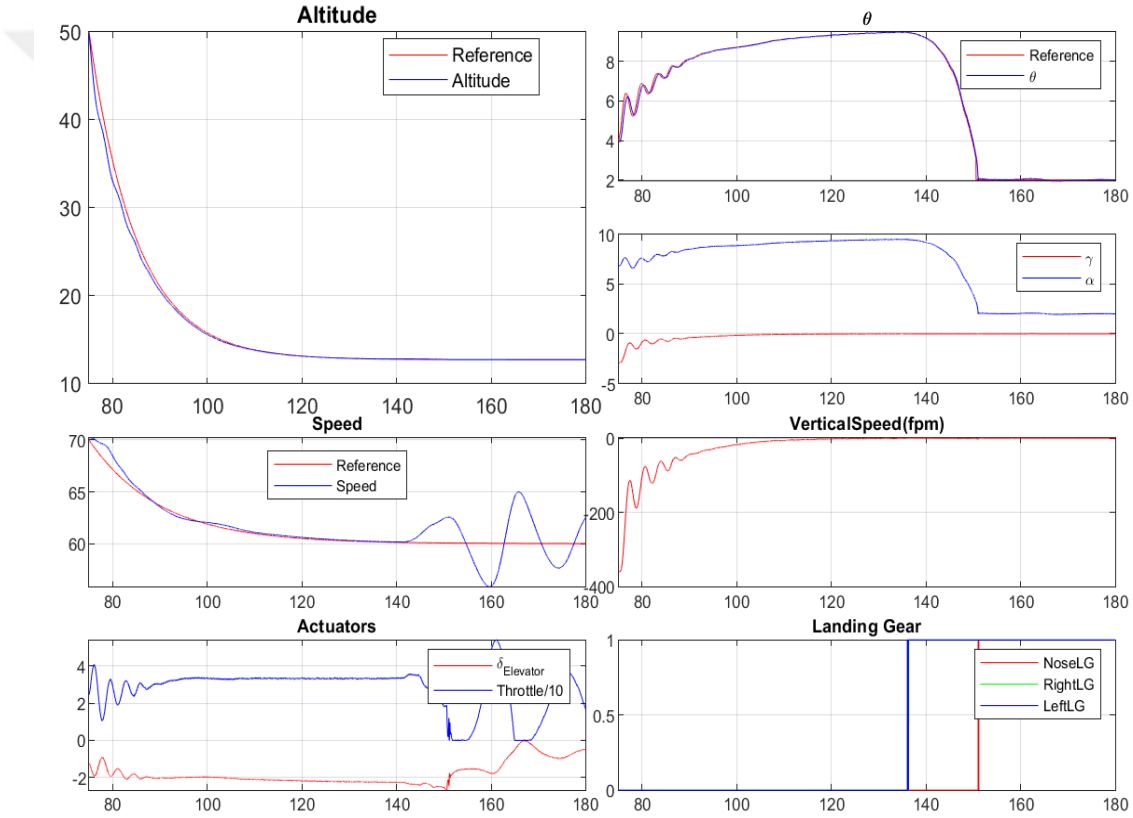

Figure 6.42 : Longitudinal Performance at Flare (State Constraint AMPC Controller).

6.4.3.2 Lateral autopilot

In order for the Algebraic Model Predictive Control response to be comparable to the Model Predictive Control response, the weighting matrices are taken the same as the Model Predictive Control. In the lateral autopilot design, heading angle and

sideslip(beta) hold autopilot are designed. Roll reference was obtained by passing the heading error, the Algebraic Model Predictive Control structure was used for Roll and Beta holding as the inner loop controller. (Figure 6.43)

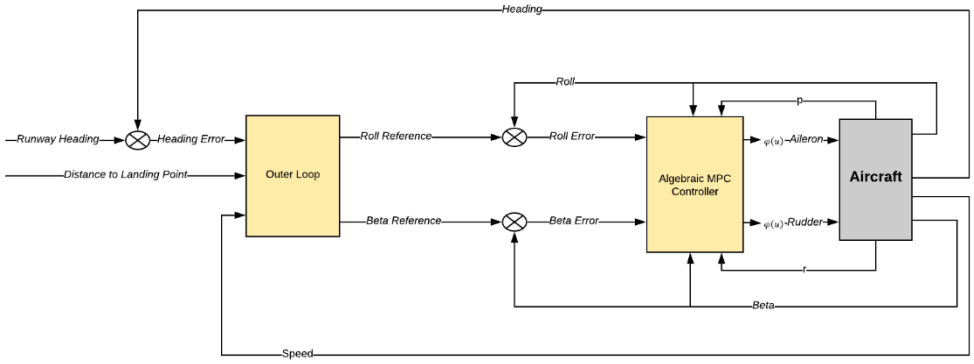

Figure 6.43 : Lateral Algebraic Model Predictive Control Scheme.

The Q and R weighting matrices for the Model Predictive Control are defined as follows.

$$Q = \begin{bmatrix} 4 & 0 \\ 0 & 1 \end{bmatrix} R = \begin{bmatrix} 500 & 0 \\ 0 & 500 \end{bmatrix} \tag{6.101}$$

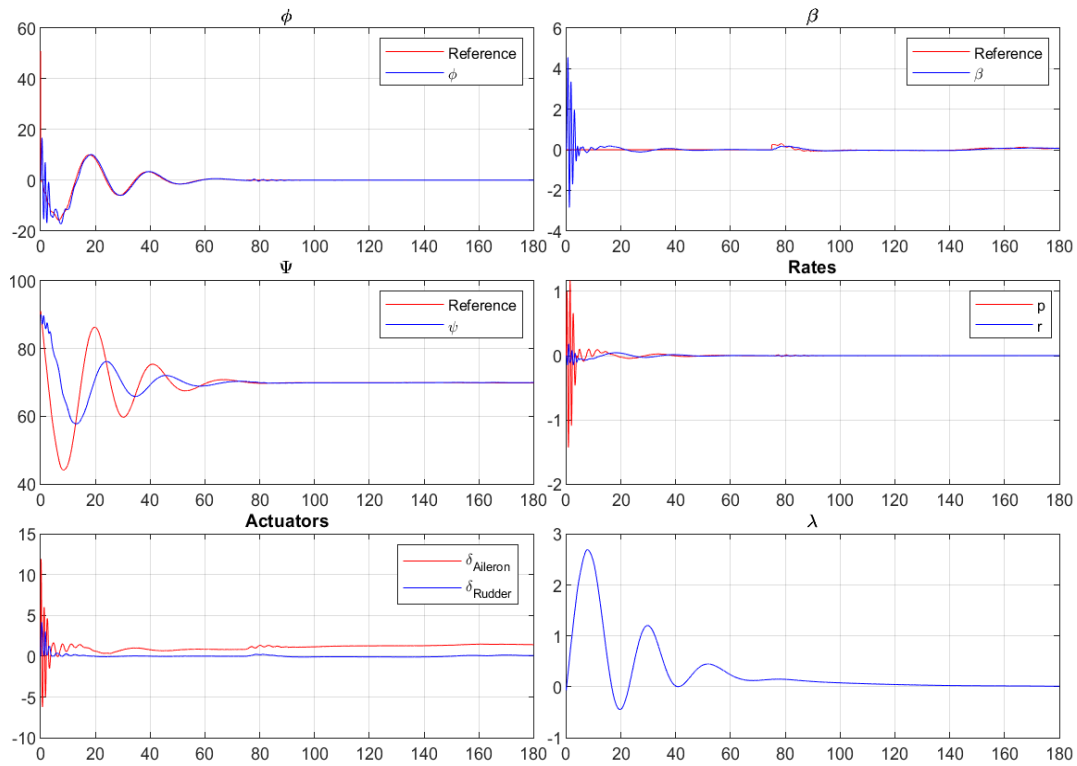

Figure 6.44 : Lateral Performance (State Constraint AMPC Controller).

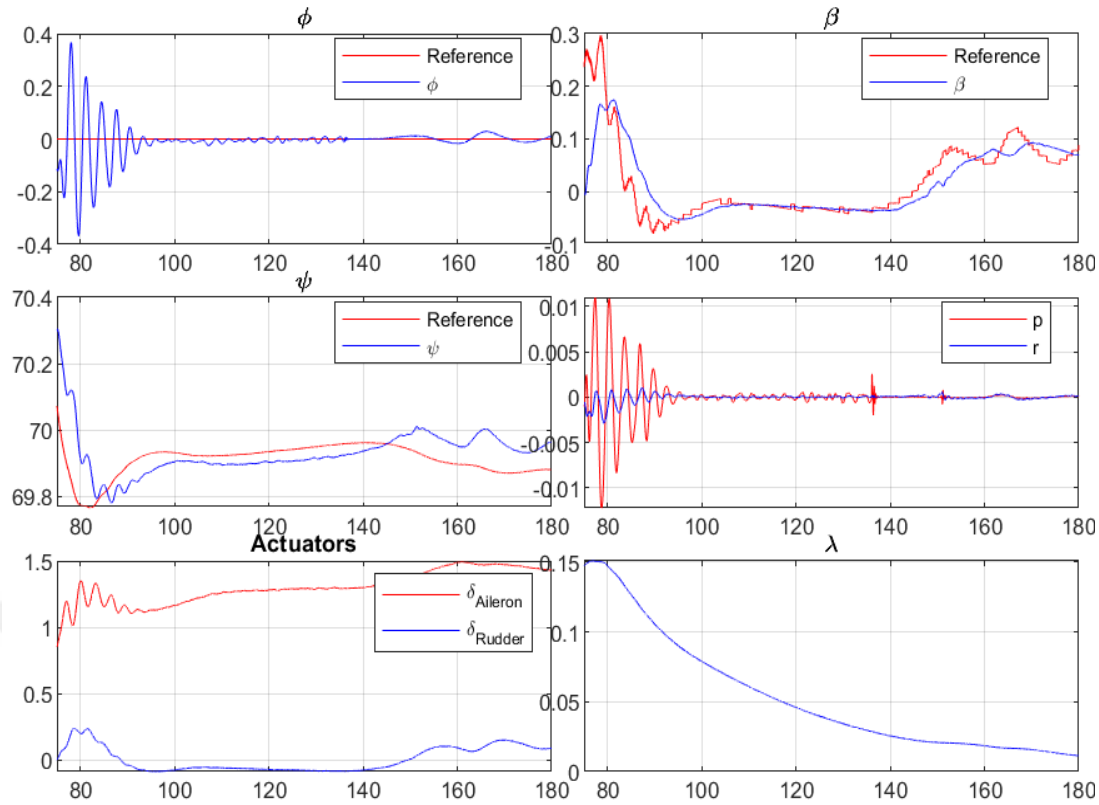

Figure 6.45 : Lateral Performance at Flare (State Constraint AMPC Controller).

If we examine the performance of the lateral part of the landing autopilot designed with an algebraic MPC controller; With the start of the landing simulation, there is a damped oscillation as can be seen in the aircraft control surface behavior, this is because the control surfaces are not in the trim condition at the start of the simulation. (Figure 6.44) In an autopilot design to be made for the entire envelope of flight, this will not occur as the initial conditions for the control surfaces will be the conditions prior to the descent transition. The roll tracking of the aircraft is seen to be successful both before and after the flare. Accordingly, it is seen that the heading holding error before the flare is getting smaller and smaller. It is seen that the beta tracking of the aircraft successfully follows the fixed 0 reference before the flare and the beta reference produced by the heading error after the flare, the lateral speed of the aircraft, the runway and the aircraft position. (Figure 6.45)

7. RESULTS

During the thesis, an automatic landing autopilot was designed with a total of 5 different control methods. These methods are respectively: PID, LQI, MPC, Input Constraint AMPC, State Constraint AMPC.

PID control method is a single-input single-output control system, the purpose of designing an automatic landing autopilot with this method is to prove that landing can be done safely with a classical feedback method, which is frequently used in the industry.

LQI control method is a multi-input multi-output control system, the purpose of designing an automatic landing autopilot with this method is to prove that an automatic landing autopilot can be designed with an integral action reference tracking.

MPC control method is a multi-input multi-output control system, augmented system matrices are used to add integral effect to the system while designing the automatic landing autopilot with this method. The resulting structure is similar to LQI, resetting the error and regulating the states. The purpose of designing an automatic landing autopilot with this method is to see the effect of using online control signals on performance and to determine the ratio of the calculation time to the system cycle. Here, the calculation time is important for the healthy control of the system.

Input Constraint AMPC control method is a multi-input multi-output control system, although it is similar to the classical state-space MPC control system with this method, it makes a difference as it can be calculated completely offline and provides a numerical solution by using an algebraic function in determining the optimal gain.

The State Constraint AMPC control method is a multi-input multi-output control system. With this method, similar to the classical state-space MPC control system, several parameters can be determined offline, but reaching the numerical solution using an algebraic function increases the computation speed of the control system.

It has been tested on a non-linear model for performance measurement of control systems. In addition, the responses of all control systems and their performance in

reference tracking have been examined, not only when the system is completely healthy, but also under various disturbance and structural deformation conditions.

The system test conditions are as follows:

- Windshear: on, off.
- Turbulance: no turbulance, light turbulance, moderate turbulance.
- Damage state: no damage, rudder off, vertical tail off, left outboard flap off, left wingtip off, left elevator off, left stabilizer off.
- Damage time: glide start, flare start, touchdown start.
- Wind speed: 0, 5, 10, 15, 20, 25.
- Wind degree: 0, 60, 120, 180, 240, 300.

Within the scope of the tests, tests were carried out for each controller under 4536 test conditions and a total of 22680 test conditions. Certain restrictions are placed on the evaluation of the test matrix:

- The altitude hold error is 5 meters below the all landing, the altitude hold error is 3 meters below the Flare phase.
- Speed hold error under 10 knots during the all landing, speed hold error under 5 knots in the Flare phase.
- Vario under 200 fpm when wheeled.
- The heading hold error is 20 degrees below the entire landing, the heading hold error is 10 degrees below the Flare phase.
- Lambda value less than 1 degree at the time of putting the wheel.

As a result of all tests, the performances of the controllers are as Table 7.1.

If we evaluate the test results;

- PID controller, which is a single-input single-output controller, is seen as the most unsuccessful in terms of performance.
- LQI controller, which is a classical feedback and multi-input multi-output controller, gives more successful results than PID controller. The reason for

this is that it can be effective in controlling feedback with different control surfaces, especially in control surface (partial or complete) losses.

- The MPC controller is constantly calculating gains to revise the control signal, so higher performance is expected before the problem is addressed. The results are also in line with expectations.
- The performance of algebraic MPC's input constraint solution seems to be lower than that of classical MPC, one of the reasons for this is that there is no online optimization. However, the LQI seems to be successful compared to the controller, the performance of the Input Constraint AMPC in saturation control surface conditions is also seen in [50].

  State Constraint AMPC, on the other hand, is the most successful among the 5 controllers, where the ideal control signal is determined more ideally due to online optimization, and its applicability is seen to be high in real platform applications with its high-speed solution capability from MPC.

Table 7.1 : Controller Compare.

Controller	Total Succesful Landing	Total Test - Successful Landing Rate
PID	369	%8.13
LQI	498	%10.98
MPC	1050	%23.15
AMPC (Input Constraint)	918	%20.24
AMPC (State Constraint)	1281	%28.40

REFERENCES

[1] **McLean, D.** (2003). Automatic flight control systems. *Measurement and Control*, *36*(6), 270–310. https://doi.org/10.1177/002029400303600602

[2] **Singh, S., & Padhi, R.** (2009). Automatic path planning and control design for autonomous landing of UAVs using dynamic inversion. *Proceedings of the American Control Conference*. https://doi.org/10.1109/ACC.2009.5160444

[3] **Juang, J. G., & Cheng, K. C.** (2006). Application of neural networks to disturbances encountered landing control. *IEEE Transactions on Intelligent Transportation Systems*, *7*(4). https://doi.org/10.1109/TITS.2006.884885

[4] **Lungu, M.** (2020). Backstepping and dynamic inversion combined controller for auto-landing of fixed wing UAVs. *Aerospace Science and Technology*, *96*. https://doi.org/10.1016/j.ast.2019.105526

[5] **Lungu, M.** (2019). Auto-landing of fixed wing unmanned aerial vehicles using the backstepping control. *ISA Transactions*, *95*. https://doi.org/10.1016/j.isatra.2019.05.019

[6] **Kato, A., & Inagaki, Y.** (2008). Control law for automatic landing using fuzzy-logic control. *Transactions of the Japan Society for Aeronautical and Space Sciences*, *50*(170). https://doi.org/10.2322/tjsass.50.274

[7] **Lungu, M., & Lungu, R.** (2019). Autonomous Adaptive Control System for Airplane Landing. *Asian Journal of Control*, *21*(3). https://doi.org/10.1002/asjc.1810

[8] **Lu, K., & Liu, C.** (2019). A L1 adaptive control scheme for UAV carrier landing using nonlinear dynamic inversion. *International Journal of Aerospace Engineering*, *2019*. https://doi.org/10.1155/2019/6917393

[9] **Rossiter, J. A.** (2017). Model-based predictive control: A practical approach. In *Model-Based Predictive Control: A Practical Approach*. https://doi.org/10.1201/9781315272610

[10] **Clarke, D. W., Mohtadi, C., & Tuffs, P. S.** (1987). Generalized predictive control-Part I. The basic algorithm. *Automatica*, *23*(2). https://doi.org/10.1016/0005-1098(87)90087-2

[11] **Kothare, S. L. D. O., & Morari, M.** (2000). Contractive model predictive control for constrained nonlinear systems. *IEEE Transactions on Automatic Control*, *45*(6). https://doi.org/10.1109/9.863592

[12] **Muske, K. R., & Rawlings, J. B.** (1993). Model predictive control with linear models. *AIChE Journal*, *39*(2). https://doi.org/10.1002/aic.690390208

[13] **Henson, M. A.** (1998). Nonlinear model predictive control: Current status and future directions. *Computers and Chemical Engineering*, *23*(2). https://doi.org/10.1016/S0098-1354(98)00260-9

[14] **Morari, M., & H. Lee, J.** (1999). Model predictive control: Past, present and future. *Computers and Chemical Engineering*, *23*(4–5). https://doi.org/10.1016/S0098-1354(98)00301-9

[15] **García, C. E., Prett, D. M., & Morari, M.** (1989). Model predictive control: Theory and practice-A survey. *Automatica*, *25*(3). https://doi.org/10.1016/0005-1098(89)90002-2

[16] **Mayne, D. Q., Rawlings, J. B., Rao, C. V., & Scokaert, P. O. M.** (2000). Constrained model predictive control: Stability and optimality. *Automatica*, *36*(6). https://doi.org/10.1016/S0005-1098(99)00214-9

[17] **Wang, Y., & Boyd, S.** (2010). Fast model predictive control using online optimization. *IEEE Transactions on Control Systems Technology*, *18*(2). https://doi.org/10.1109/TCST.2009.2017934

[18] **Oravec, J., Jiang, Y., Houska, B., & Kvasnica, M.** (2017). Parallel Explicit MPC for Hardware with Limited Memory. *IFAC-PapersOnLine*, *50*(1). https://doi.org/10.1016/j.ifacol.2017.08.506

[19] **Kvasnica, M., Bakaráč, P., & Klaučo, M.** (2019). Complexity reduction in explicit MPC: A reachability approach. *Systems and Control Letters*, *124*. https://doi.org/10.1016/j.sysconle.2018.12.002

[20] **Bemporad, A., Borrelli, F., & Morari, M.** (2002). Model predictive control based on linear programming - The explicit solution. *IEEE Transactions on Automatic Control*, *47*(12). https://doi.org/10.1109/TAC.2002.805688

[21] **Kale, M. M., & Chipperfield, A. J.** (2005). Stabilized MPC formulations for robust reconfigurable flight control. *Control Engineering Practice*, *13*(6). https://doi.org/10.1016/j.conengprac.2004.09.001

[22] **Gopinathan, M., Boskovic, J. D., Mehra, R. K., & Rago, C.** (1998). Multiple model predictive scheme for fault-tolerant flight control design. *Proceedings of the IEEE Conference on Decision and Control*, *2*. https://doi.org/10.1109/cdc.1998.758477

[23] **Maciejowski, J. M., & Jones, C. N.** (2003). MPC fault-tolerant flight control case study: Flight 1862. *IFAC Proceedings Volumes (IFAC-PapersOnline)*, *36*(5). https://doi.org/10.1016/S1474-6670(17)36480-7

[24] **Garcia, G. A., & Keshmiri, S.** (2011). Nonlinear model predictive controller for navigation, guidance and control of a fixed-wing UAV. *AIAA Guidance, Navigation, and Control Conference 2011*. https://doi.org/10.2514/6.2011-6310

[25] **Gros, S., Quirynen, R., & Diehl, M.** (2012). Aircraft control based on fast non-linear MPC & multiple-shooting. *Proceedings of the IEEE Conference on Decision and Control*. https://doi.org/10.1109/CDC.2012.6426439

[26] **Wolowicz, C. H., Bowman, J. S., & Gilbert, W. P.** (1979). SIMILITUDE REQUIREMENTS AND SCALING RELATIONSHIPS AS APPLIED TO MODEL TESTING. In *NASA Technical Paper* (Issue 1435).

[27] MIL-F-8785C: Flying Qualities of Piloted Airplanes. (1980). In *United States Department of Defense* (Issues MIL-F-8785C).

[28] **Bossert, D. E., Morris, S. L., Hallgren, W. F., & Yechout, T. R.** (2003). Introduction to Aircraft Flight Mechanics. In *Introduction to Aircraft Flight Mechanics*. https://doi.org/10.2514/4.862069

[29] **Federal Aviation Administration**. (2016). Airplane Flying Handbook. *U.S. Department of Transportation*.

[30] **Conway, E.** (2006). Blind landings: Low-visibility operations in American aviation, 1918-1958. In *Blind Landings: Low-Visibility Operations in American Aviation, 1918-1958*. https://doi.org/10.5860/choice.44-5075

[31] **Diamond, H., & Dunmore, F. W.** (1930). A RADIO SYSTEM FOR BLIND LANDING OF AIRCRAFT IN FOG. *Proceedings of the National*

Academy of Sciences, *16*(11). https://doi.org/10.1073/pnas.16.11.678

[32] **Goblet, V., Fala, N., & Marais, K.** (2015). Identifying phases of flight in general aviation operations. *15th AIAA Aviation Technology, Integration, and Operations Conference*. https://doi.org/10.2514/6.2015-2851

[33] **Commercial Aviation Safety Team / Common Taxonomy Team**. (2013). *Phase of Flight: Definitions and Usage Notes: Vol. 1.3* (Issue April).

[34] **McRuer, D., & Graham, D.** (1981). Eighty years of flight control - Triumphs and pitfalls of the systems approach. *Journal of Guidance, Control, and Dynamics*, *4*(4). https://doi.org/10.2514/3.19743

[35] **Stevens, B. L., Lewis, F. L., & Johnson, E. N.** (2015). Aircraft control and simulation: Dynamics, controls design, and autonomous systems: Third edition. In *Aircraft Control and Simulation: Dynamics, Controls Design, and Autonomous Systems: Third Edition*. https://doi.org/10.1002/9781119174882

[36] **Nelson, R. C.** (1989). Flight Stability and Automatic Control. In *Book*.

[37] **Military Standarts-USAF**. (2008). *Flight Control Systems - Design, Installation and Test of Piloted Aircraft, General Specification for (MIL-DTL-9490E)* (Issue April).

[38] **Cooper, G. E., & Harper, R. P.** (1969). The Use of Pilot Ratings in the Evaluation of Aircraft Handling Qualities. *Advisory Group for Aerospace Research and Development Neuilly-Sur-Seine, AGARD-567*.

[39] **Nho, K., & Agarwal, R. K.** (2000). Automatic landing system design using fuzzy logic. *Journal of Guidance, Control, and Dynamics*, *23*(2). https://doi.org/10.2514/2.4522

[40] **Shue, S. P., & Agarwal, R. K.** (1999). Design of automatic landing systems using mixed H2/H∞ control. *Journal of Guidance, Control, and Dynamics*, *22*(1). https://doi.org/10.2514/2.4356

[41] **Liao, F., Wang, J. L., Poh, E. K., & Li, D.** (2005). Fault-tolerant robust automatic landing control design. *Journal of Guidance, Control, and Dynamics*, *28*(5). https://doi.org/10.2514/1.12611

[42] **Juang, J. G., Chien, L. H., & Lin, F.** (2011). Automatic landing control system design using adaptive neural network and its hardware realization. *IEEE Systems Journal*, *5*(2). https://doi.org/10.1109/JSYST.2011.2134490

[43] **Laiacker, M., Kondak, K., Schwarzbach, M., & Muskardin, T.** (2013). Vision aided automatic landing system for fixed wing UAV. *IEEE International Conference on Intelligent Robots and Systems*. https://doi.org/10.1109/IROS.2013.6696777

[44] **Lungu, R., & Lungu, M.** (2016). Automatic Control of Aircraft in Lateral-Directional Plane during Landing. *Asian Journal of Control*, *18*(2). https://doi.org/10.1002/asjc.1133

[45] **John H. Blakelock**. (1991). Automatic control of aircraft and missiles. In *John Wiley & Sons*.

[46] **Bristol, E. H.** (1966). On a new measure of interaction for multivariable process control. *IEEE Transactions on Automatic Control*, *11*(1). https://doi.org/10.1109/TAC.1966.1098266

[47] **Young, P. C., & Willems, J. C.** (1972). An approach to the linear multivariable servomechanism problem. *International Journal of Control*, *15*(5), 961–979. https://doi.org/10.1080/00207177208932211

[48] **Wang, L.** (2009). Model Predictive Control System Design and Implementation

Using MATLAB®. In *Springer*. https://doi.org/10.1007/978-1-84882-331-0

[49] **Dursun, U.** (2020). *Hidrolik Test Sistemlerinin Kontrolü*.

[50] **Dursun, U., Yıldız Taşçıkaraoğlu, F., & Üstoğlu, İ.** (2021). An algebraic and suboptimal solution of constrained model predictive control via tangent hyperbolic function. *Asian Journal of Control*, *23*(5). https://doi.org/10.1002/asjc.2357

CURRICULUM VITAE

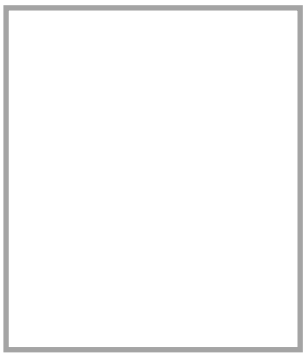

Name Surname **:** Talha Ulukır

EDUCATION **:**

- **B.Sc.** **:** 2018, Yildiz Technical University, Electric and Electronic Engineering, Control and Automation Engineering

PROFESSIONAL EXPERIENCE AND REWARDS:

- 2018-Now Turkish Aerospace / Flight Control Law and Algorithm Design Engineer